WATER RESOURCES research center

Publication No. 27

A Physical Model for Prediction and Control of Saltwater Intrusion in the Floridan Aquifer

By
Bent A. Christensen
and
Andrew J. Evans, Jr.

Department of Civil & Coastal Engineering
University of Florida
Gainesville

UNIVERSITY OF FLORIDA

Publication No. 27

A Physical Model for Prediction and Control of Saltwater Intrusion in the Floridan Aquifer

By
Bent A. Christensen
and
Andrew J. Evans, Jr.

Department of Civil & Coastal Engineering
University of Florida
Gainesville

A PHYSICAL MODEL FOR PREDICTION AND CONTROL OF SALTWATER INTRUSION IN THE FLORIDAN AQUIFER

By

Bent A. Christensen
and
Andrew J. Evans, Jr.

PUBLICATION NO. 27

FLORIDA WATER RESOURCES RESEARCH CENTER

RESEARCH PROJECT TECHNICAL COMPLETION REPORT

OWRR Project Number A-022-FLA

Annual Allotment Agreement Number

14-31-0001-3809

Report Submitted: January 29, 1974

The work upon which this report is based was supported in part by funds provided by the United States Department of the Interior, Office of Water Resources Research as Authorized under the Water Resources Research Act of 1964

ACKNOWLEDGEMENTS

Appreciation is extended to the Office of Water Resources Research, United States Department of the Interior, for financial support of this project, and to Dr. W. H. Morgan for his administrative assistance, and Ms. Mary Robinson for accounting assistance. The participation of Mr. Floyd Combs in all aspects of the project was especially valuable.

The efforts of Mr. C. L. White, Mr. William Whitehead and the staff of the Mechanical Engineering machine shop in the construction of the model are gratefully acknowledged. The assistance of Mr. Richard Sweet in the operation of the model and the patient attention of Ms. Cheryl Combs in typing the report deserve special thanks.

TABLE OF CONTENTS

TABLE OF CONTENTS (Continued)

LIST OF TABLES

LIST OF FIGURES

LIST OF FIGURES (Continued) Page

KEY TO SYMBOLS OR ABBREVIATIONS

SYMBOLS

- A = area, Fourier coefficient
- b = width of model and prototype
- B = body force, Fourier coefficient
- f = subscript denoting fresh-water, Floridan aquifer
- g = acceleration due to gravity
- h = height of water
- j = summation limit
- k = intrinsic permeability
- K = hydraulic conductivity
- l = distance between storativity tubes, subscript denoting leaky layer
- L = distance center to center of groove in anisotropic zone, flow meter tube length
- m = subscript denoting model
- n_e = effective porosity
- p = pressure, subscript denoting prototype
- q = specific discharge
- Q = total flow
- r = subscript denoting ratio
- R = accretion
- R_e = Reynolds' number
- S_o = specific storage
- t = time
- T = transmissivity
- U = volume
- V = velocity
- x = horizontal direction parallel to test section
- y = horizontal direction perpendicular to test section
- z = vertical direction

KEY TO SYMBOLS OR ABBREVIATIONS (Continued)

1,2,3	=	subscripts denoting zone 1, zone 2 and zone 3
α	=	width adjustment factor
γ	=	unit weight
λ	=	length adjustment factor
μ	=	absolute viscosity
ξ	=	geometric parameter in anisotropic zone
ρ	=	mass density
υ	=	kinematic viscosity
ϕ	=	potentiometric head
Φ	=	velocity potential, potential

ABBREVIATIONS

$\frac{D}{Dt}$	=	substantial derivative
∇^2	=	Laplace operator
Δ	=	difference operator
°C	=	Centigrade
cfs	=	cubic feet per second
°F	=	Fahrenheit
fps	=	feet per second
g/cm^3	=	grams per cubic centimeter
gpd	=	gallons per day
Hg	=	Mercury
I.D.	=	inner diameter
msl	=	mean sea level
O.D.	=	outer diameter
pcf	=	pounds per cubic feet
psid	=	pounds per square inch differential
psig	=	pounds per square inch gage
RPM	=	revolutions per minute

ABSTRACT

Continuing development of the coastline zone in the middle Gulf area of Florida is increasing the demand for ground water supplies, and in turn increasing the probability of salt-water intrusion. Methods must be developed to make long-range predictions on the effects of increased demands on the Floridan aquifer.

A Hele-Shaw model is a physical model which fits the requirements for long-range planning. It is well suited to handling anisotropic aquifers, difficult boundary conditions and can simulate years of field conditions in minutes of model time.

The section selected for study lies in a line from the Gulf coast near Tarpon Springs to a point near Dade City and passes through the Eldridge-Wilde well field. The Eldridge-Wilde well field is the major water producer for Pinellas County. This region has experienced several years of dry weather, and pumping has lowered the water levels in the aquifer by a significant amount. This loss of fresh-water head is certain to induce salt-water intrusion.

A Hele-Shaw model has been built for this section, and all pertinent geological and hydrological features of the area are included. Steady-state characteristics of the aquifer system have been considered. In particular, the long-term effects due to pumping and artificial recharge were examined.

CHAPTER I

INTRODUCTION AND STATEMENT OF PROBLEM

Florida, with the possible exception of California, is the fastest growing state of the United States. The rapid influx of people since World War II has greatly increased the demands for land and water. In the past, there has been an almost total lack of wide-range planning for the uses of these resources. Even fewer investigations have been made into the consequences of their rapid and unordered development. Recently, water supplies have had to be rationed in South Florida. Overall, land and wetlands required for fish and wildlife have so diminished that, in some instances, there has been a marked decrease in their numbers. It seems reasonable to conclude that in some areas of the state, land and water resources cannot support much larger populations with current locally available supplies without almost irrecoverable damage to the ground water system in the form of salt-water encroachment.

With the growing affluence of the American people, and the availability of economically priced air-conditioning units, it can be expected that even more people will leave the colder northern climates for the southern and western states. Florida can expect to receive more than its share of the migration. Frequently now, environmental protection groups are making forecasts of impending doom. At worst, their predictions may come true and people are beginning to look at all growth with a jaundiced eye.

It is doubtful, however, that growth and development can be stopped. The history of man indicates a continual effort to better his life style, his private environment. There is little doubt that this has sometimes caused a degradation of other portions of his world. Unless the cessation of all growth and development is acceptable, new ways must be found of forecasting, or predicting, the results of all growth so as to combat possible undesirable results. Consequences of all growth must be known, even of those resulting when pragmatic short-term solutions are used.

Hopefully, the remainder of this report will present a modeling method which will be useful in forecasting the results of pumpage and use of ground water in our coastal zones so that we may better plan their usage. But first, a little background on Florida.

Topography

Florida lies between latitudes 24°-40' and 31°-00' North, and longitudes 80°-00' and 87°-40' West, and is the most southerly unit of the continental United States. In its southernmost extension it is less than 1° of latitude north of the Tropic of Cancer.

Florida is bounded on the east by the Atlantic Ocean; on the south by the Straits of Florida and the Gulf of Mexico; on the west by the Gulf of Mexico and the state of Alabama; and on the north by Alabama and Georgia. The shape of the state in relation to the remainder of the United States suggests two distinctive parts: the Floridan panhandle and the peninsula of Florida. The panhandle is a strip roughly 225 miles long that stretches in an east-west direction. The peninsula is a south-southeast extension at approximate bearing S 17° E. From the northern boundary of the state to the tip, not including the chain of keys, the peninsula is approximately 415 miles long and includes 2/3's of the land mass of the entire state. Its coastline, some 1350+ miles long, is the longest with the exception of Alaska. No place in the interior of Florida is more than 60 miles from either the Gulf or the Atlantic coast.

Cooke (1945) divided the terrain of Florida into five sections, Figure 1; the Western Highlands, the Marianna Lowlands, the Tallahassee Hills, and a narrow band of Coastal Lowlands, which comprise the panhandle, and the Central Highlands and Coastal Lowlands, which comprise the peninsula. The topography of each is described briefly.

Western Highlands

Extending eastward from the Perdido River (the western boundary of Florida) to the Apalachicola River, the northern part of this region near the Alabama stateline is not much higher than 300 feet. It is considered to be hilly when compared to the broad gently rolling southern parts of this region which drop to 100 feet elevation as one approaches the coastal lowlands. The highest elevation in the state, 345 feet, is found in this region in the northwest corner of Walton County. The western highlands are underlain with sand of the Pliocene Citronelle Formation. The steepness of the bankslopes at the headwaters of the many streams is the most unique physiographic characteristic of this section.

Marianna Lowlands

This roughly triangular-shaped region of Holmes, Jackson and Washington Counties, with somewhat smaller contributions from Bay and Calhoun Counties lies between the Tallahassee hills and the western highlands. It is difficult

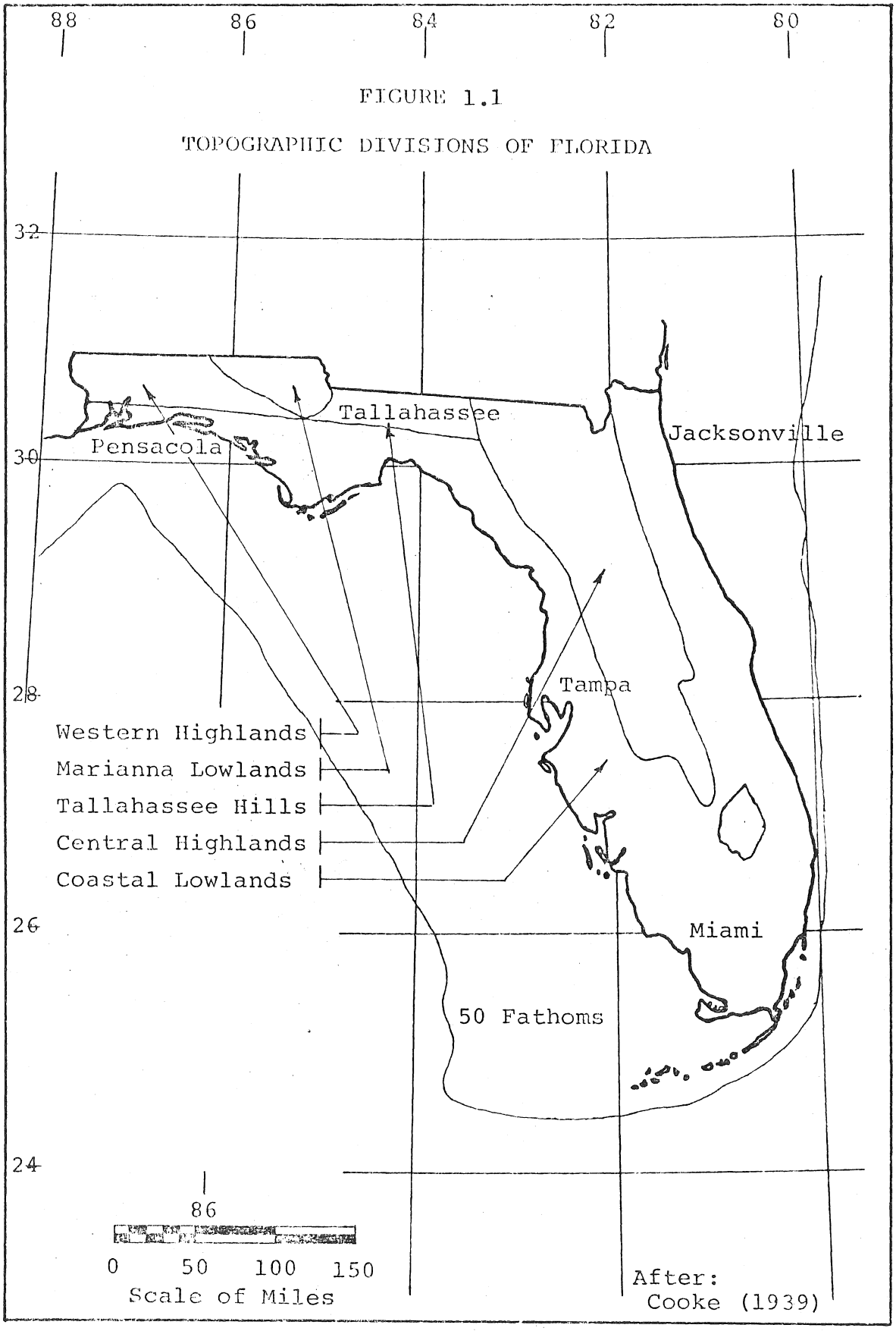

FIGURE 1.1

TOPOGRAPHIC DIVISIONS OF FLORIDA

to recognize this area of gently rolling hills as lowlands. Cooke (1945) attributes the lower elevations to the solubility and consequent degradation of the underlying limestone. This area is one of the two in the state where the Ocala Formation is exposed to the surface and the only area of the state where the Marianna limestone, the soft white limestone of the Oligocene Age, is found exposed. The region is dotted with sinks, sinkhole lakes and springs.

Tallahassee Hills

From the Apalachicola River east to the Withlacoochee River, the Tallahassee hills extends along the Georgia-Florida border and is only 25 miles in width. The western section is a nearly level plateau some 300 feet above mean sea level. The remainder consists of rolling hills carved out of the Citronelle Formation. In addition to this, a red clayey sand and Fuller's earth of the Hawthorn Formation are found in this area. This is a fertile farming region.

Central Highlands

The central highlands forms the backbone of the Floridan peninsula and extends from the Georgia line between the Withlacoochee and St. Mary's Rivers south-southeastward some 250 miles into Glades County west of Lake Okeechobee. This region is highly diversified. It includes high swampy plains, hills and innumerous lakes. Soils are sandy. Much of them were derived from Pleistocene (Ice Age) marine terraces. However, a distinquishable amount comes from the Miocene Hawthorn and Pliocene Citronelle Formations. The lakes and sinks which dot the entire area indicate the presence of limestone below the surface. Elevations of this region average just slightly more than 150 feet; however, they vary from less than 100 feet to approximately 300 feet.

Coastal Lowlands

The coastal lowlands, or coastal plains as it is sometimes called, borders the entire 1350 mile Florida coastline. Flanking on both sides of the central highlands, the coastal lowlands is widest just south of Lake Placid and narrowest between the western border and the Choctawhatchee Bay just south of the western highlands. The elevations everywhere within this region are less than 100 feet. The soil for the most part is sandy except in the Everglades and Big Cypress Swamp locales where Pliocene limestone, muck and peat prevail near the surface. The keys, which extend some 100 miles into the Straits of Florida, are mostly sandy oolitic limestone like that of the mainland; however, some limestone with coral heads is found. The islands seldom reach 15 feet elevation. The entire region is generally flat, typical of recently deposited material with little or no erosion.

Climate

The sea surface temperatures east and west of Florida average, respectively, 78° and 77° Fahrenheit. Water temperatures range from 74° to 83° Fahrenheit in the east and 70° to 84° Fahrenheit in the west. The coldest month in both cases is February; the warmest month is likewise August. The relative homogeneous distribution of sea temperature, the lack of high relief and the peninsula shape of Florida contribute greatly to its climate. The temperature is everywhere subtropical. Mean annual average temperature in the north is 68° Fahrenheit, and in the southern tip 75° Fahrenheit.

The tradewinds, which shift from northern Florida to southern Florida and back semiannually, bring a mildly-monsoon effect to Florida. In November, the tradewinds are at their southernmost extension and Florida's climate is controled by frontal, or cyclonic, activity moving in from the continental United States. Rainfall during this period is of low intensity and longer duration.

Beginning in early May, the tradewinds move north, again bringing with them the moist warm air of the Atlantic. The cyclonic activity is greatly reduced over the state and convectional instability begins to become established. June through September is known as the rainy season in Florida. The thunderstorms of this period are intense and very spacially varied. They usually occur during the hottest part of the day and only on rare occasions last longer than two hours. About 60 percent of the total average annual rainfall occurs during this period, Figure 2. The mean average rainfall of Florida is in the neighborhood of 53 inches. It varies from 38 to 40 inches in the lower keys to over 65 inches in the southeast corner of the peninsula and the western portion of the panhandle. Most of the interior, that is the central highlands, receive approximately the mean annual average.

Geology

The Floridan peninsula and the offshore submerged lands above 50 fathoms, which Vaughn (1910) called the Floridian Plateau, have existed for several million years. The region has not been subject to violent earth movement and, consequently, there has been a gentle doming resulting in the formation of an oval arch above the basement rock. The rock of the core underlying the plateau is hypothesized to be pre-Cambrian; however, no drill has penetrated the core. The oldest rocks penetrated, to date, are a quartzite found at about 4500 feet below the surface in Marion County. The borehole encountered another 1680 feet of

FIGURE 1.2

MEAN ANNUAL PRECIPITATION
(In Inches)

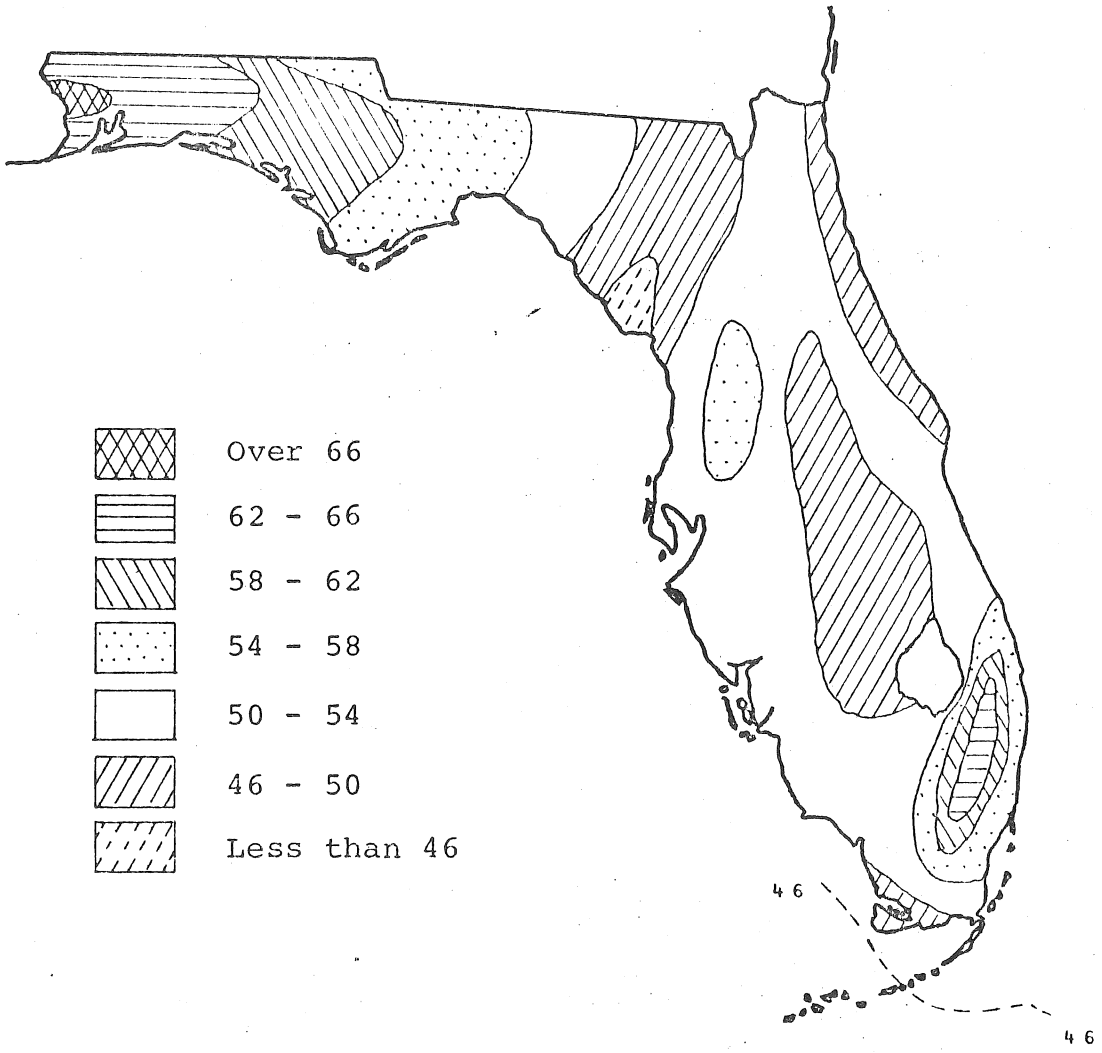

Note: Precipitation normals compiled from records published in Climatological Data: Florida Section, Dec, 1971.

quartzite before drilling was suspended. This metamorphized rock, believed to be a continuation of the Piedmont region of Georgia, was assigned by Cooke (1945) to the Pennsylvanian period. The arch above the metamorphized basement, composed of almost pure porous limestone, is known as the Lake City, Avon Park and Ocala Formations. Dated in the Eocene period, the Ocala Formation has an estimated maximum thickness of 360 feet. It is found at, or above, mean sea level throughout northeast and north central Florida and is this section's principal aquifer. In southern Florida, in the vicinity of the Everglades, the Ocala is found at depths approaching 1200 feet. The Lake City and Avon Park limestones found below the Ocala are the principal aquifer used by agricultural interests in central and south central Florida and are known locally as the Floridan aquifer.

Above the Eocene series are the formations of the Oligocene epoch. These are represented by the Marianna limestone and the Byran limestones found and mined in the Marianna lowlands of the northern part of the state, and the Suwanne limestone found over the Ocala Formation as far south as Hillsborough County.

The next higher formations are those of the Miocene epoch. These are well represented by the Tampa limestone of the early Miocene which are found above the Suwanne and Ocala limestone in south Florida, the Chipola and Shoal River Formations of the Alum Bluff group found in northwest and north central Florida, the Hawthorn Formation and the Duplin marls. The latter three formations, Alum Bluff, Hawthorn and Duplin, chiefly are sands, clays and marls that form a confining layer over the Eocene and Oligocene limestones.

The Hawthorn, with the possible exception of the Ocala, is the most extensive formation within the state. It occurs at, or near, the surface in most of north Florida. It overlies the Tampa limestone formation in Hillsborough County, and is, itself, overlain by the Duplin marls and younger deposits in the south central and southern parts of the state.

The surface material of most of the coastal lowlands are of the Pliocene, Pleistocene and Recent periods. The most widely distributed are the sands formed along the old shorelines of previous ocean levels. Cooke (1945) defines seven of these marine terraces. Some small deposits of coquina, oolite, coral reef limestone and fresh-water marls are found among these deposits.

CHAPTER II

MODELS, NUMERICAL AND PHYSICAL

The purpose of this chapter is to enumerate some of the more widely used modeling techniques in ground water flow, along with a brief description of each. The reader is referred to Bear (1972) for additional information and references.

A: NUMERICAL METHODS

Numerical methods are used in many cases where the partial differential equations governing flow through porous media cannot be solved exactly. Various techniques have been developed for obtaining numerical solutions.

Method of Finite Differences

The method of finite differences is one such technique. The first step is to replace the differential equations by algebraic finite difference equations. These difference equations are relationships among values of the dependent variable at neighboring points of the applicable coordinate space.

The resulting series of simultaneous equations is solved numerically and gives values of the dependent variables at a predetermined number of discrete or "grid" points throughout the region of investigation.

If the exact solution of the difference equations is called D, the exact solution of the differential equation is called S, and the numerical solution of the difference equation is called N, two quantities of interest may be defined. They are the truncation error, $|S - D|$, and the round-off error, $|D - N|$. In order for the solution to converge, it is necessary that $|S - D| \Rightarrow 0$ everywhere in the solution domain. The stability requirement is such that $|D - N| \Rightarrow 0$ everywhere in the solution domain. The general problem is to find N so that $|S - N|$ is smaller than some predetermined error. Noting that $(S - N) = (S - D) + (D - N)$, it is seen that the total error is composed of the truncation error and the round-off error. The arbitrary form selected for the finite difference equation leads to the truncation error. This error is frequently the major part of the total error.

The actual computation proceeds by one of two schemes. They are the explicit, or forward-in-time, scheme and the implicit, or back-in-time, scheme. The explicit scheme is simpler but more time consuming than the implicit scheme due to the stability constraint. The implicit scheme is more efficient but requires a more complicated program as compared to the explicit scheme.

Method of Finite Elements

The finite element technique employs a funtional associated with the partial differential equation, as opposed to the finite difference method which is based on a finite difference analog of the partial differential equation. A correspondence which assigns a real number to each function or curve belonging to some class is termed a functional.

The calculus of variations is employed to minimize the partial differential equation under consideration. This is done by satisfying a set of associated equations called the Euler equations. Thus, one seeks the functional for which the governing equations are the Euler equations and proceeds to solve the minimization problem directly, rather than solving the differential equation.

The procedure is continued by partitioning the flow field into elements, formulating the variational functional within each element and taking derivatives with respect to the dependent variables at all nodes of the elements. The equations of all the elements are then collected. The boundary condition is expressed in terms of nodal values and incorporated into the equations. The equations are then solved.

Relaxation Methods

This method may be applied to steady-state problems which are adequately described by the Laplace or Poisson equations. The process involves obtaining steadily improved approximations of the solution of simultaneous algebraic difference equations.

The first step of the procedure is to replace the continuous flow domain under investigation by a square or rectangular grid system. The governing differential equation is also replaced by corresponding difference equations. Next, a residual, say R_o, is defined corresponding to the point o on the grid. R_o represents the amount by which the equation is in error at that point. If all values of the equation are correct, R_o will be zero everywhere. In the initial computational step, values are assigned at all grid points and , in general, the initial residuals will not be zero everywhere. The process now consists in adjusting values at each point so that eventually all residuals approach zero, to at least some required accuracy.

The reduction of residuals is achieved by a "relaxation pattern" which is repeated at different grid points so as to gradually spread the residuals and reduce their value.

B: PHYSICAL MODELS

As implied in section A, direct analytical solutions are frequently inadequate or impractical for engineering application. In many cases, the analytical solutions which are found are difficult to interpret in a physical context. In an attempt to circumvent some of the shortcomings of a purely mathematical approach, model and analog methods are frequently employed. The analog may be considered as a single purpose computer which has been designed and built for a given problem.

Modeling, then, is the technique of reproducing the behavior of a phenomenon on a different and more convenient scale. In modeling, two systems are considered: the prototype, or system under investigation, and the analog system. These systems are analogous if the characteristic equations describing their dynamic and kinematic behavior are similar in form. This occurs only if there is a one-to-one correspondence between elements of the two systems. A direct analogy is a relationship between two systems in which corresponding elements are related to each other in a similar manner.

A model is an analog which has the same dimensions as the prototype, and in which every prototype element is reproduced, differing only in size. An analog is based on the analogy between systems belonging to entirely different physical categories. Similarity is recognized in an analog by two characteristics: (1) for each dependent variable and its derivatives in the equations describing one system, there corresponds a variable with corresponding derivatives in the second system's equations, and (2) independent variables and associated derivatives are related to each other in the same manner in the two sets of equations. The analogy stems from the fact that the characteristic equations in both systems represent the same principles of conservation and transport that govern physical phenomena. It is possible to develop analogs without referring to the mathematical formulation; an approach which is particularly advantageous when the mathematical expressions are excessively complicated or are unknown.

Analogs may be classed as either discrete or continuous with respect to space variables. In both cases, time remains a continuous independent variable.

The need for complete information concerning the flow field of a prototype system is obvious, and no method of solution can bypass this requirement. However, in many practical cases involving complicated geology and boundary

conditions, it is usually sufficient to base the initial construction of the analog on available data and on rough estimates of missing data. The analog is then calibrated by reproducing in it the known past history of the prototype. This is done by adjusting various analog components until a satisfactory fit is obtained between the analog's response and the response actually observed in the prototype. Once the analog reproduces past history reliably, and within a required range of accuracy, it may be used to predict the prototype's response to planned future operations.

The Sandbox Model

A reduced scale representation of a natural porous medium domain is known as a sandbox model, or a seepage tank model. Inasmuch as both prototype and model involve flow through porous media, it is a true model.

A sandbox model is composed of a rigid, watertight container, a porous matrix filler (sand, glass beads, or crushed glass), one or several fluids, a fluid supply system and measuring devices. The box geometry corresponds to that of the investigated flow domain, the most common shapes being rectangular, radial and columnar. For one-dimensional flow problems, the sand column is the most common experimental tool. Transparent material is preferred for the box construction, especially when more than one liquid may be present and a dye tracer is to be used. Porosity and permeability variations in the prototype may be simulated by varying the corresponding properties of the material used as a porous matrix in the model according to the appropriate scaling rules. The porous matrix may be anisotropic. In order to measure piezometric heads and underpressures, piezometers and tensiometers may be inserted into the flow domain of the model.

Wall effects are often eliminated by gluing sand grains to the walls of the box. This effect can also be reduced by making the porous matrix sufficiently large in the direction normal to the wall. Inlets and outlets in the walls connected to fixed-level reservoirs or to pumps are used to simulate the proper boundary and initial conditions of the prototype.

Water is usually used in models which simulate ground water aquifers, although liquids of a higher viscosity may be used to achieve a more suitable time scale.

The sandbox model is used extensively because of its special features which permit studies of phenomena related to the microscopic structure of the medium such as: hydrodynamic dispersion, unsaturated flow, miscible and immiscible displacement, simultaneous flow of two or more liquids at different relative saturations, fingering, wettability and capillary pressure. The capillary fringe in a sandbox model

is disproportionately larger than the corresponding capillary rise in the prototype, and for this reason the sandbox model is usually used to simulate flow under confined rather than phreatic conditions.

The Hele-Shaw Analog

The Hele-Shaw or viscous flow analog is based on the similarity between the differential equations governing two-dimensional, saturated flow in a porous medium and those describing the flow of a viscous liquid in a narrow space between two parallel planes. In practice, the planes are transparent plates, and the plates are usually mounted in a vertical or horizontal orientation.

The vertical Hele-Shaw analog was selected for this study because it is more appropriate for the prototype system under investigation. Also, it is not possible to model a free ground water table or percolation in a horizontal model.

A detailed description of this analog is presented in Chapter III of this report.

Electric Analog

Three types of electric analogs are powerful tools in the study of flow through porous media. They are the continuous electric analog, the discrete electric analog and the ion motion analog.

The Continuous Electric Analog

This analog takes two forms: the electrolytic tank and the conducting paper analogs. The analogy rests on the similarity between the differential equations that govern the flow of a homogeneous fluid through a porous medium, and those governing the flow of electricity through conducting materials.

In particular, Darcy's law for flow in a porous medium and Ohm's law for the flow of an electric current in a conductor may be compared. Also, the continuity equation for an incompressible fluid flowing through a rigid porous medium may be compared with the equation for the steady flow of electricity in a conductor. One concludes from this comparison that any problem of steady flow of an incompressible fluid having a potential may be simulated by the flow of electric current in an analog.

The Discrete Electric Analog

This analog also takes two forms: the resistance network analog for steady flow, and the resistance-capacitance network for unsteady flow.

In this analog, electric circuit elements are concentrated in the network's node points to simulate the properties of portions of the continuous prototype field around them. The unknown potentials are the solution of the problem, and

they can only be obtained for those points which correspond to the nodes of the analog network. The discrete electric analog is based on the finite-difference approximation of the equations to be solved; therefore, the errors involved in the discrete representation are the same as those occuring in this approximation.

The electric resistor corresponds to the resistance of soil to flow through it, and capacitors are used at the nodes to simulate storage capacity of the prototype.

The Ion Motion Analog

This analogy uses the fact that the velocity of ions in an electrolytic solution under the action of a DC voltage gradient is analogous to the average velocity of fluid particles under imposed potential gradients in a porous medium. In this case, both electric and elastic storativities are neglected. The primary advantage of the ion motion analogy is that, in addition to the usual potential distribution, it permits a direct visual observation of the movement of an interface separating two immiscible fluids. In ground water interface problems where gravity is involved, this analog cannot be used. Scaling for the analog is based on the similarity between Darcy's law and Ohm's law governing the ion motion in an electrolytic solution.

Physically the analog consists of an electrolytic tank having the same geometry as the investigated flow domain. Inflow and outflow boundaries are simulated by positive and negative electrodes, and two- and three-dimensional flow domains may be investigated.

The Membrane Analog

The membrane analog consists of a thin rubber sheet, stretched uniformly in all directions and clamped to a flat plane frame. The achievement of equilibrium of various forces and stresses in the membrane (caused by distorting the frame or transversal loads) leads to the Laplace equation and the Poisson equation. The analogy is based on the similarity between these two equations and the corresponding equations that describe the flow in the prototype.

This method is applicable mainly to cases of steady two-dimensional flow involving complicated boundary geometry and point sources and sinks within the flow field.

Summary

Following Bear (1972), Table 2.1 is presented as a summary of the models and analogs discussed in section B of this chapter. In section A, the numerical methods discussed are most likely to be carried out on a digital computer. It is important for the investigator to examine both the cost and the applicability of these various numerical and physical

TABLE 2.1

APPLICABILITY OF MODELS AND ANALOGS

Characteristic	Sandbox Model	Hele-Shaw Analog		Electric Analogs			Membrane Analog
		Vertical	Horizontal	Electrolytic	RC Network	Ion Motion	
Dimensions of field	two or three	two	two	two or three	two or three	two (horizontal)	two (horizontal)
Steady or unsteady flow	both	both	both	steady	both	steady	steady
Simulation of phreatic surface	yes[1]	yes[1]	no	yes[2]	no[3]	no	no
Simulation of capillary fringe and capillary pressure	yes	yes	no	no	no	no	no
Simulation of elastic storage	yes, for two dimensions	yes	yes	yes, for two dimensions	yes	no	no
Simulation of anisotropic media[4]	yes	yes $k_x \neq k_z$	yes $k_x \neq k_y$	yes	yes	yes $k_x \neq k_y$	yes $k_x \neq k_y$
Simulation of medium inhomogeneity	yes	yes[5]	yes[5]	yes	yes	yes	yes
Simulation of leaky formations	yes	yes	yes	yes[5]	yes	no	no
Simulation of accretion	yes	yes	yes	yes, for two dimensions	yes	no	yes
Flow of two liquids with an abrupt interface	approximately	yes	yes	no[6]	no[6]	yes	no
Simultaneous flow of two immiscible fluids	yes	no	no	no	no	no	no
Hydrodynamic dispersion	yes	no	no	no	no	no	no
Observation of streamlines	yes, for two dimensions, near transparent walls for three dimensions	yes	yes	no	no	no	no

1 Subject to restrictions because of the presence of a capillary fringe.

2 By trial and error for steady flow.

3 By trial and error for steady flow, or, as an approximation, for relatively small phreatic surface fluctuations.

4 By scale distortion in all cases, except for the RC network and sometimes the Hele-Shaw analog where the hydraulic conductivity of the analog can be made anisotropic.

5 With certain constraints.

6 For a stationary interface by trial and error.

methods to his particular case. An analog is usually preferred to a digital solution when the accuracy and/or amount of field data is small. In many simple cases, the analog is likely to be less expensive than a digital computer; whereas, for large regions or unsteady three-dimensional problems, the computer may be less expensive.

The Hele-Shaw model also has definite advantages when demonstration of the salt-water intrusion phenomenon to a public body, or other laymen involved in political decision-making, is considered. This type of model allows for direct observation of the phenomenon without the numerical interpretations used in the computer models.

CHAPTER III

THE HELE-SHAW MODEL

The viscous flow analog, more commonly referred to as a parallel-plate or Hele-Shaw model, was first used by H. S. Hele-Shaw (1897, 1898, 1899) to demonstrate two-dimensional potential flow of fluid around a ship's hull and other variously shaped objects. The analog is based on the similarity of the differential equations which describe two-dimensional laminar flow, or potential flow for that matter, of a viscous fluid between two closely spaced parallel plates; and those equations which describe the field of flow below the phreatic surface of ground water, namely Darcy's law:

$$q_x = - K_x \frac{\partial \phi}{\partial x} \; ; \quad q_z = - K_z \frac{\partial \phi}{\partial z} \qquad (3.1a;b)$$

where:

q_x, q_z = Darcy velocity of specific discharge in the x-direction and z-direction, respectively.
K_x, K_z = hydraulic conductivity in the x-direction and z-direction, respectively.
x = horizontal direction (major flow direction).
z = vertical direction.
ϕ = potentiometric head

and, by use of the conservation of mass principle, the Laplace equation:

$$\frac{\partial^2 \phi}{\partial x^2} + \frac{\partial^2 \phi}{\partial z^2} = 0 \qquad (3.2)$$

Viscous Flow Analog

To demonstrate the analogy of model and prototype, the equations of motion and continuity for laminar flow of a viscous fluid between two closely spaced parallel plates will be developed and then compared to equations 3.1a, 3.1b and 3.2.

Consider a viscous incompressible fluid flowing ever so slowly between two parallel plates which are spaced such that the Reynolds' number, R_e, based on the interspace width is less than 500 (Aravin and Numerov, 1965). In Cartesian coordinates, the general Navier-Stokes equations, i.e., the equations of motion, are:

$$\frac{DV_x}{Dt} = B_x + \frac{1}{\rho}\{-\frac{\partial p}{\partial x} + \mu\nabla^2 V_x\} \qquad (3.3a)$$

$$\frac{DV_y}{Dt} = B_y + \frac{1}{\rho}\{-\frac{\partial p}{\partial y} + \mu\nabla^2 V_y\} \qquad (3.3b)$$

$$\frac{DV_z}{Dt} = B_z + \frac{1}{\rho}\{-\frac{\partial p}{\partial z} + \mu\nabla^2 V_z\} \qquad (3.3c)$$

where:

$$\frac{D}{Dt} = \text{substantial derivative} = \frac{\partial}{\partial t} + V_x\frac{\partial}{\partial x} + V_y\frac{\partial}{\partial y} + V_z\frac{\partial}{\partial z}$$

$$\nabla^2 = \text{Laplace operator} = \frac{\partial^2}{\partial x^2} + \frac{\partial^2}{\partial y^2} + \frac{\partial^2}{\partial z^2}$$

V_x, V_y, V_z = velocity in the x-, y- and z-directions, respectively.
B_x, B_y, B_z = body forces in the x-, y- and z-directions respectively.
p = pressure.
ρ = density of the fluid.
μ = absolute viscosity of the fluid.
y = horizontal direction (minor flow direction).
t = time.

Referring to the free-body diagram of the idealized flow regime shown in Figure 3.1, if no slip conditions (adherence to the walls) of the fluid particles are assumed in the molecules closest to the walls of the parallel plates, it is easily seen that the velocity gradient in the y-direction is much larger than the velocity gradient in either the x- or z-directions. Thus, the first and second order partial derivatives taken with respect to both x and z may be neglected when compared to those taken in the y-direction. Secondly, because of the very low velocities ("creeping" motion) the inertia terms, that is the terms on the left side of equations 3.3, are very small when compared to the viscous

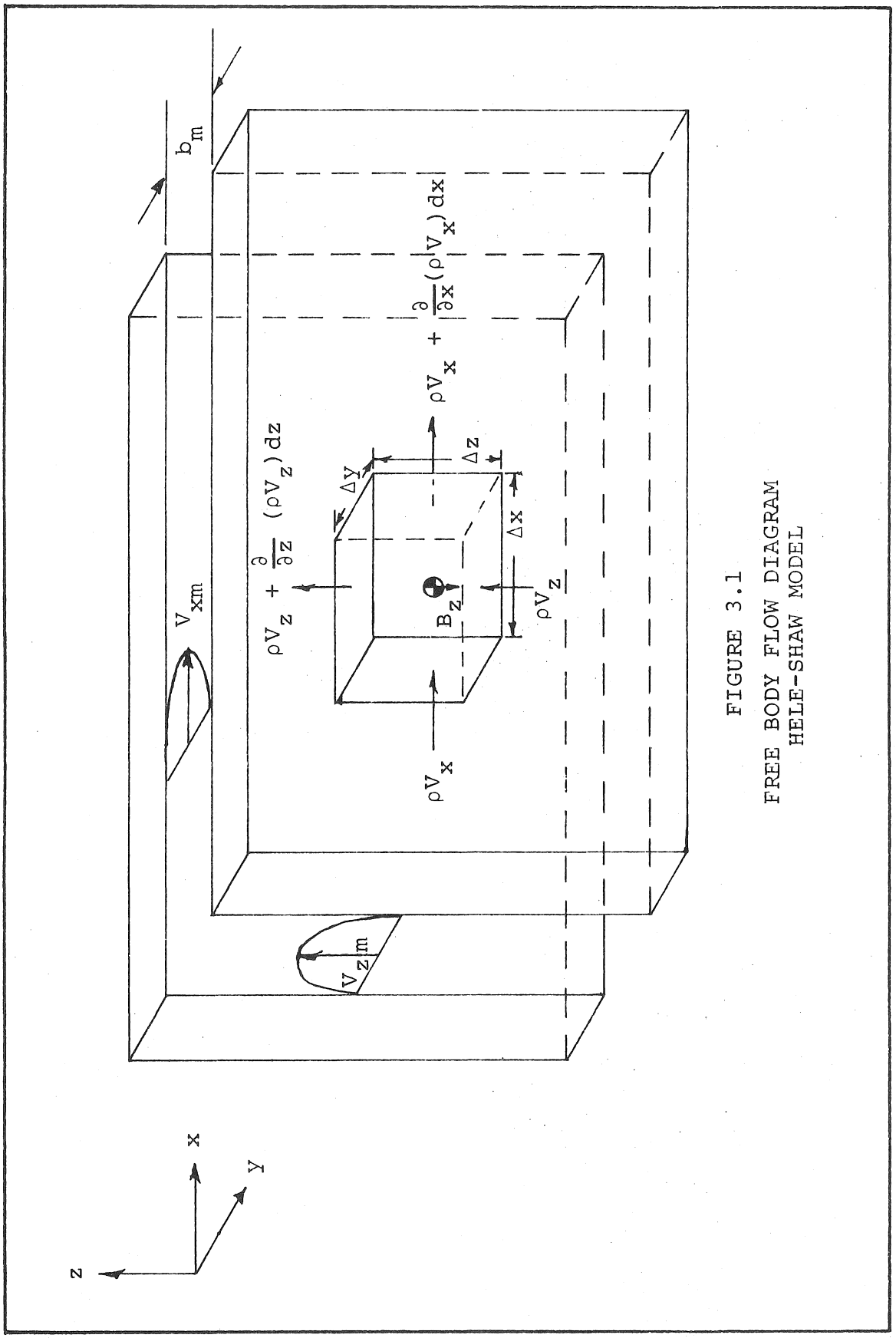

FIGURE 3.1
FREE BODY FLOW DIAGRAM
HELE-SHAW MODEL

terms, those on the right side of equations 3.3, and may be neglected. Thirdly, because of the restriction to two dimensions, the velocity in the y-direction is taken to be zero; consequently, all rates of change of velocity in the y-direction must be zero. Finally, the only non-cancelable body force acting on the fluid is gravity which acts only in the vertical. Mathematically, $B_x = -\frac{\partial}{\partial x}(gz) = 0$; $B_y = -\frac{\partial}{\partial y}(gz) = 0$; and $B_z = -\frac{\partial}{\partial z}(gz) = -g = -32.17$ ft./sec.^{2}. Incorporating all of the above arguments and values into equations 3.3, the equation of motion becomes:

$$-\frac{\partial p}{\partial x} + \mu \frac{\partial^2 V_x}{\partial y^2} = 0 \qquad (3.4a)$$

$$-\frac{\partial p}{\partial y} = 0 \qquad (3.4b)$$

$$-\rho g - \frac{\partial p}{\partial z} + \mu \frac{\partial^2 V_z}{\partial y^2} = 0 \qquad (3.4c)$$

Defining the potentiometric head, or potential, $\phi = z + p/\gamma$, where γ equals the unit weight of the fluid, and taking the partial derivative with respect to x, y and z, the following results are obtained after multiplying through by the unit weight of the fluid:

$$\gamma \frac{\partial \phi}{\partial x} = \frac{\partial p}{\partial x}; \quad \gamma \frac{\partial \phi}{\partial y} = \frac{\partial p}{\partial y}; \quad \gamma\{\frac{\partial \phi}{\partial z} - 1\} = \frac{\partial p}{\partial z} \qquad (3.5a;b;c)$$

Introducing these relationships into equations 3.4 and dividing through by the unit weight yields:

$$\frac{\partial \phi}{\partial x} = \frac{\mu}{\gamma} \frac{\partial^2 V_x}{\partial y^2} \qquad (3.6a)$$

$$\frac{\partial \phi}{\partial y} = 0 \qquad (3.6b)$$

$$\frac{\partial \phi}{\partial z} = \frac{\mu}{\gamma} \frac{\partial^2 V_z}{\partial y^2} \qquad (3.6c)$$

It is evident from equation 3.6b that the potentiometric head is constant in the y-direction. It is possible then to integrate the first and third equations of equations 3.6 with respect to y. After separating

variables and integrating once, using the boundary condition $y = 0$, $\frac{\partial V_x}{\partial y} = 0$ and $\frac{\partial V_z}{\partial y} = 0$, the following equations are obtained:

$$y \frac{\partial \phi}{\partial x} = \frac{\mu}{\gamma} \frac{\partial V_x}{\partial y} \tag{3.7a}$$

$$y \frac{\partial \phi}{\partial z} = \frac{\mu}{\gamma} \frac{\partial V_z}{\partial y} \tag{3.7b}$$

Integrating, once again, using the second boundary condition $y = \pm b/2$, $V_x = 0$ and $V_z = 0$ (no slip) the above becomes, after solving for the respective velocities:

$$V_x = \frac{\gamma}{2\mu} \left\{y^2 - \frac{b^2}{4}\right\} \frac{\partial \phi}{\partial x} \tag{3.8a}$$

$$V_z = \frac{\gamma}{2\mu} \left\{y^2 - \frac{b^2}{4}\right\} \frac{\partial \phi}{\partial z} \tag{3.8b}$$

Note, where b is the spacing between the plates, that if a potential $\Phi = - \frac{\gamma \phi}{2\mu} \left\{y^2 - \frac{b^2}{4}\right\}$ is defined, equations 3.8 can be written:

$$V_x = - \frac{\partial \Phi}{\partial x} \; ; \quad V_z = - \frac{\partial \Phi}{\partial z} \tag{3.9a;b}$$

Φ is what Shames (1962) calls a velocity potential. It is dependent only on y. Integrating the velocity profiles established by equations 3.8 between the limits of $\pm b/2$, and dividing by b, the directional specific discharges are obtained:

$$q_x = \frac{1}{b} \int_{-b/2}^{+b/2} V_x dy = \frac{1}{b} \frac{\gamma}{2\mu} \frac{\partial \phi}{\partial x} \left\{\frac{y^3}{3} - \frac{b^2 y}{4}\right\}_{-b/2}^{+b/2} = - \frac{b^2}{12} \frac{\gamma}{\mu} \frac{\partial \phi}{\partial x} \tag{3.10a}$$

$$q_z = \frac{1}{b} \int_{-b/2}^{+b/2} V_z dy = \frac{1}{b} \frac{\gamma}{2\mu} \frac{\partial \phi}{\partial z} \left\{\frac{y^3}{3} - \frac{b^2 y}{4}\right\}_{-b/2}^{+b/2} = - \frac{b^2}{12} \frac{\gamma}{\mu} \frac{\partial \phi}{\partial z} \tag{3.10b}$$

It is obvious that for a model of constant spacing b, the quantity $\frac{b^2}{12}\frac{\gamma}{\mu}$ does not vary in either the x- or z-direction. Defining the model hydraulic conductivity as $K_{xm} = K_{zm} = \frac{b^2}{12}\frac{\gamma}{\mu}$, equations 3.10a and 3.10b become:

$$q_x = - K_{xm} \frac{\partial \phi}{\partial x} \; ; \quad q_z = - K_{zm} \frac{\partial \phi}{\partial z} \qquad (3.11a;b)$$

which, of course, is analogous to equations 3.1.

Consider, now, the two-dimensional continuity equation for flow between parallel plates:

$$\frac{\partial V_x}{\partial x} + \frac{\partial V_z}{\partial z} = 0 \qquad (3.12)$$

The specific discharge, or Darcy velocity, is related to the velocity by the vector equation $n_e \vec{q} = \vec{V}$, where n_e is the effective porosity of the flow media. In the model, n_e equals 1. From the analogy $V_x = q_x$; $V_z = q_z$, and substituting the relationship obtained from equation 3.11 into equation 3.12:

$$- K_{xm} \frac{\partial}{\partial x} \left\{\frac{\partial \phi}{\partial x}\right\} - K_{zm} \frac{\partial}{\partial z} \left\{\frac{\partial \phi}{\partial z}\right\} = 0 \qquad (3.13)$$

or dividing by $- K_m$ and recalling that for a model $K_m = K_{xm} = K_{zm}$:

$$\frac{\partial^2 \phi}{\partial x^2} + \frac{\partial^2 \phi}{\partial z^2} = 0 \qquad (3.14)$$

which is clearly analogous to equation 3.2.

The similarity of equations 3.1 and 3.11 and equations 3.2 and 3.14 establish the analogy.

Scaling

The two-dimensional equation along the free surface, or water table, of an anisotropic porous media given by Bear (1972) is:

$$K_{xp} \left\{\frac{\partial \phi_p}{\partial x_p}\right\}^2 + K_{zp} \left[\left\{\frac{\partial \phi_p}{\partial z_p}\right\}^2 - \frac{\partial \phi_p}{\partial z_p}\right] = n_{ep} \frac{\partial \phi_p}{\partial t_p} \qquad (3.15)$$

where the subscript p denotes the prototype. For a Hele-Shaw model, using the subscript m, the equation can be written as:

$$K_{xm}\left\{\frac{\partial\phi_m}{\partial x_m}\right\}^2 + K_{zm}\left(\left\{\frac{\partial\phi_m}{\partial z_m}\right\}^2 - \frac{\partial\phi_m}{\partial z_m}\right) = n_{em}\frac{\partial\phi_m}{\partial t_m} \qquad (3.16)$$

Introducing the similitude ratios, denoted by the subscript r, of the corresponding parameter of model and prototype:

$$K_{xr} = \frac{K_{xm}}{K_{xp}} \; ; \quad K_{zr} = \frac{K_{zm}}{K_{zp}} \qquad (3.17a;b)$$

$$x_r = \frac{x_m}{x_p} \; ; \quad z_r = \frac{z_m}{z_p} \qquad (3.17c;d)$$

$$\phi_r = \frac{\phi_m}{\phi_p} \; ; \quad n_{er} = \frac{n_{em}}{n_{ep}} \qquad (3.17e;f)$$

$$t_r = \frac{t_m}{t_p} \qquad (3.17g)$$

and substituting these relationships into equation 3.15, the following is obtained:

$$\frac{K_{xm}}{K_{xr}}\left\{\frac{\partial(\phi_m/\phi_r)}{\partial(x_m/x_r)}\right\}^2 + \frac{K_{zm}}{K_{zr}}\left(\left\{\frac{\partial(\phi_m/\phi_r)}{\partial(z_m/z_r)}\right\}^2 - \frac{\partial(\phi_m/\phi_r)}{\partial(z_m/z_r)}\right) = \frac{n_{em}}{n_{er}} \cdot \frac{\partial(\phi_m/\phi_r)}{\partial(t_m/t_r)} \qquad (3.18)$$

The ratios of model to prototype quantities are constant and can be removed from behind the differential; therefore, equation 3.18 can be rearranged in the following way:

$$\frac{x_r^2}{K_{xr}\phi_r^2}K_{xm}\left\{\frac{\partial\phi_m}{\partial x_m}\right\}^2 + K_{zm}\left(\frac{z_r^2}{K_{zr}\phi_r^2}\left\{\frac{\partial\phi_m}{\partial z_m}\right\}^2 - \frac{z_r}{K_{zr}\phi_r}\left\{\frac{\partial\phi_m}{\partial z_m}\right\}\right) = \frac{t_r}{n_{er}\phi_r}n_{em}\frac{\partial\phi_m}{\partial t_m} \qquad (3.19)$$

Comparing the equations 3.16 and 3.19, it is evident that, if the equations are identical, the following must be true:

$$1 = \frac{x_r^2}{K_{xr}\phi_r} = \frac{z_r^2}{K_{zr}\phi_r} = \frac{z_r}{K_{zr}\phi_r} = \frac{t_r}{n_{er}\phi_r} \qquad (3.20)$$

Solving the third equality for z_r, the following important relationship is found:

$$z_r = \phi_r \qquad (3.21)$$

The second equality, after cross-multiplying, yields:

$$\left\{\frac{x_r}{z_r}\right\}^2 = \frac{K_{xr}}{K_{zr}} \qquad (3.22)$$

Recalling the definitions of K_{xr} and K_{zr} (equations 3.17a;b) and remembering that $K_{xm} = K_{zm}$ in an isotropic model, the above equation can be rewritten:

$$\left\{\frac{x_r}{z_r}\right\}^2 = \frac{K_{xm}/K_{xp}}{K_{zm}/K_{zp}} = \frac{K_{zp}}{K_{xp}} \qquad (3.23)$$

The ratio of $\frac{K_{zp}}{K_{xp}}$ is called the ratio or degree of anisotropy of the prototype.

Time

Using the fourth equality of equation 3.20, the time ratio of the model and prototype is established:

$$t_r = \frac{n_{er} z_r}{K_{zr}} \; ; \quad t_r = \frac{n_{er} x_r^2}{K_{xr}\phi_r} \qquad (3.24a;b)$$

Substituting the vertical ratio, z_r, for the potentiometric head established by equation 3.20 and the similitude ratios of time, hydraulic conductivity and porosity into equation 3.24b results in:

$$\frac{t_m}{t_p} = \frac{n_{em}}{n_{ep}} \frac{K_{xp}}{K_{xm}} \frac{x_r^2}{z_r} \qquad (3.25)$$

The effective porosity of an isotropic model, n_{em}, is unity. The hydraulic conductivity of the model was defined previously as $\frac{b^2 g}{12\upsilon}$, thus the time scale for the model is finally written as:

$$t_m = \frac{12}{g} \frac{\upsilon}{n_{ep}} \frac{K_{xp}}{b^2} \frac{x_r^2}{z_r} t_p \qquad (3.26)$$

Anisotropy

The Hele-Shaw model is normally isotropic. This is because of the non-variance of the spacing of the parallel plates. There are, however, two methods for simulating anisotropy in a model. Equation 3.23 gives a clue as to the first possibility of simulating anisotropy:

$$\left\{\frac{x_r}{z_r}\right\}^2 = \frac{K_{xm}/K_{xp}}{K_{zm}/K_{zp}} = \frac{K_{zp}}{K_{xp}} \qquad (3.23)$$

Since $K_{xm} = K_{zm}$, the x or z ratio can be adjusted so that the model's hydraulic conductivities are kept equal. This is usually done by choosing a suitable horizontal ratio. Knowing the prototype parameters, a vertical scale for the model is computed so that the aforementioned conductivities are kept equal, demonstrating:

$$z_r = \frac{z_m}{z_p} = \left\{\frac{K_{xp}}{K_{zp}}\right\}^{1/2} \frac{x_m}{x_p} \qquad (3.27)$$

Solving for z_m:

$$z_m = \left\{\frac{K_{xp}}{K_{zp}}\right\}^{1/2} \frac{x_m}{x_p} z_p \qquad (3.28)$$

Unfortunately, the geometric distortion method is adequate for modeling only one ratio of anisotropy. If there is a second aquifer, within the prototype which has a different vertical or horizontal hydraulic conductivity, the second aquifer cannot be correctly simulated; unless, of course, the second aquifer's ratio of anisotropy is the same as the ratio of the first. This restriction would severely limit the use of the Hele-Shaw analog in modeling of regional ground water problems unless another method were available to correct the ratio of anisotropy.

Polubarinova-Kochina (1962) suggests using a grooved plate within the model to correct the ratio of anisotropy of the second flow zone. The plate may be grooved in any

one of several methods. It matters little whether a grooved plate is sandwiched between the parallel plates, or if rectangular bars are attached to the front or back plate. The degree of anisotropy of the second aquifer and the amount of geometric distortion used to model the first flow zone determines the directions the grooves, or bars, are placed; however, the grooves are normally placed horizontally or vertically. Collins and Gelhar (1970) have developed the conductivity equations for the flow zone in which Polubarinova-Kochina's grooved plate is used. The analysis assumes one-dimensional flow and can be used equally well with either vertical or horizontal orientation of the grooves.

Following Collins and Gelhar (1970), consider flow in a grooved portion of a model. For simplicity, assume Figure 3.2 is a plan section of the grooved zone. Assuming such, the horizontal direction then corresponds to the x-direction and the grooves, which are vertical, lie in the z-direction. Area 1 is associated with the wider spacing of length αb. Area 2 is associated with the narrower spacing of length b. Since flow area 1 is the much larger of the two areas, most of the frictional head loss occurring through the total length L is developed in flow area 2 which has length $(1-\lambda)L$. Lambda, λ, is a length correction factor. Referring to Figure 3.3, the potentiometric gradient $\frac{\partial \phi_2}{\partial x}$, across area 2 is:

$$\frac{\partial \phi_2}{\partial x} = \frac{\Delta \phi_2}{(1-\lambda)L} \tag{3.29}$$

For high values of α:

$$\frac{\partial \phi}{\partial x} = \frac{\Delta \phi}{L} \simeq \frac{\Delta \phi_2}{L} \tag{3.30}$$

but, from equation 2.29, $\frac{\Delta \phi_2}{L} = (1-\lambda)\ \frac{\partial \phi_2}{x}$ so that:

$$\frac{\partial \phi}{\partial x} \simeq (1-\lambda)\ \frac{\partial \phi_2}{\partial x} \tag{3.31}$$

Applying Darcy's law to area 2:

$$q_x = - K_{x_2}\ \frac{\partial \phi_2}{\partial x} \tag{3.32}$$

and, substituting the previous expression for $\frac{\partial \phi_2}{\partial x}$:

$$q_x = - \frac{K_{x2}}{(1-\lambda)}\ \frac{\partial \phi}{\partial x} \tag{3.33}$$

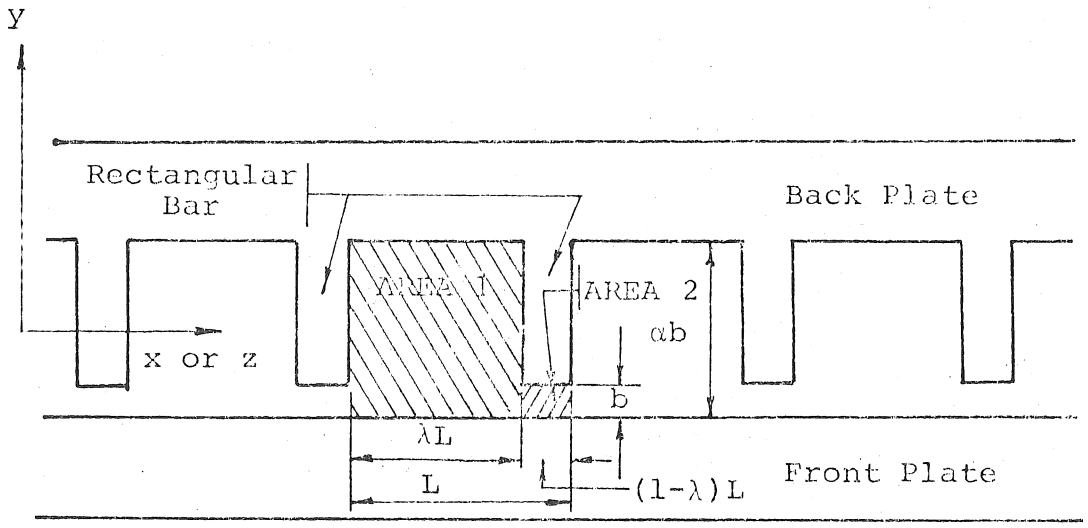

FIGURE 3.2

PLAN SECTION OF ANISOTROPIC GROOVED ZONE
IN HELE-SHAW MODEL

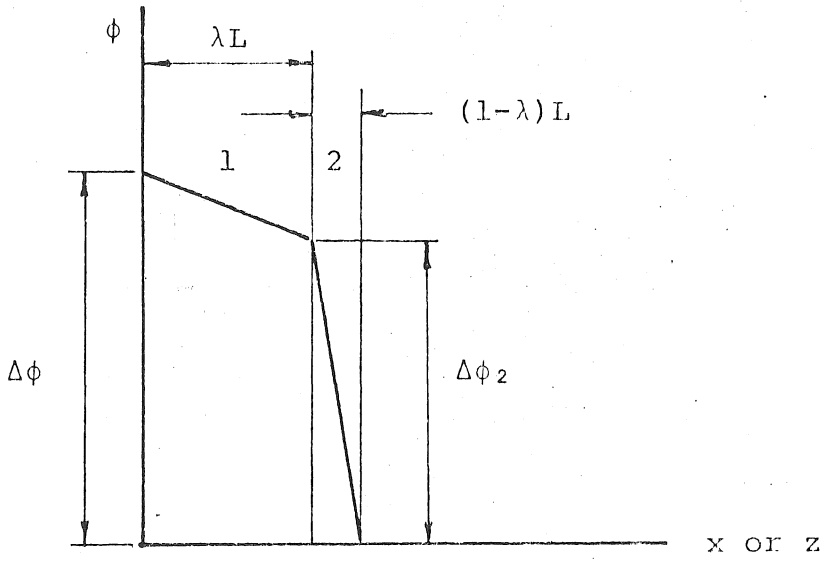

FIGURE 3.3

HEADLOSS IN GROOVED ANISOTROPIC ZONE

The effective hydraulic conductivity in the x-direction then is:

$$K_{xm} = \frac{K_{x2}}{(1-\lambda)} = \frac{b^2 g}{12\upsilon(1-\lambda)} \tag{3.34}$$

Consider vertical flow through the grooved zone illustrated in Figure 3.2. In particular, consider flow downward through areas 1 and 2. The total discharge through these areas can be written as the sum of the discharge through each, that is, $Q_{zm} = Q_1 + Q_2$. Applying Darcy's law for the total discharge, Q:

$$Q_1 = - K_{z_1} \frac{\partial \phi}{\partial z} (\alpha b \lambda L) \tag{3.35}$$

$$Q_2 = - K_{z_2} \frac{\partial \phi}{\partial z} (1-\lambda) Lb \tag{3.36}$$

Adding Q_1 and Q_2:

$$Q_{zm} = - \{K_{z_1} (\alpha\lambda) + K_{z_2} (1-\lambda)\} bL \frac{\partial \phi}{\partial z} \tag{3.37}$$

For flow area 2 it is not unreasonable to assume that the frictional forces in the fluid boundary to either side of area 2 are negligible. Therefore, the horizontal conductivity in this area is the same as defined by the earlier analysis, that is:

$$K_{z_2} = \frac{b^2}{12} \frac{\gamma}{\mu} = \frac{b^2}{12} \frac{g}{\upsilon} \tag{3.38}$$

where υ is the kinematic viscosity. Furthermore, if $b/\alpha b << 1$, the flow in area 1 can be assumed roughly equivalent to flow through a rectangular hole. According to Rouse (1959), the equation of motion through a rectangular cross-section of length λL and width αb is given by:

$$V_z = \frac{\gamma}{2\mu} \frac{\partial \phi}{\partial z} x(x - \lambda L) + \sum_{j=1}^{\infty} \sin \frac{j\pi x}{\lambda L} \cdot$$

$$\{A_j \cosh \frac{j\pi y}{\lambda L} + B_j \sinh \frac{j\pi y}{\lambda L}\} \tag{3.39}$$

where:

$$A_j = - \frac{2\gamma(\lambda L)^2}{\mu j^3 \pi^3} \frac{\partial \phi}{\partial z} (\cos j\pi - 1) \tag{3.40}$$

and,

$$B_j = -A_j \left(\frac{\cosh \frac{j\alpha b\pi}{\lambda L} - 1}{\sinh \frac{j\alpha b\pi}{\lambda L}} \right) \tag{3.41}$$

By integrating V_z over the area and dividing by the total area $\lambda L \alpha b$, the mean velocity is given by:

$$\bar{V}_z = - \xi \frac{\gamma}{\mu} \frac{(\alpha b)^2}{12} \frac{\partial \phi}{\partial z} \tag{3.42}$$

where:

$$\xi = 1 - \frac{12 \cdot 16}{\pi^5} \left\{ \frac{\alpha b}{\lambda L} \right\} \sum_{j=1}^{\infty} \frac{\{\cos(j\pi) - 1\}^2}{4 j^5} \tanh \frac{j\pi\lambda L}{2\alpha b} \tag{3.43}$$

Since the terms of the infinite series decrease as j^5, only the first term of the series need be considered and retained, so that:

$$\xi \simeq 1 - \frac{192}{\pi^5} \left\{ \frac{\alpha b}{\lambda L} \right\} \tanh \frac{\pi\lambda L}{2\alpha b} \tag{3.44}$$

From equation 3.42, the equivalent hydraulic conductivity in area 1 is given by:

$$K_{z_1} = \frac{\gamma}{\mu} \frac{(\alpha b)^2}{12} \xi \tag{3.45}$$

Finally, introducing the values found for K_{z_1} and K_{z_2} into equation 3.37:

$$Q_{zm} = - \frac{\gamma}{\mu} \left\{ \frac{(\alpha b)^2}{12} \xi (\alpha\lambda) + \frac{b^2}{12} (1-\lambda) \right\} \frac{\partial \phi}{\partial z} bL \tag{3.46}$$

or,

$$Q_{zm} = - \frac{\gamma}{\mu} \left\{ \frac{b^2}{12} (\alpha^3 \lambda \xi + 1 - \lambda) \right\} \frac{\partial \phi}{\partial z} bL \tag{3.47}$$

from which it's seen that the effective vertical hydraulic conductivity is given by:

$$K_{zm} = \frac{\gamma}{\mu} \frac{b^2}{12} (\alpha^3 \lambda \xi + 1 - \lambda) \tag{3.48}$$

after defining $Q_{zm}/bL = V_z$, where $V_z = q_z$ is the effective vertical specific discharge. Equations 3.34 and 3.48 give the second method available to correct the hydraulic conductivity of a model so that it can simulate the true ratios of anisotropy found in the prototype.

Leakage

An aquiclude can be defined as a soil stratification in which the hydraulic conductivities are zero. In certain geo-hydrologic problems, it is convenient to assume such conditions. However, in reality few soil masses are truly impervious. The degree of perviousness in a stratum is referred to as leakance and it is generally assumed that the direction of flow is only vertical. There is no horizontal flow, that is,

$$K_{xp} = 0 \tag{3.49}$$

Bear, et al., (1968) suggests the use of vertical slots to model such a semi-pervious layer. To accomplish this, the spacing between the parallel plates of the Hele-Shaw analog is filled with a slotted middle plate. See Figure 3.4.

The analysis to determine the effective vertical hydraulic conductivity of a model's leaky layer closely parallels that for an anisotropic grooved zone. Again, following Collins (1970), Darcy's law for flow through a vertical slot is:

$$Q_z = - K_z \frac{\partial \phi}{\partial z} \lambda L \alpha b \tag{3.50}$$

The effective specific discharge through the slot found by integrating the Rouse equation (equation 3.39) is the same as equation 3.42 from which is found the hydraulic conductivity:

$$K_z = \frac{\gamma}{\mu} \frac{(\alpha b)^2}{12} \xi \tag{3.51}$$

and, introducing the above into equation 3.50:

$$Q_z = - \frac{\gamma}{\mu} \frac{(\alpha b)^2}{12} \xi \lambda L \alpha b \frac{\partial \phi}{\partial z} \tag{3.52}$$

Again, the effective specific discharge, or mean velocity, is equal to:

$$\bar{V}_z = \frac{Q_z}{bL} = - \frac{\gamma}{\mu} \alpha^3 \lambda \xi \frac{b^2}{12} \frac{\partial \phi}{\partial z} \tag{3.53}$$

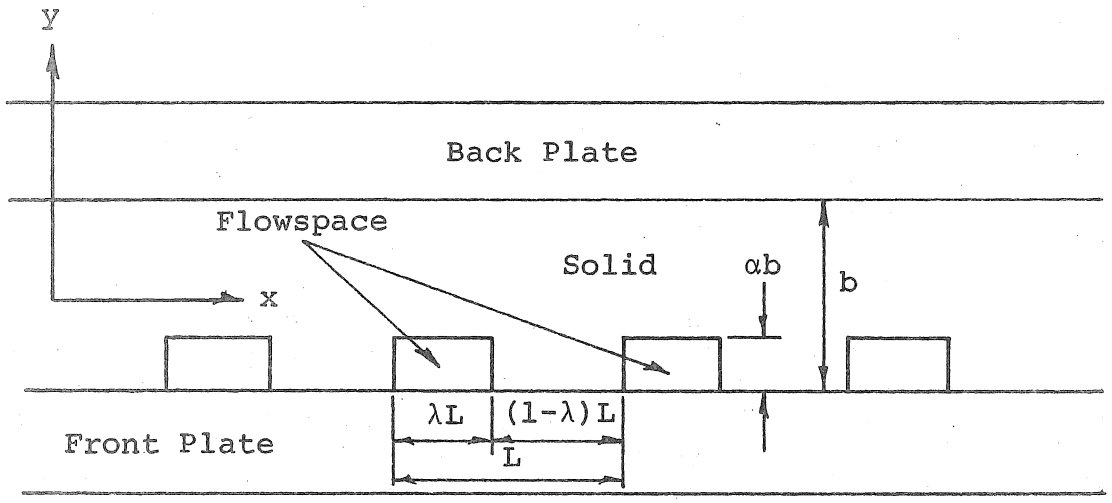

FIGURE 3.4

PLAN SECTION OF LEAKY ZONE
IN HELE-SHAW MODEL

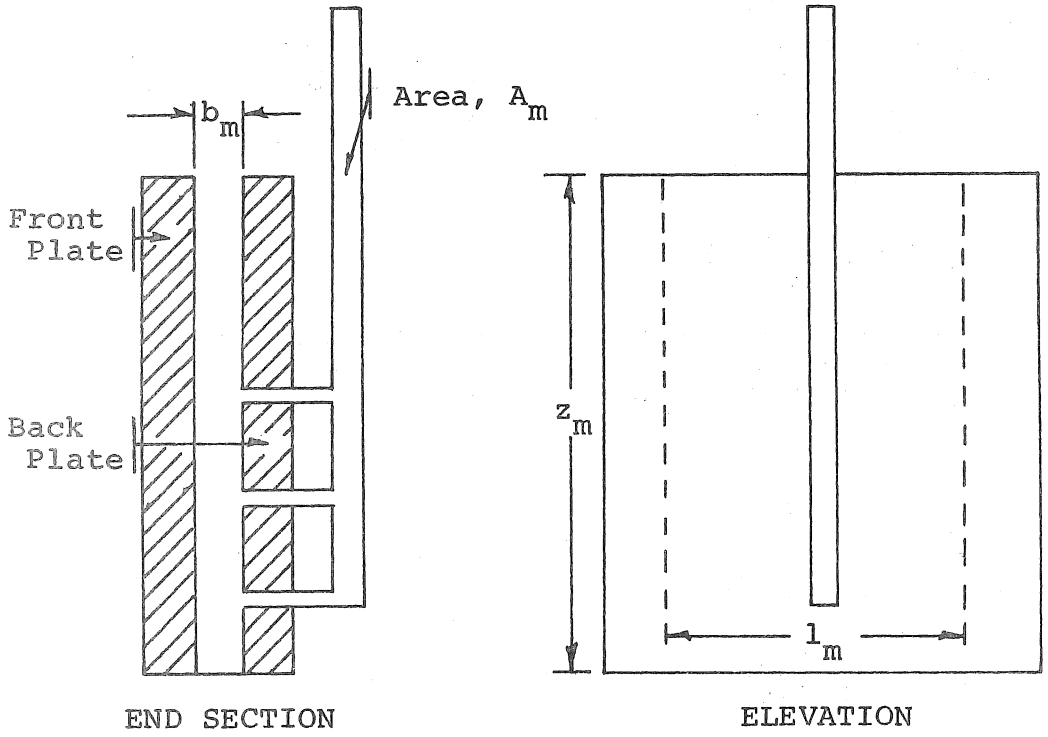

FIGURE 3.5

STORATIVITY

so that the effective hydraulic conductivity of a leaky layer in the model is:

$$K_{zm} = \frac{\gamma}{\mu} \alpha^3 \lambda \xi \frac{b^2}{12} \tag{3.54}$$

Storativity

While the problem of storage has not been completely solved, it has, in general, been neglected by most researchers. Bear (1960) suggests that discrete tubes attached to either the front or back plate and connected to the aquifer be used to model the specific storage of a confined aquifer. For a non-isotropic aquifer, the right-hand side of equation 3.13 is not zero, but, in fact, equals the specific storage, S_o, times the rate of change of the potentiometric head. Rewriting the two-dimensional equation 3.13 for both model and prototype to include the above is as follows:

$$K_{xp} \frac{\partial^2 \phi_p}{\partial x^2_p} + K_{zp} \frac{\partial^2 \phi_p}{\partial z^2_p} = S_{op} \frac{\partial \phi_p}{\partial t_p} \tag{3.55}$$

$$K_{xm} \frac{\partial^2 \phi_m}{\partial x^2_m} + K_{zm} \frac{\partial^2 \phi_m}{\partial z^2_m} = S_{om} \frac{\partial \phi_m}{\partial t_m} \tag{3.56}$$

Defining a ratio of storativity:

$$S_{or} = \frac{S_{om}}{S_{op}} \tag{3.57}$$

it follows from inspection that,

$$K_{xr} \frac{z_r}{x_r^2} = \frac{K_{zr}}{z_r} = S_{or} \frac{z_r}{t_r} \tag{3.58}$$

or that,

$$S_{or} = \frac{K_{zr} t_r}{z_r^2} = \frac{S_{om}}{S_{op}} \tag{3.59}$$

Referring to Figure 3.5, the storage represented by the model in the discrete length l_m is equal to:

$$S_{om} = \frac{A_m}{b_m l_m z_m} \tag{3.60}$$

where A_m is the cross-sectional area of the storativity tube. Introducing the above into equation 3.59 and solving for A_m:

$$A_m = b_m l_m z_m \, S_{op} \, K_{zr} \, \frac{t_r}{z_r^2} \tag{3.61}$$

Discharge

The discharge scales are obtained from Darcy's law. Written for both prototype and model with the usual subscripting, these are in the x-direction:

$$Q_{xp} = - K_{xp} \, \frac{\partial \phi_p}{\partial x_p} \, b_p z_p \tag{3.62}$$

and,

$$Q_{xm} = - K_{xm} \, \frac{\partial \phi_m}{\partial x_m} \, b_m z_m \tag{3.63}$$

Dividing equation 3.63 by equation 3.62 and recalling the definitions for the various parameters' ratios, it follows that:

$$Q_{xr} = K_{xr} \, \phi_r \, b_r \, \frac{z_r}{x_r} = K_{xr} \, b_r \, \frac{z_r^2}{x_r} \tag{3.64}$$

Similarly, in the z-direction,

$$Q_{zr} = K_{zr} \, \phi_r \, b_r \, \frac{x_r}{z_r} = K_{zr} \, b_r \, x_r \tag{3.65}$$

Solving equation 3.22 for the hydraulic conductivity in the x-direction:

$$K_{xr} = K_{zr} \left\{ \frac{x_r}{z_r} \right\}^2 \tag{3.66}$$

and, substituting this result into equation 3.64, it follows that:

$$Q_{xr} = K_{zr} \left\{\frac{x_r}{z_r}\right\}^2 b_r \frac{z_r^2}{x_r} = K_{zr}\, b_r\, x_r \tag{3.67}$$

or,

$$Q_{xr} = Q_{zr} = Q_r \tag{3.68}$$

Accretion

Accretion, R, is the rate at which a net quantity (percipitation and surface inflow minus evapotranspiration, runoff, etc.) of liquid is taken into the flow system at the phreatic surface. It is measured as a volume per unit horizontal area per unit time, that is:

$$R_r = \frac{Q_r}{b_r x_r} \tag{3.69}$$

From equations 3.64 or 3.65, it follows that:

$$R_r = \frac{K_{xr} z_r^2}{x_r^2} = K_{zr} \tag{3.70}$$

Volume

On occasion, volume, U, is of some importance. The volume scale follows directly from continuity, that is:

$$U_r = Q_r t_r \tag{3.71}$$

Substituting the values found from equations 3.65 and 3.24a for Q_r and t_r, respectively, the above equation becomes:

$$U_r = K_{zr}\, b_r\, x_r\, n_{er} \frac{z_r}{K_{zr}} = b_r\, n_{er}\, x_r\, z_r \tag{3.72}$$

As inferred earlier by this section's opening sentence, the volume scale is usually neglected; however, in the case of free surface water bodies, lakes, rivers, etc., if the volume exchange of liquid is of interest and has to be modeled, the volume scale requires an additional restriction. In the following analysis, the bar above the width dimension indicates the free water surface of a river, lake, ocean, or such.

In the portion of the model simulating the body of water, the spacing of the model is increased to maintain hydrostatic pressure distributions within the model. The narrower spacing of the model is, of course, a measure of the hydraulic conductivity of the aquifer. In the prototype, however, the width of the open water and the aquifer are equal and this leads to the following (Bear, 1960) for the model and prototype, respectively:

$$U_r = n_{er}\, b_r\, x_r\, z_r \tag{3.73a}$$

$$\bar{U}_r = \bar{n}_{er}\, \bar{b}_r\, x_r\, z_r \tag{3.73b}$$

The same volume ratio must be applicable to both the narrow and the enlarged interspace; therefore, $\bar{U}_r = U_r$. It follows that:

$$\bar{n}_{er}\, \bar{b}_r = n_{er}\, b_r \tag{3.74}$$

but,

$$\bar{n}_{er} = \frac{\bar{n}_{em}}{\bar{n}_{ep}} = 1 \tag{3.75}$$

so,

$$\bar{b}_r = n_{er}\, b_r \tag{3.76}$$

Note that for an anisotropic media, n_{em} does not necessarily equal one.

CHAPTER IV

SITE SELECTION AND PROTOTYPE GEOLOGY AND HYDROLOGY

Site Selection

The site selected for this study is the middle Gulf area of Florida. This region has a rapidly expanding population with a corresponding growth in water demand. The increased pumping to satisfy this demand also increases the likelihood of salt-water intrusion, and, in fact, a number of municipal supply wells in the coastal zone have been shut down in recent years due to chloride contamination.

One of the major water supply systems in this region is the Pinellas County Water System, and this study is centered around the Eldridge-Wilde well field of this system. The location of Eldridge-Wilde in relation to several of the population centers of this region is shown in Figure 4.1. It is about 8 miles east of the Gulf of Mexico and encompasses an area in the northeast corner of Pinellas County, at the intersection of the boundaries of Pinellas, Hillsborough and Pasco Counties.

In 1970 (Black, Crow and Eidsness, Inc., 1970), the waterworks facilities at Eldridge-Wilde included: sixty-one water wells, over 11 miles of raw-water collection piping, water treatment facilities consisting of aeration and chemical treatment, including chlorination and fluoridation, and high service pumping units.

All wells are open hole and penetrate the Floridan aquifer at depths from 140 to 809 feet below ground surface, averaging 354 feet. The design capacity of the field at the present time is 69 million gallons per day, although the maximum allowable pumpage has been set by the Southwest Florida Water Management District at 28 million gallons per day on the average with a maximum day of 44 million gallons per day.

In selecting the prototype location within the site area, two characteristics of the vertical Hele-Shaw analog must be considered. The first characteristic is that there can be no general flow normal to the parallel walls of the model. This means that the flow from one end of the model to the other is streamline flow. The second characteristic is that the ends of the model are finite.. Therefore, the prototype must be along a streamline in the flow domain and have boundary conditions which are "infinite" reservoirs or water divides.

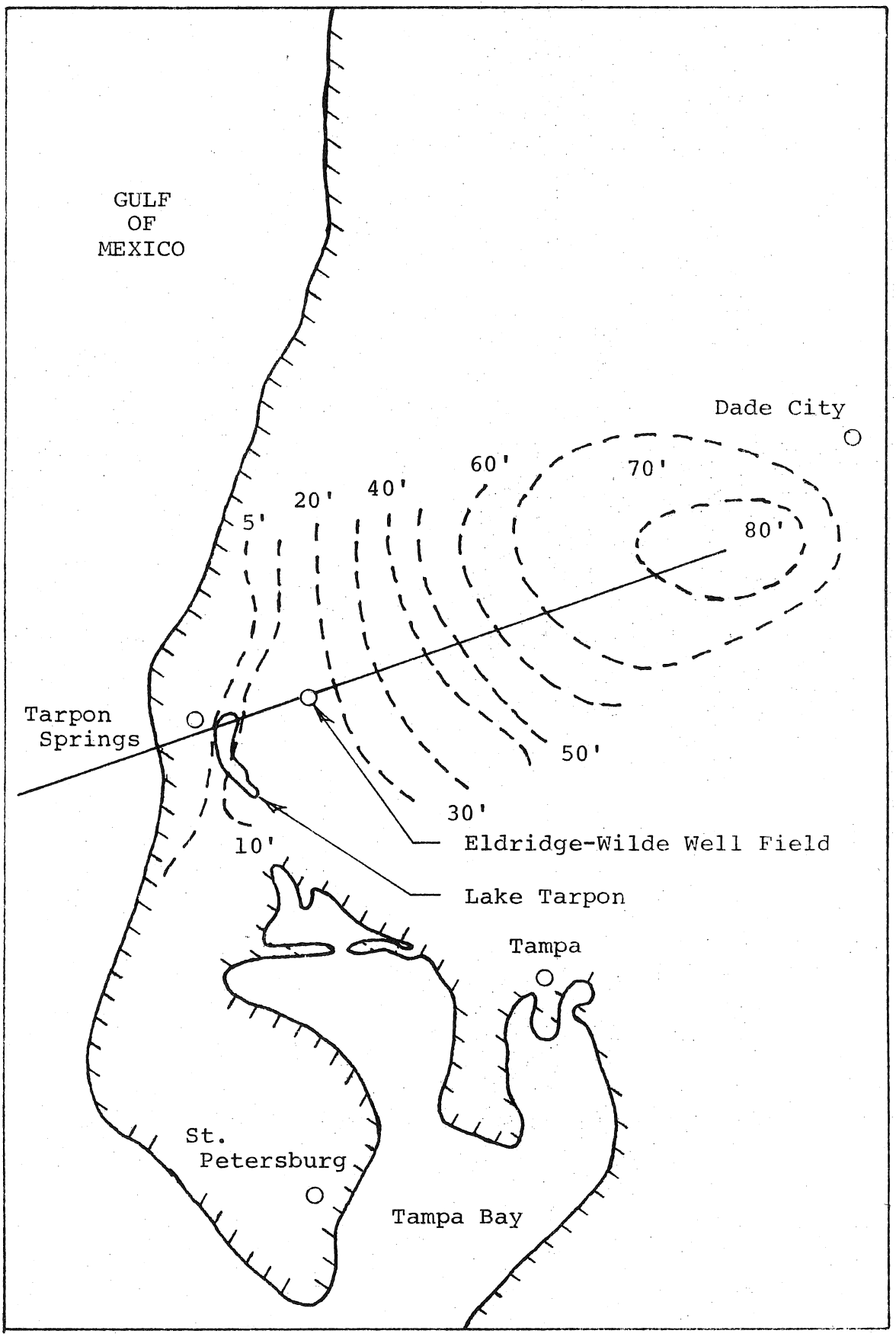

FIGURE 4.1
REGIONAL AREA OF PROTOTYPE

The prototype selected meets the above requirements and includes the point of interest, i.e., Eldridge-Wilde well field. The center line of the prototype is shown in Figure 4.1 as the unbroken line passing through Eldridge-Wilde in a southwest to northeast direction. The dotted contours in the figure define the potentiometric surface of the Floridan aquifer in feet above mean sea level as of May, 1971. They were obtained from a map publication entitled "Potentiometric Surface of Floridan Aquifer Southwest Florida Water Management District, May, 1971" prepared by the U. S. Geological Survey in cooperation with the Southwest Florida Water Management District and the Bureau of Geology, Florida Department of Natural Resources. Now, in a flow field, streamlines are perpendicular to potentiometric lines. As can be seen from the figure, the prototype orientation reasonably satisfies the streamline requirement. The prototype is terminated on the southwestern end at the 15 feet depth contour in the Gulf of Mexico, and it is assumed that this satisfies the infinite reservoir boundary condition. The northeastern terminus is located in the center of the 80 feet contour, southwest of Dade City. This location satisfies the water divide boundary condition. The area in the vicinity of the 80 feet contour is known as the Pasco High. The overall length of the prototype is 36 statute miles. The width of the prototype is taken to be 3.5 statute miles. This dimension is sufficient to include the cone of depression caused by pumping in Eldridge-Wilde well field, and is based on the results of a study by Mr. Evans (employing a numerical model) for Black, Crow and Eidsness, Inc. The land surface contours of the prototype are obtained from U. S. Geological Survey topographic maps. The bottom boundary of the prototype is taken to be the base of the Lake City Formation, with depths being determined from available well logs of wells in the prototype vicinity. The maximum depth from highest land surface to deepest point is 1340 feet.

Prototype Geology

Stewart (1968) identifies eight formations as being of interest in terms of water production in the prototype area. They are in descending order, the Undifferentiated Deposits, Tampa Limestone, Suwannee Limestone, Crystal River Formation, Williston Formation, Inglis Formation, Avon Park Limestone and Lake City Limestone. Underlying the Lake City Limestone is the Oldsmar Limestone which is not used as a source of water at present.

The Undifferentiated Deposits are interbedded sand, silt and clay of Post-Miocene age and range in thickness from zero near the Pasco High to 60 feet in the Eldridge-Wilde well field. The thickest deposits are in northeast

Pinellas County around the north end of Lake Tarpon where sand dunes, as much as 40 feet high, overlie alternating layers of clay, thin limestone beds and sand greater than 70 feet thick.

The Tampa Limestone is a hard, dense, sandy, white to light-tan or yellowish-tan fossiliferous limestone of Miocene age. This limestone is near the surface in the area of the Pasco High and about 80 feet below land surface at the Eldridge-Wilde well field. At Eldridge-Wilde, the thickness varies erractically from about 20 to 240 feet. The Tampa Limestone is a poor to fair producer of water.

The Suwannee Limestone is a soft to hard, nodular or granular, fossiliferous white to tan limestone of Oligocene age and is about 200 feet thick. The Suwannee and Tampa Limestones are the major water producers for wells in the area.

The Crystal River, Williston and Inglis Formations comprise the Ocala Group of late Eocene age. The Crystal River and Williston Formations are lithologically similar units of white to cream, porous, soft, coquinoid limestone and are generally poor producers of water. The Inglis Formation is a hard, cream to brown to gray fossiliferous limestone and is generally a good producer of water.

The Avon Park and Lake City Limestones are lithologically similar units of soft to hard, cream to brown, fossiliferous limestone with beds of dolomitic limestone and some gypsum. Both formations are good producers of poor quality water.

The Oldsmar Limestone is a fragmental dolomitic limestone with lenses of chert, thin shale beds and some gypsum.

In this report, two formations are considered, the Undifferentiated Deposits and the Floridan aquifer. The Floridan aquifer is considered to contain all formations from the Tampa to, and including, the Lake City Limestone.

The transmissivity of the Floridan aquifer ranges from about 165,000 to 550,000 gallons per day per foot, and the coefficient of storage ranges from about 0.0005 to 0.0015. The coefficient of leakage is approximately 0.0015 gallons per day per cubic foot.

Based on ground water discharge and water levels, the estimated recharge (leakance) to the Floridan aquifer was computed (Stewart, 1968) to be about 103 million gallons per day. Based on aquifer test data, the estimated recharge for a 250 square mile area was 90 million gallons per day.

The Undifferentiated Deposits act as a confining layer, and the Floridan aquifer is thus under artesian conditions.

Prototype Hydrology

The surface waters of the area consist of many lakes and few streams. Because of the flat topography, little water runs off into streams, and swampy wetlands are numerous. Most rainfall evaporates or is transpired by plants.

The Floridan aquifer is recharged through the Undifferentiated Deposits by surface and ground water derived from local rainfall. Many millions of gallons of water are also admitted to the aquifer by numerous sinkholes in the region. Water levels in the Floridan aquifer respond to rainfall since this is the recharge source. This response is not immediate, but usually fluctuates with the wet and dry seasons. Water levels in wells which are not directly affected by local pumping show yearly lows in the dry season, April and May, and yearly highs during the wet season, late summer or early fall, (Black, Crow and Eidsness, Inc., 1970).

The aquifer recharge has been estimated (Black, Crow and Eidsness, Inc., 1970) from available data and the use of the following formula:

$$\text{Aquifer Recharge} = P + SWI + GWI - ET - R - GWO$$

The basin area is 575 square miles, changes in storage are assumed zero, and evapotranspiration is assumed to be 75% of the precipitation. The applicable values are listed below in million gallons per day:

P	= Precipitation	=	+ 1492
SWI	= Surface Water Inflow	=	+ 0
GWI	= Ground Water Inflow	=	+ 0
ET	= Evapotranspiration	=	- 1119
R	= Runoff	=	- 218
GWO	= Ground Water Outflow	=	- 37
	Aquifer Recharge	=	118

This value is in reasonable agreement with previous reported values (Stewart, 1968).

CHAPTER V

DESIGN, CONSTRUCTION AND OPERATION OF MODEL

Design

Prototype

The selection of the prototype area was discussed in Chapter IV. Table 5.1 is a summary of the prototype characteristics. The *leaky layer* is synonymous with the *undifferentiated deposits*. The top and bottom of the Floridan aquifer were determined by straight-line extrapolation from available well logs.

The hydraulic data are within the reported range of values and are the result of a trial and error process to stay within the range and still produce a reasonable model.

Model

The purpose of the Hele-Shaw analog in this study is to model salt-water intrusion. Before discussing the model design, it seems appropriate at this point to provide some background about salt-water intrusion. Water, in general, whether it be surface water or ground water, is continually migrating towards the sea, where an equilibrium, or moving fresh-water/salt-water interface, is established. The two fluids are messible, but because of the difference in densities and the very low velocities, the interface is formed. Across the interface, the salinity varies from that of the fresh ground water to that of the ocean. The transition zone, as it is called, is due to hydrodynamic dispersion and, although it is anything but abrupt, it is usually assumed to be. The interface then is generally selected to occur at some measured electric conductivity or salt (chloride) concentration.

The earliest investigations of salt-water encroachment were made by Badon-Ghyben (1888) in Holland and Herzberg (1901) in Germany. Working independently, both investigated the equilibrium relationships between the shape and position of the fresh-water/salt-water interface. Figure 5.1 shows a coastal phreatic aquifer and the Ghyben-Herzberg interface model. Badon-Ghyben and Herzberg assumed static equilibrium and a hydrostatic pressure distribution in the fresh ground water and stationary saline ground water near the interface.

TABLE 5.1

PROTOTYPE PARAMETERS

Parameters	Floridan Aquifer	Leaky Layer
a. Geometric		
x_p (ft.)	190,080	190,080
z_p (ft.)	1,340	55
b_p (ft.)	18,480	18,480
b. Hydraulic		
T_{xp} (gpd/ft.)	225,000	-
T_{zp} (gpd/ft.)	184,426	-
$\frac{K_{xp}}{K_{zp}}$	1.218	0
Leakance (gpd/ft.^{3})	-	0.0015
K_{zp} (gpd/ft.^{2})	161.4	0.09
K_{xp} (gpd/ft.^{2})	196.7	0
S	0.00158	-
ν_p @ 77° F (ft.^{2}/sec.)	0.965 (10^{-5})	0.965 (10^{-5})
g_p = 32.2 ft./sec.^{2}		

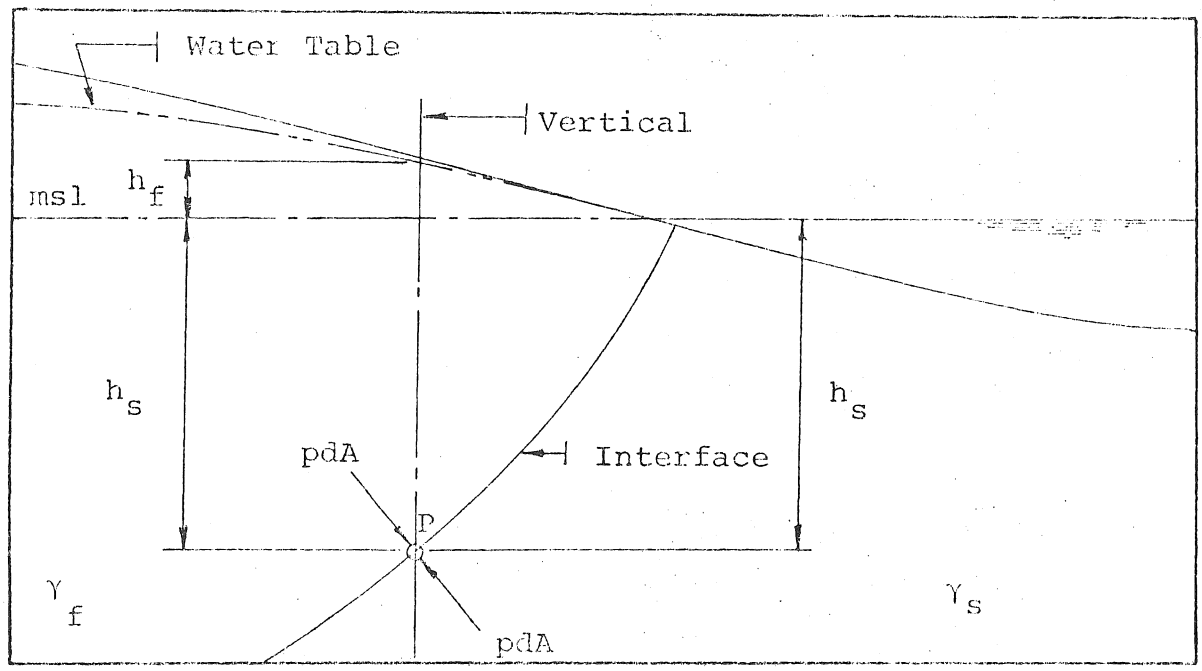

FIGURE 5.1

GHYBEN-HERZBERG INTERFACE MODEL

Considering a point P on the interface, and choosing mean sea level as the datum, the pressure at point P is:

$$P_p = h_s \gamma_s \tag{5.1}$$

where:

h_s = vertical distance from mean sea level to point P.
γ_s = unit weight of sea water.

This pressure may, also, be expressed by:

$$P_p = (h_f + h_s)\ \gamma_f \tag{5.2}$$

in which h_f equals the vertical distance from mean sea level to the phreatic line at the location of P and γ_f equals the unit weight of fresh-water. Equating the preceding two equations:

$$h_s \gamma_s = h_f \gamma_f + h_s \gamma_f \tag{5.3}$$

and, rearranging,

$$h_s \gamma_s - h_s \gamma_f = h_f \gamma_f \tag{5.4}$$

Solving for h_s:

$$h_s = \frac{\gamma_f}{\gamma_s - \gamma_f} h_f \tag{5.5}$$

Introducing $\gamma = \rho g$, where ρ is the density, factoring and canceling out the gravity term, the Ghyben-Herzberg relation is found:

$$h_s = \frac{\rho_f}{\rho_s - \rho_f} h_f \tag{5.6}$$

for a salt-water density of 1.025 lb sec.^{2}/ft.^{4} and a fresh-water density of 1.000 lb sec.^{2}/ft.^{4}, the quantity $\rho_f/(\rho_s - \rho_f) = 40$. The implications of equation 5.6 are rather dramatic. For instance, for every foot of fresh-water above the datum, there is 40 feet of fresh-water below the datum. More importantly however, consider the

effects of lowering the phreatic surface. For every one foot drop of the water table, the interface raises 40 feet. It must be remembered that the above analysis assumes static conditions. This, in fact, is not always the case. The position of the interface is a function of dynamic conditions rather than static. Even so, in cases where flow is quasi-horizontal, i.e., the equipotential lines are nearly vertical, equation 5.6 is valid.

Many investigators have incorporated dynamic forces into the analysis of the stationary interface. Hubbert (1940) was able to ascertain a more accurate determination of the shape of the interface near the coast line. He assumed that at the interface the tangential velocity was zero in the salt-water, but increases with horizontal distance in the fresh-water as the coast line is approached. This then is the cause for the interface to tilt upwards as the sea is approached and the greater depths found than those estimated by the Ghyben-Herzberg relationship. Hubbert showed that the Ghyben-Herzberg equation holds between points on the water table and the interface along an equipotential line, rather than along a vertical plane.

R. E. Glover (1959) modeled an infinitely deep coastal aquifer by assuming no flow in the salt-water region, a horizontal water table and a horizontal seepage face located seaward of the coast line. He found an exact solution for the shape of the wedge, giving the following relationship:

$$z^2 = \frac{2qx}{K\{\frac{\rho_s-\rho_f}{\rho_f}\}} + \frac{q^2}{K^2\{\frac{\rho_s-\rho_f}{\rho_f}\}^2} \qquad (5.7)$$

where x and z are the horizontal and vertical directions, respectively, q is the seepage rate per unit width and K is the hydraulic conductivity. De Wiest (1962) using complex variables and a velocity potential of $\Phi = K_x\phi \cdot (\rho_s-\rho_f)/\rho_f$ derived the same equation.

Bear and Dagan (1964), using the Dupuit assumptions and the Ghyben-Herzberg equation, developed the approximate shape of the interface for a shallow aquifer of constant depth.

All of the above investigated the equilibrium position of the salt-water/fresh-water interface.

If there is a change in the fresh-water flow regime, a transition period is caused during which the interface moves to a new point of equilibrium. The non-linear boundary conditions along the interface make the solution for the shape and position of the transient interface all but impossible except for the simpliest geometries.

Bear and Dagan (1964b), as well as other investigators, have used the Dupuit assumptions to approximate the rate of movement of an interface in a confined aquifer. Following Polubarinova-Kochina's (1962) suggestion, they assumed quasi-steady flow and were able to approximate the interface shape and position for both a receding motion and landward motion of the interface.

Characteristically, the solutions obtained by investigators to date have all had simple geometries and involved simplifying assumptions, some of which have had little resemblance to actual conditions. Therein lies the advantages of a Hele-Shaw analog, complex geometries and boundary conditions can be modeled with relative ease.

In order to satisfy additional similitude requirements for the flow of two liquids with an abrupt interface, as in this study, and to provide a suitable time ratio, two liquid silicone fluids were chosen to be used in the model. Dow Corning Corporation Series 200 silicone fluid was used to model fresh-water. Series 510 silicone fluid from the same company was used to simulate salt-water. The 200 Series fluid and the 510 Series fluid have densities of 0.977 gm/cm^3 and 1.00 gm/cm^3, respectively, at 25° C. Both fluids have absolute viscosities of 500 centistokes at 25° C. Dow Corning 200 fluid is a clear dimethyl siloxane which is characterized by oxidation resistance, a relatively flat viscosity-temperature slope and low vapor pressure. Dow Corning 510 fluid is a clear phenylmethyl polysiloxane which also has a relatively flat viscosity-temperature slope. In order to locate and follow the interface movement, the denser fluid was dyed blue and the lighter fluid dyed orange.

The dimensions of the model were selected so that a unit of reasonable size would be produced. These dimensions are 11.75 feet long, 0.5 inch wide inside and 2 feet deep. The parameters x_r, z_r, and b_r are therefore set, and the result is a distorted model. This distortion requires the use of a slatted inner zone as discussed in Chapter III. Tables 5.2 and 5.3 list the applicable parameters.

The following analysis is shown for the design of the model Floridan aquifer, leaky layer and storage coefficient:

a) Slatted Anisotropic Zone for the Floridan Aquifer.

1) Compute k_{xm}/k_{zm} from Eq. 3.22

$$\left\{\frac{x_r}{z_r}\right\}^2 = \frac{K_{xr}}{K_{zr}} \qquad (3.22)$$

Noting that $k = K \frac{\nu}{g}$ (5.8)

TABLE 5.2

MODEL PARAMETERS

Parameters	Floridan Aquifer	Leaky Layer
a. Geometric		
x_m (ft.)	11.75	11.75
z_m (ft.)	2.0	0.082
b_m (ft.)	0.0417	0.0417
α	16.50	.25
λ	0.8097	0.3846
b (in.)	0.030	0.500
L (in.)	1.235	1.235
ξ	0.6905	0.8349
αb (in.)	0.495	0.125
λL (in.)	1.00	0.475
$(1 - \lambda)L$ (in.)	0.235	0.760
b. Hydraulic		
k_{xm} (in.^{2})	3.94×10^{-4}	0
k_{zm} (in.^{2})	.1884	1.05×10^{-4}
k_{xm}/k_{zm}	.00209	0
S_{om} (ft.$^{-1}$)	0.0369	-
ν_m @ 77° F (ft.^{2}/sec.)	5.382×10^{-3}	5.382×10^{-3}
$g_m = 32.2$ ft./sec.^{2}		

TABLE 5.3

SIMILARITY RATIOS

Parameters	Floridan Aquifer	Leaky Layer
a. Geometric		
x_r	6.182×10^{-5}	6.182×10^{-5}
z_r	1.493×10^{-3}	1.493×10^{-3}
b_r	2.255×10^{-6}	2.255×10^{-6}
b. Hydraulic		
k_{xr}	3×10^{4}	-
k_{zr}	1.748×10^{7}	1.748×10^{7}
k_{zr}/k_{xr}	582.8	-
S_{or}	2.677×10^{4}	-
ν_r @ 77° F	557.7	557.7
R_r	3.136×10^{4}	3.136×10^{4}
Q_r	4.372×10^{-6}	4.372×10^{-6}
t_r	1.903×10^{-6}	1.903×10^{-6}
g_r	1	1

Then (3.22) becomes,

$$\left\{\frac{x_r}{z_r}\right\}^2 = \frac{k_{xm}}{k_{xp}} \cdot \frac{k_{zp}}{k_{zm}} \qquad (5.9)$$

and finally,

$$\frac{k_{xm}}{k_{zm}} = \frac{k_{xp}}{k_{zp}} \left\{\frac{x_r}{z_r}\right\}^2 = (1.22)\left\{\frac{6.182 \times 10^{-5}}{1.493 \times 10^{-3}}\right\}^2 = 0.00209$$

This is the value which the slatted zone must produce.

2) Select dimensions for the slatted zone as shown in Figure 3.2, as follows:

i) hold $\alpha b \simeq 0.5$ inch
ii) select b
iii) find α
iv) select $(1 - \lambda)L$
v) select λL
vi) find L
vii) find λ

3) Compute $k_{xm} = \frac{b^2}{12} \frac{1}{(1 - \lambda)}$ (3.34)

4) Compute $k_{zm} = \frac{b^2}{12} (\alpha^3 \lambda \xi + 1 - \lambda)$ (3.48)

5) Compute k_{xm}/k_{zm} and compare to the results of step (1).

6) Repeat the process until the result of step (5) equals the result of step (1).

b) Slotted Leaky Layer. Refer to Figure 3.4 for this section.

$$k_{xlm} = 0 \qquad (5.10)$$

$$k_{zlm} = \frac{b^2}{12} \alpha^3 \xi \lambda \qquad (3.54)$$

Also, continuity of flow between the leaky layer and the Floridan aquifer requires that:

$$Q_{lr} = Q_{fr} \qquad (5.11)$$

Also,

$$Q_r = Q_{zr} = Q_{xr} = K_{zr} b_r x_r \qquad (3.67) \text{ \& } (3.68)$$

Therefore,

$$K_{zlr} b_r x_r = K_{zfr} b_r x_r \qquad (5.12)$$

so,

$$K_{zlr} = K_{zfr} \tag{5.13}$$

or,

$$k_{zlr} = k_{zfr} \tag{5.14}$$

Therefore,

$$k_{zlm} = k_{zlp}\, k_{zfr} \tag{5.15}$$

Now rewrite Eq. 3.54 as,

$$\alpha^3 \xi \lambda = k_{zlm} \frac{12}{b^2}$$

1) set b = 0.5 inch

2) $\alpha^3 \xi \lambda$ = constant, since b is set and k_{zlm} can be computed from previous information.

3) select αb and find α

4) select λL & L and find λ

5) compute ξ

6) compute $\alpha^3 \xi \lambda$

7) compare the result of step (6) to the result of step (2).

8) repeat the process until the result of step (6) equals the result of step (2).

9) make sure the physical size of this layer is compatible to the slatted layer, especially in terms of slot spacing, i.e., blockage.

c) Storage Coefficient Manifolds. Refer to Figure 3.5 for this section.

1) take average storage coefficient and average depth in prototype to compute S_{op}.

2) select convenient time ratios, in this case 1 minute = 1 year, and compute S_{or} from Eq. 3.59.

3) compute S_{om}

4) Eq. 3.60 is now used to compute A_m for various l_m's with z_m averaged over l_m.

In this case the model was apportioned into five zones with one manifold per zone.

Construction

Because the Hele-Shaw analog is capable of modeling complex geometries and boundary conditions, it is desirable that it be as adaptable to as many different prototype geometries and hydraulic parameters as possible. This would facilitate model construction and investigations of many different areas in the state of Florida where salt-water intrusion is, or in the future might be, a problem. A reduction in cost of investigation would also be achieved if many of the parts were reusable.

A list of general specifications would then be as follows:

1) The Hele-Shaw model should be housed in a frame in which it can be easily installed and removed.
2) The front and back plates with interior model parts should not be permanently sealed together.
3) The front and back plates should be as adaptable as possible to different situations.
4) The model should have as few opaque parts as possible.
5) The model should be mobile.

Frame

As shown in Figure 5.2, the frame is composed of two assemblies; the cradle and the cradle dolly. The function of the cradle is to support and orient the Plexiglas plates. It also contains the inflatable neoprene hose which seals the plates. It is fabricated of 2-1/2" x 2" x 3/8" steel angles which are welded into a channel 2-1/2" high by 4" wide. The channel has the shape of an elongated rectangular "U" which is 32-1/2" high and 147" long.

The function of the cradle dolly is to support the the cradle and provide mobility. The cradle dolly is constructed of 3-1/2" x 3-1/2" x 1/4" steel tubing. The length of the center tube is 14 feet, the short cross-pieces at the ends are 2 feet long. The cradle load is transmitted to the cradle dolly through two stub shafts and pillow blocks which are mounted on pedestals at each end of the center tube. The center line of the stub shafts is aligned on the cradle so that the cradle may be easily rotated as shown in Figure 5.3. This rotational ability allows easy insertion or removal of the model into or out of the cradle. It also allows a convenient orientation to be selected for working on the model.

The height of the stub shaft center line from the floor is 37". When the cradle is rotated into a horizontal position, its internal supports correspond to the height of the table upon which the model is built and assembled. This allows the model to be slid from the table and into

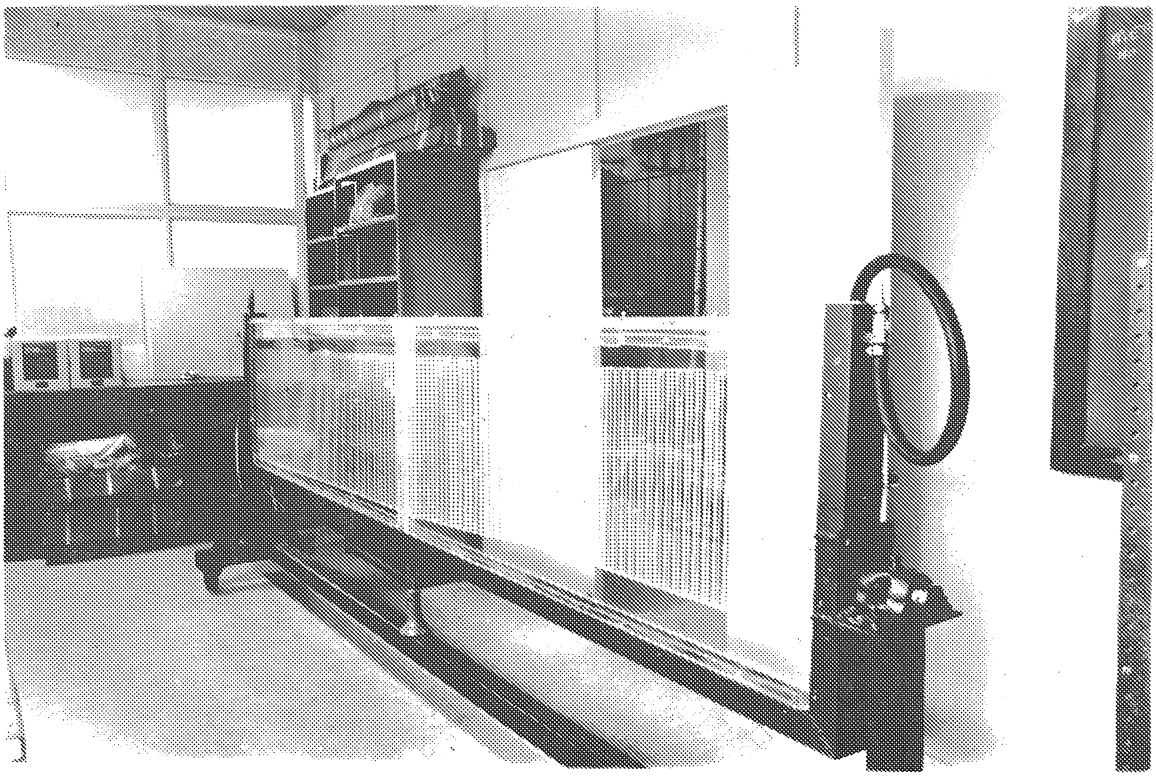

FIGURE 5.2
CRADLE AND CRADLE DOLLY

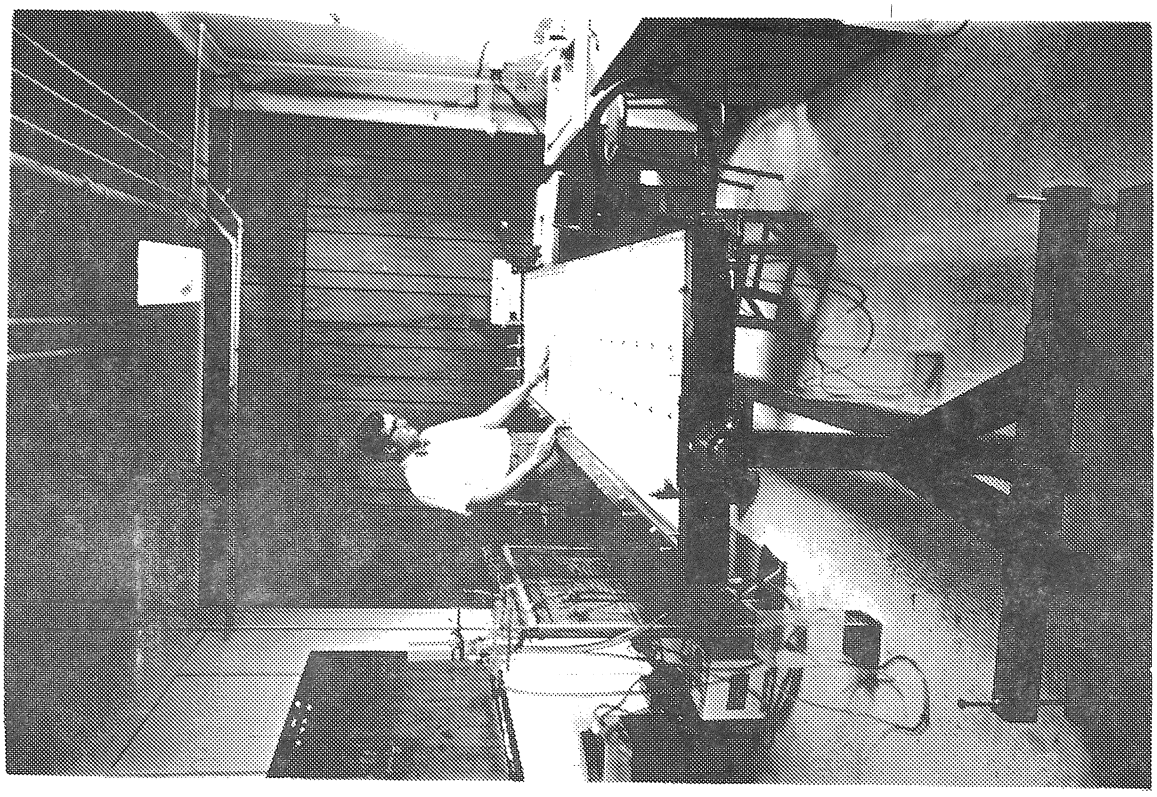

FIGURE 5.3
CRADLE ROTATION

the cradle. The cradle is then rotated into the vertical position and the whole assembly rolled into the laboratory for testing. Figure 5.4 shows the frame and model in a completed set-up.

Figure 5.5 shows the air hose and valve arrangement for pressurizing the hose seal around the model.

Figure 5.6 shows the stub shaft and pillow block mounting arrangement. Each pillow block has a jam screw which is tightened against the stub shaft to hold the designed orientation of the cradle. Spreader arms are added to the cross member at the bottom of the cradle dolly to provide stability, anchoring and leveling capabilities. The spreader arms increase the cross member length to 48".

Figure 5.7 shows the back-up pressurizing system consisting of SCUBA bottle, regulator and air hose.

Figure 5.8 shows a typical cross-section of the internal support and sealing system. The Plexiglas plates are supported on pairs of angle brackets and fastened into the cradle with cap screws and bolts. There are nine pairs of angles in the bottom of the cradle and two pairs in each end. The sides of the cradle are drilled slightly oversize to permit adjustment in the angle brackets and Plexiglas plates. The neoprene sealing hose is 1" O.D. with 1/8" walls. It is contained in an aluminum channel which provides lateral support and proper alignment with the Plexiglas plates. A pressure of 25 psig was found sufficient to swell the hose against the inner edges of the plates and provide positive sealing. Figure 5.9 shows a portion of the front plate of the model with support angles and bolts located in the cradle channel.

Plexiglas Plates and Manifolds

The front and back plates of the model were fabricated from 5' x 6' x 1/2" sheets of G grade Plexiglas. The sheets were sawn in half to obtain two pieces 2-1/2' x 6' x 1/2". These pieces were then glued together to form a single plate 2-1/2' x 12' x 1/2". The bottom corners of each such plate were cut to a 4" radius to accomodate the sealing hose. Figure 5.10 shows, from left to right, the back plate with internal strips and the front plate. They are on the construction table mentioned previously. The plates are reinforced around their edges with a Plexiglas strip and a plate over the center butt joint.

Figure 5.11 and Figure 5.12 show the detail of the model leaky layer and Floridan aquifer. The 0.030" gap in the Floridan aquifer is maintained by seventy-nine stainless steel tabs which are glued to the strips at regular intervals. In Figure 5.11, (turn the page sideways), the base of the aquifer is shown as the tapered

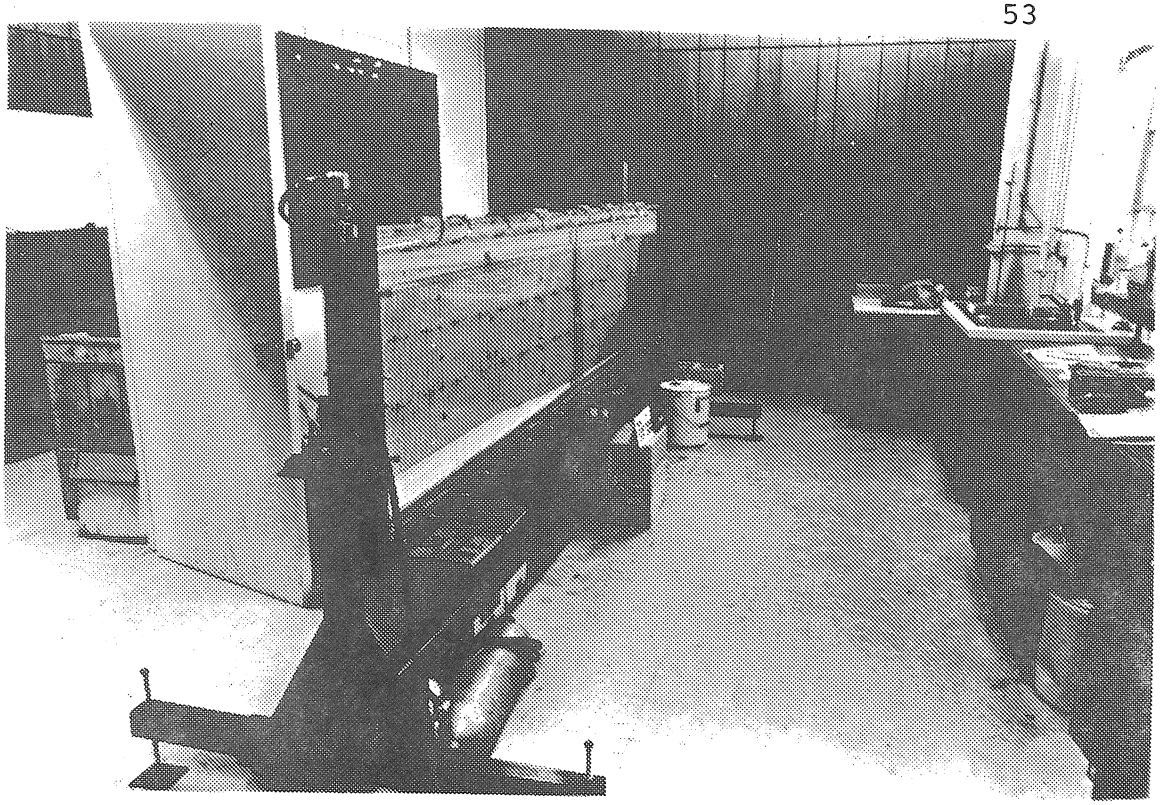

FIGURE 5.4
FRAME AND MODEL SET-UP

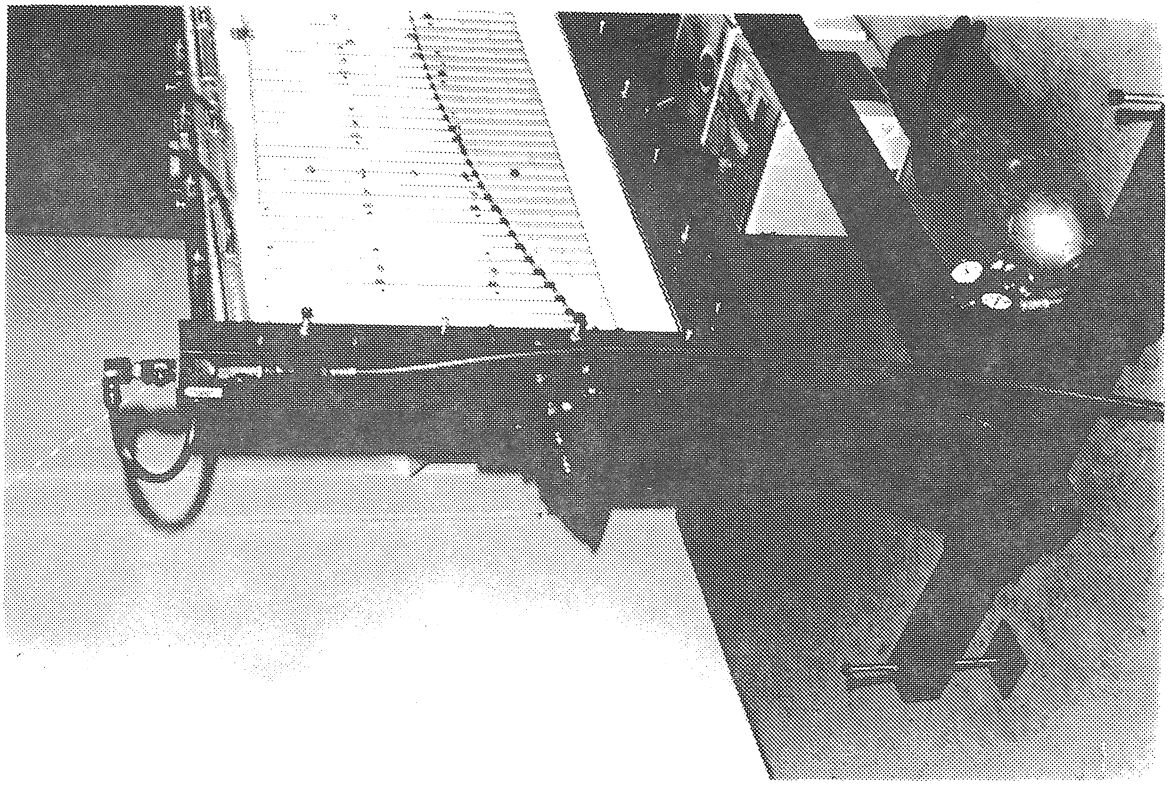

FIGURE 5.5
AIR HOSE AND VALVE ARRANGEMENT

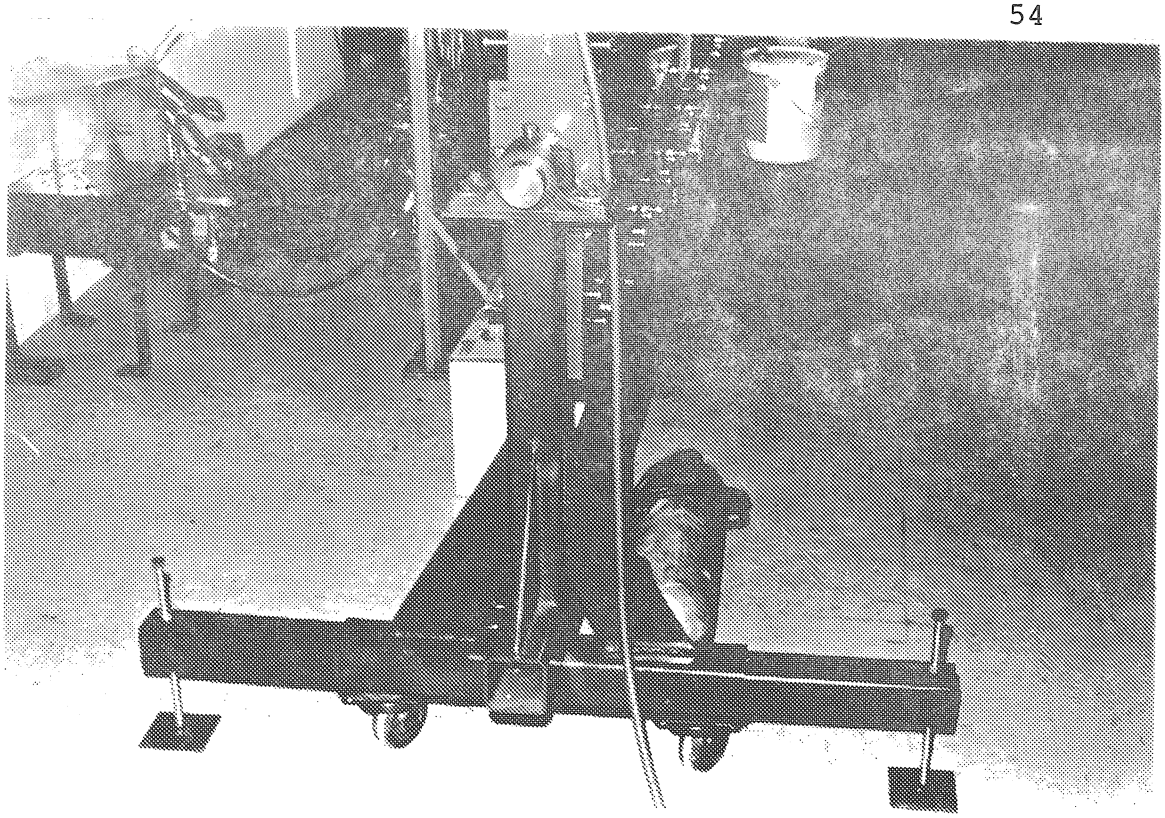

FIGURE 5.6
STUB SHAFT AND PILLOW BLOCK ARRANGEMENT

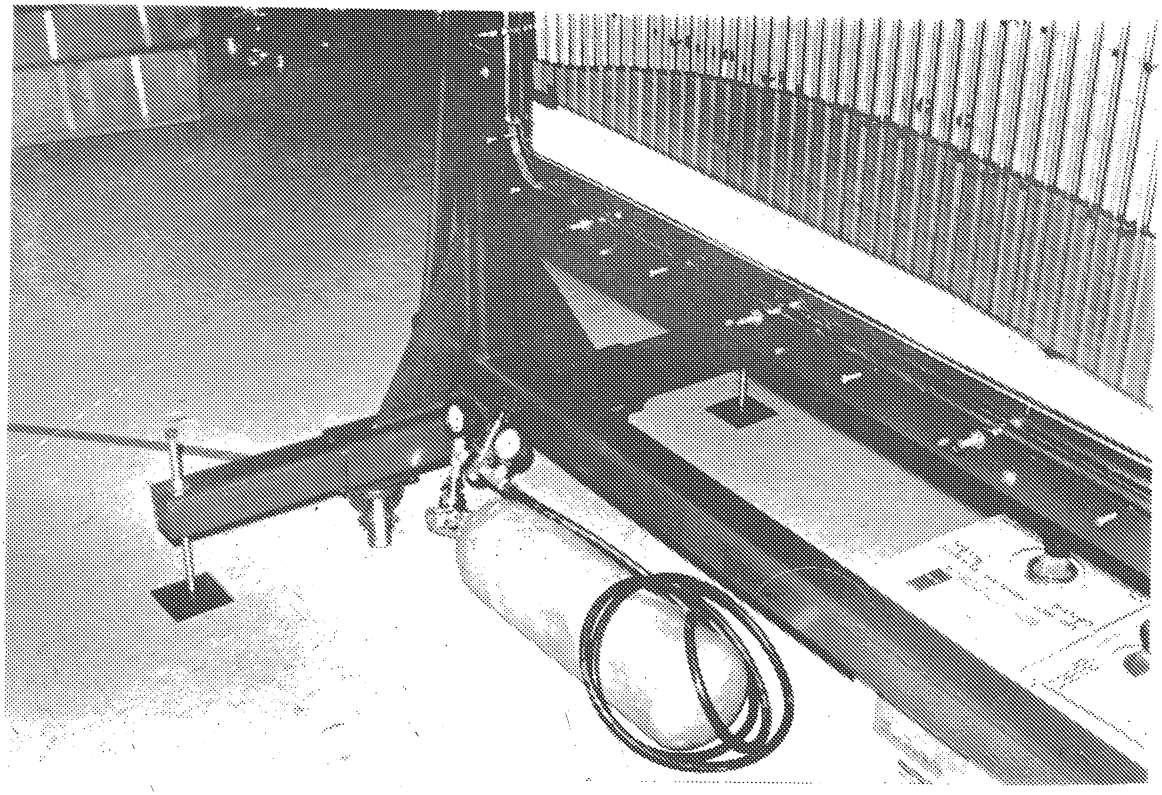

FIGURE 5.7
BACK-UP AIR SUPPLY

FIGURE 5.8
INTERNAL SUPPORT AND SEALING SYSTEM

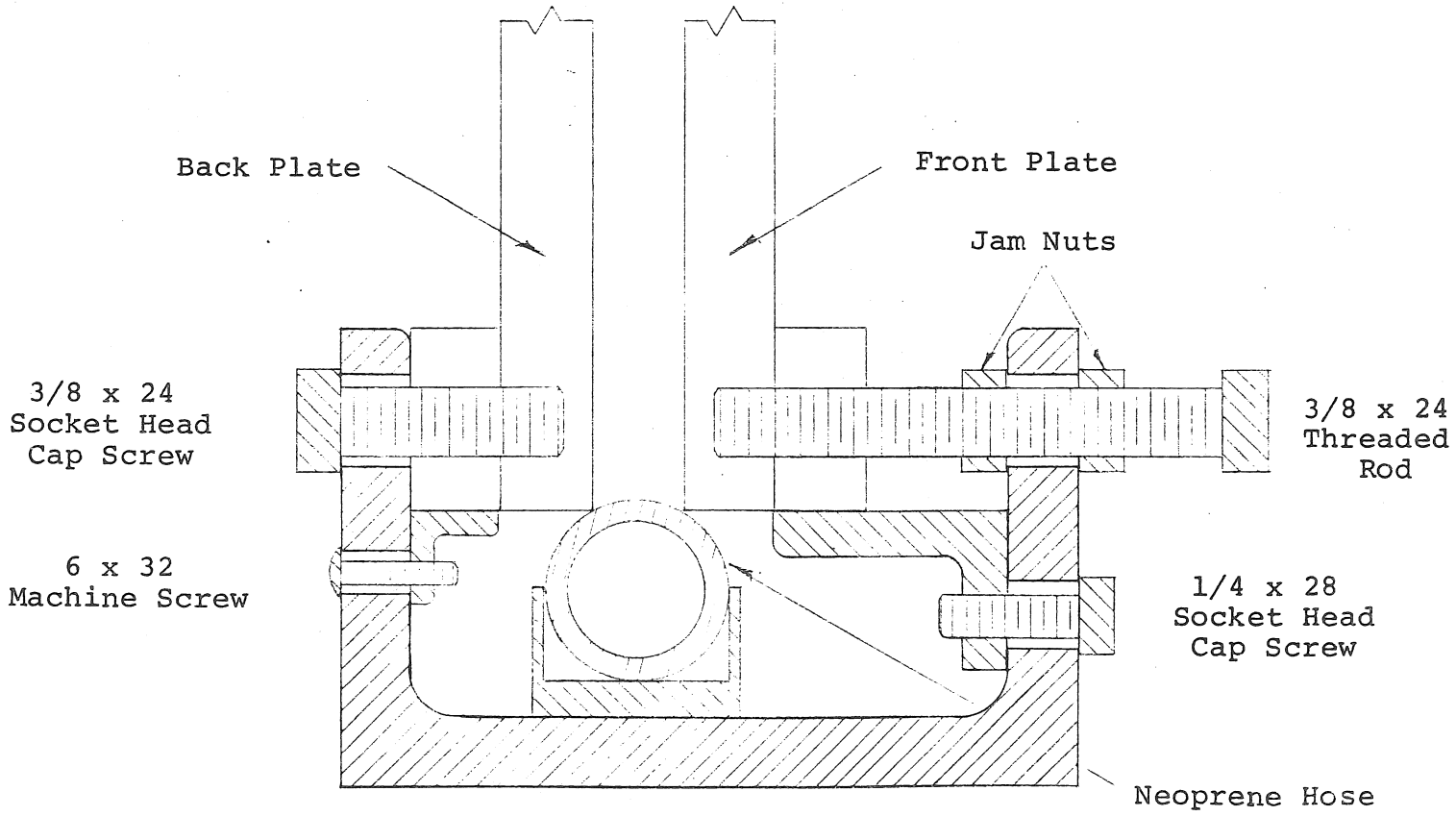

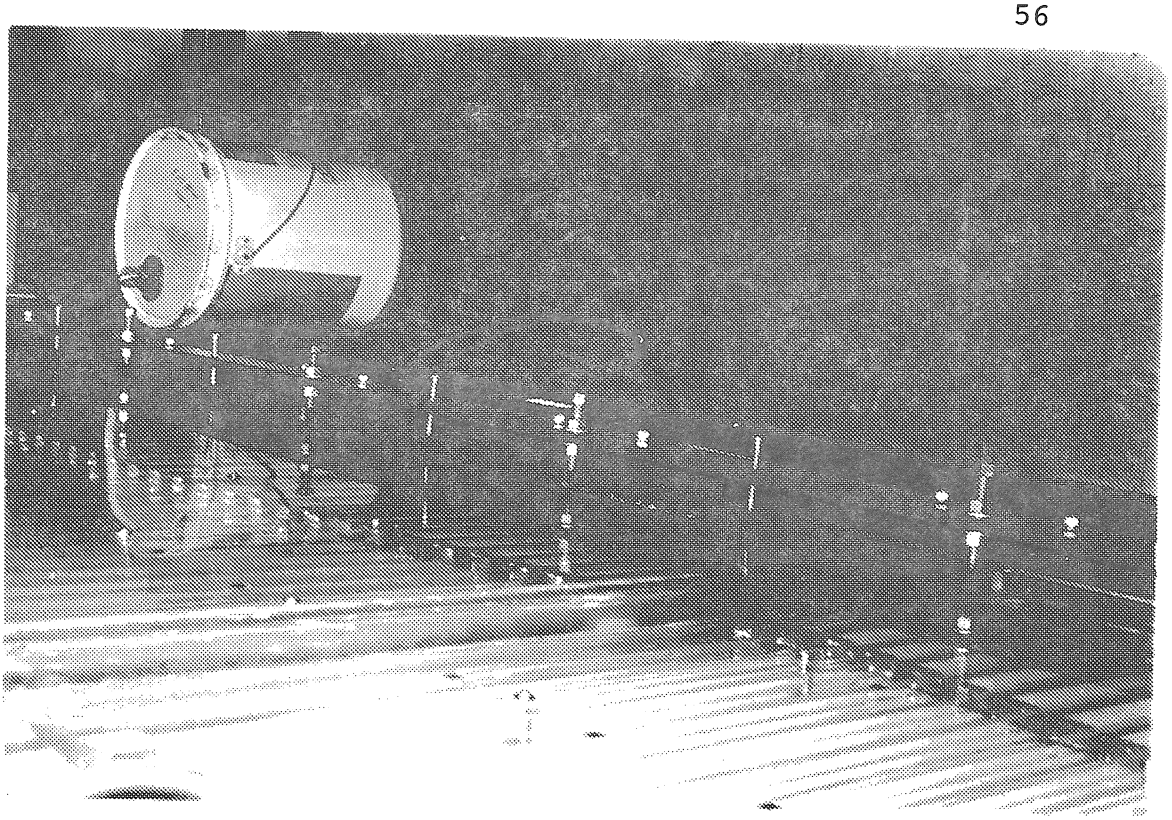

FIGURE 5.9
MODEL MOUNTING SYSTEM

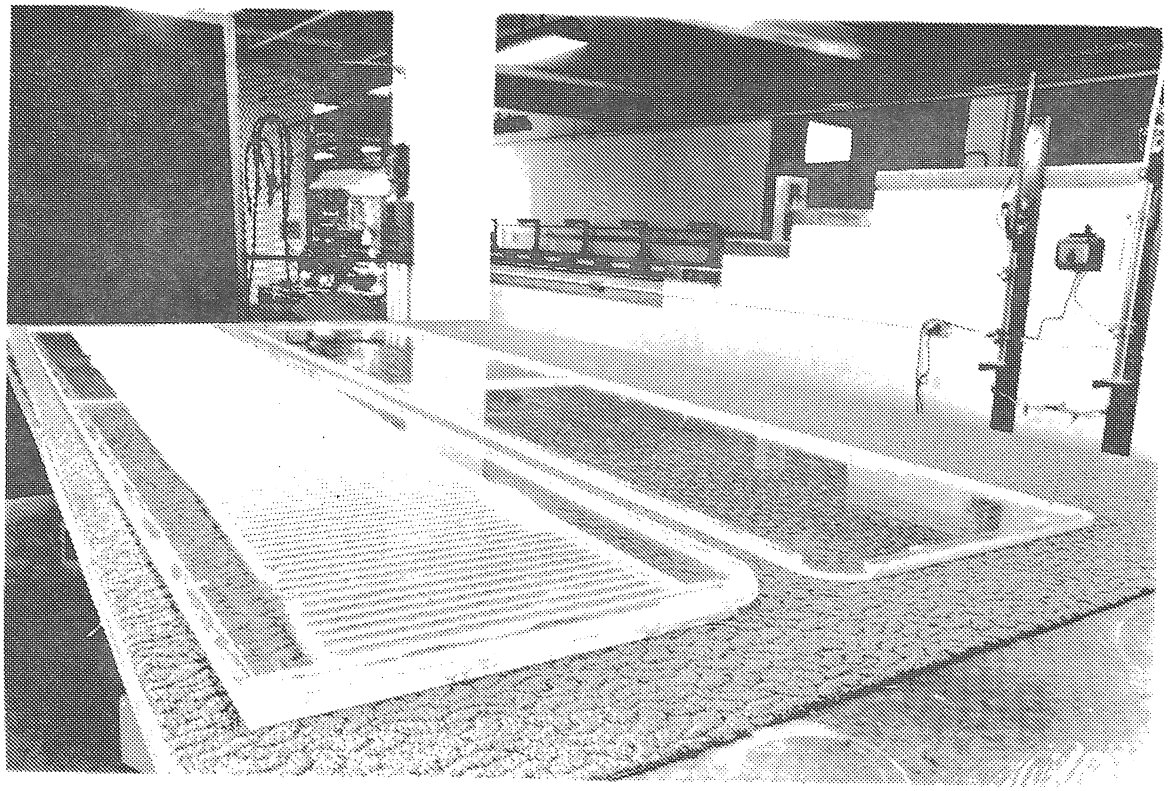

FIGURE 5.10
MODEL BACK AND FRONT PLATES

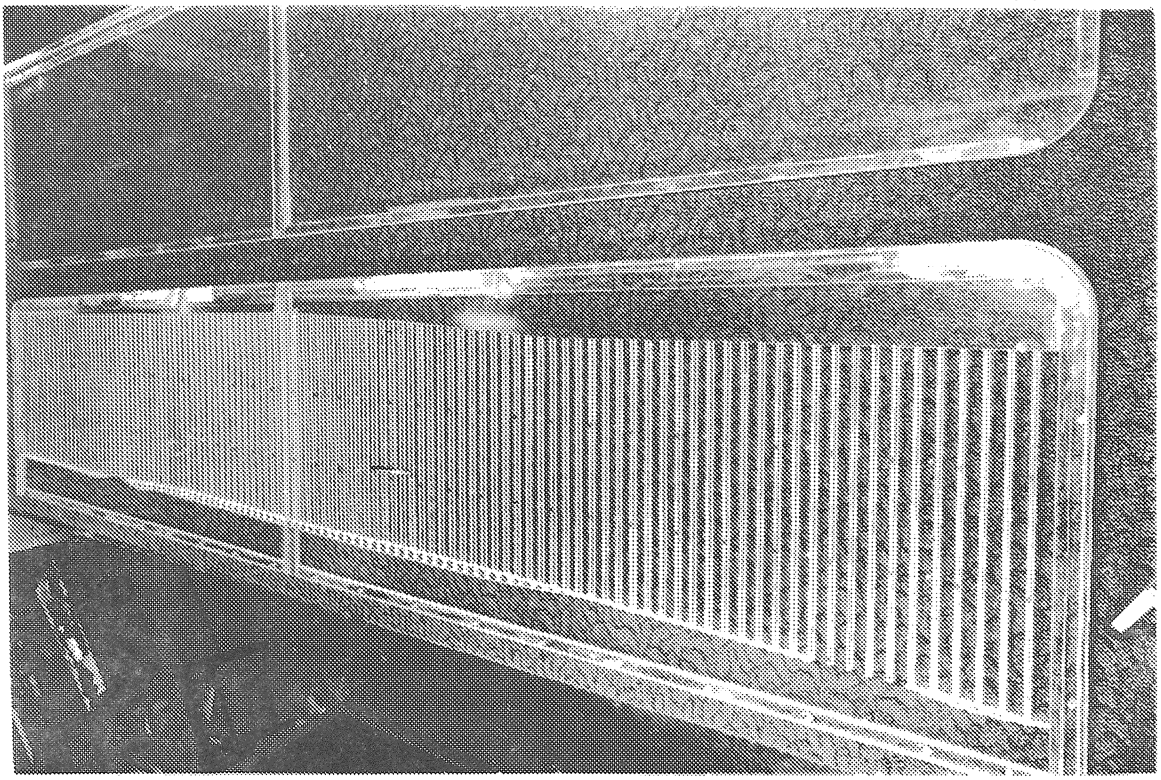

FIGURE 5.11
MODEL BACK PLATE, DETAIL

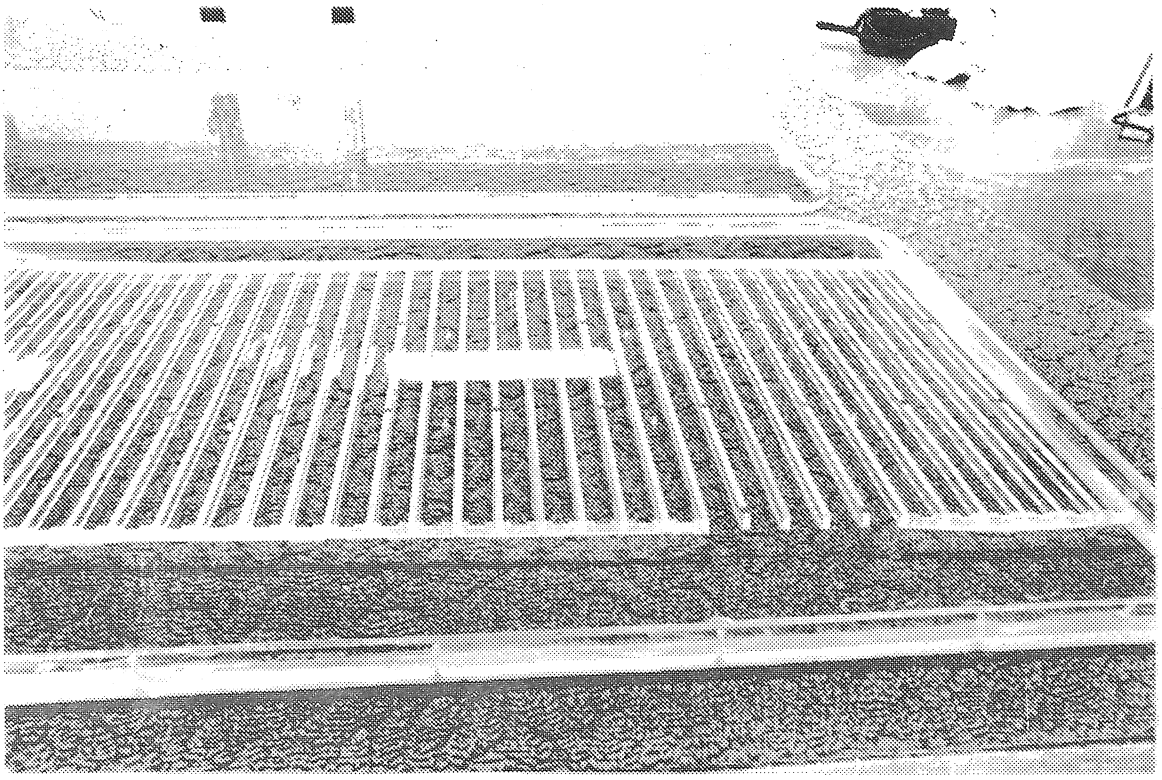

FIGURE 5.12
MODEL BACK PLATE, DETAIL

Plexiglas wedge at the right, or bottom, side of the back plate. The leaky layer is the narrow strip at the left, or top, side of the back plate. The plate from the bottom of the figure to the top (long axis) represents the prototype from the Pasco High to the Gulf of Mexico. Figure 5.12 is a closer look at the interior geometry.

Figures 5.13, 5.15 and 5.16 show some of the accretion manifolds which are mounted near the top of the front plate. There are ten individual manifolds which are available together or in any order to supply recharge to the aquifer. These manifolds are built from half sections of a 1-1/4" O.D. Plexiglas tube (1/8" wall). They are mounted at a slight angle to the horizontal and provided with an air bleed at the high end. Each manifold is fed from a flow meter through a single 1/4" I.D. tube. The fluid is delivered to the model through 3/64" holes drilled through the front plate. There are twenty holes per manifold, and the fluid runs down the inside surface of the front plate.

Figure 5.18 shows the five storage coefficient manifolds mounted on the back plate of the model. Figure 5.20 shows a detailed view of one manifold. The manifolds are constructed of 1/4" Plexiglas and have a square cross-section. They are supported from the top of the back plate and are provided with short tube connections to the model, as well as a drain valve.

Figure 5.14 shows the front and back plate being fastened together. Besides the supporting bolts located in the cradle, there are thirty-six #5 x 40 machine screws regularly spaced throughout the model to pull it together. These screws are sealed with O-rings. There are also bolts and spacers along the top of the model. There are three valves in the base of the aquifer for drainage. A grid system, a portion of which can be seen in Figure 5.16, is fastened to the back plate and denotes 1 mile increments horizontally and 100 feet increments vertically.

Figure 5.17 is a flow schematic for the fluid supply network of the model. There are two main systems: the salt-water system and the fresh-water system. The fresh-water system is composed of three subsystems: the accretion system, the well system and the flow meter system.

Figure 5.18 is an over-view of the connections between the model and the fluid supply system.

Salt-Water System

Figure 5.19 shows the salt-water reservoir and support stand. Underneath the reservoir is a small gear pump driven by a variable speed, reversible, motor-transmission set. The gear pump transfers fluid from the reservoir into a constant head tank. Figure 5.20 shows

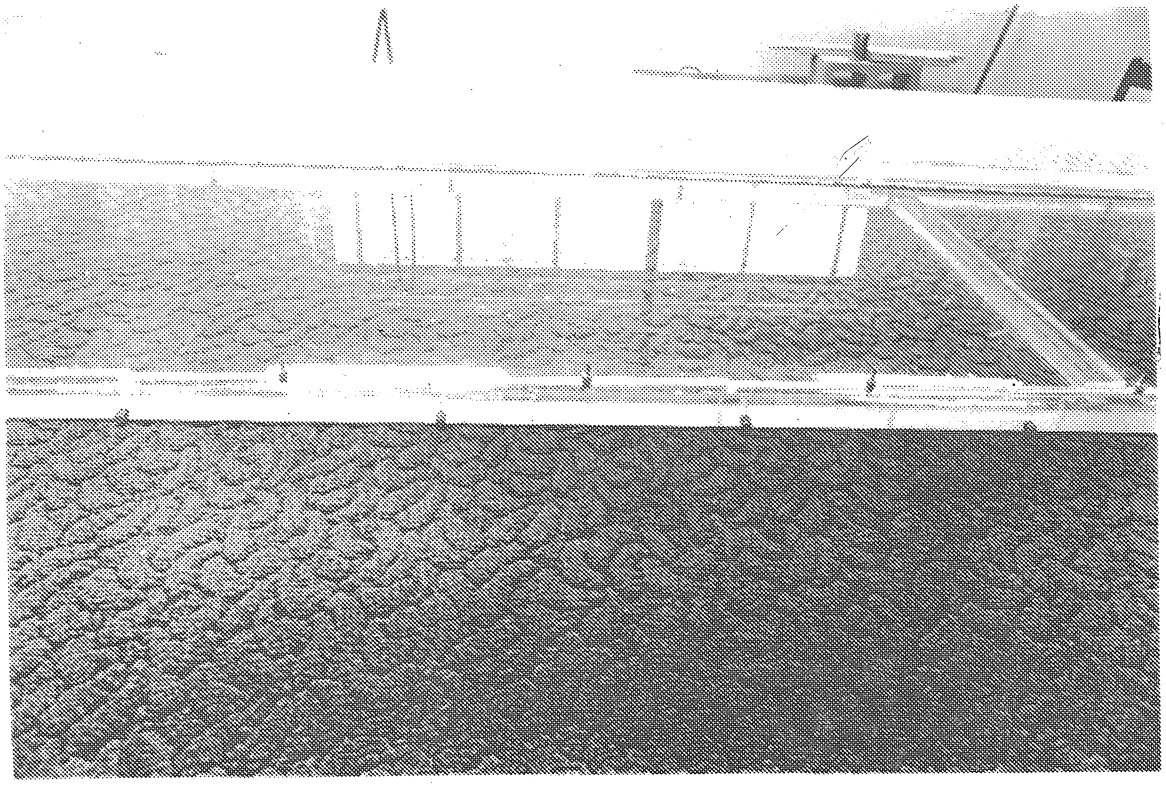

FIGURE 5.13
FRONT PLATE WITH ACCRETION MANIFOLDS

FIGURE 5.14
BACK AND FRONT PLATE CLAMP UP

FIGURE 5.15
ACCRETION MANIFOLDS

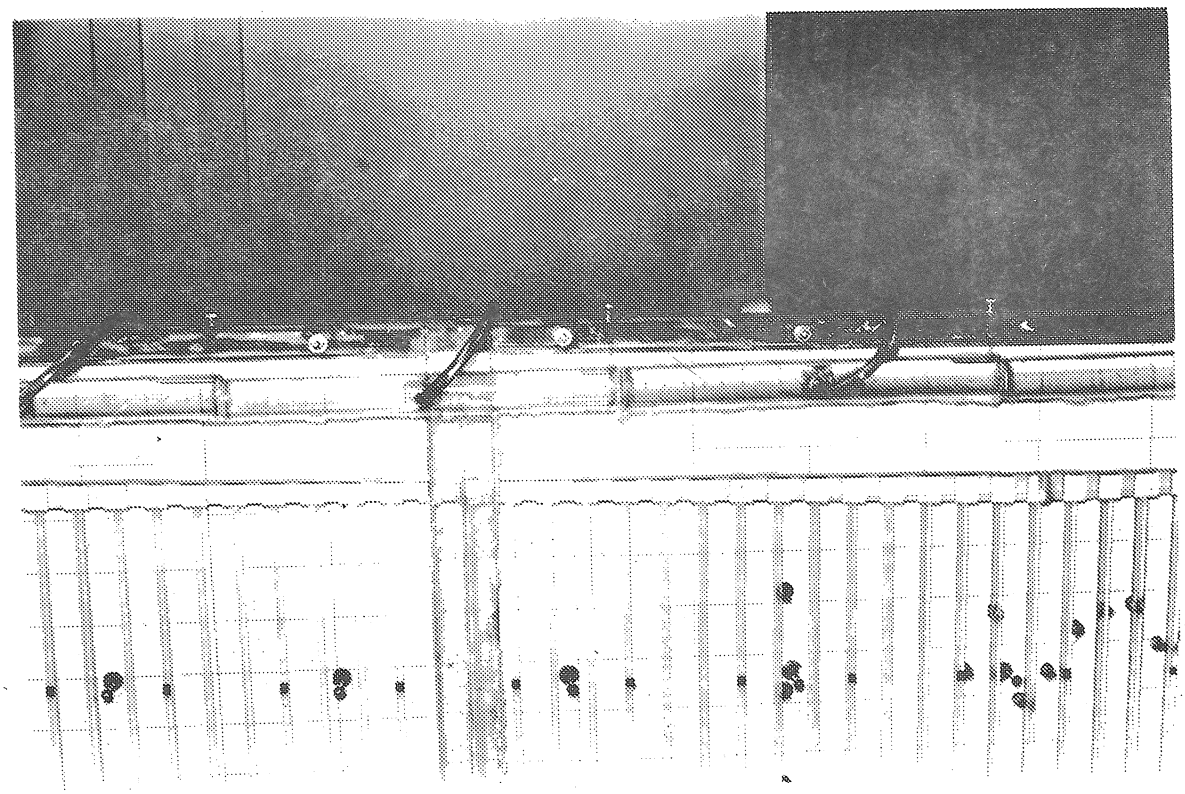

FIGURE 5.16
ACCRETION MANIFOLDS, DETAIL

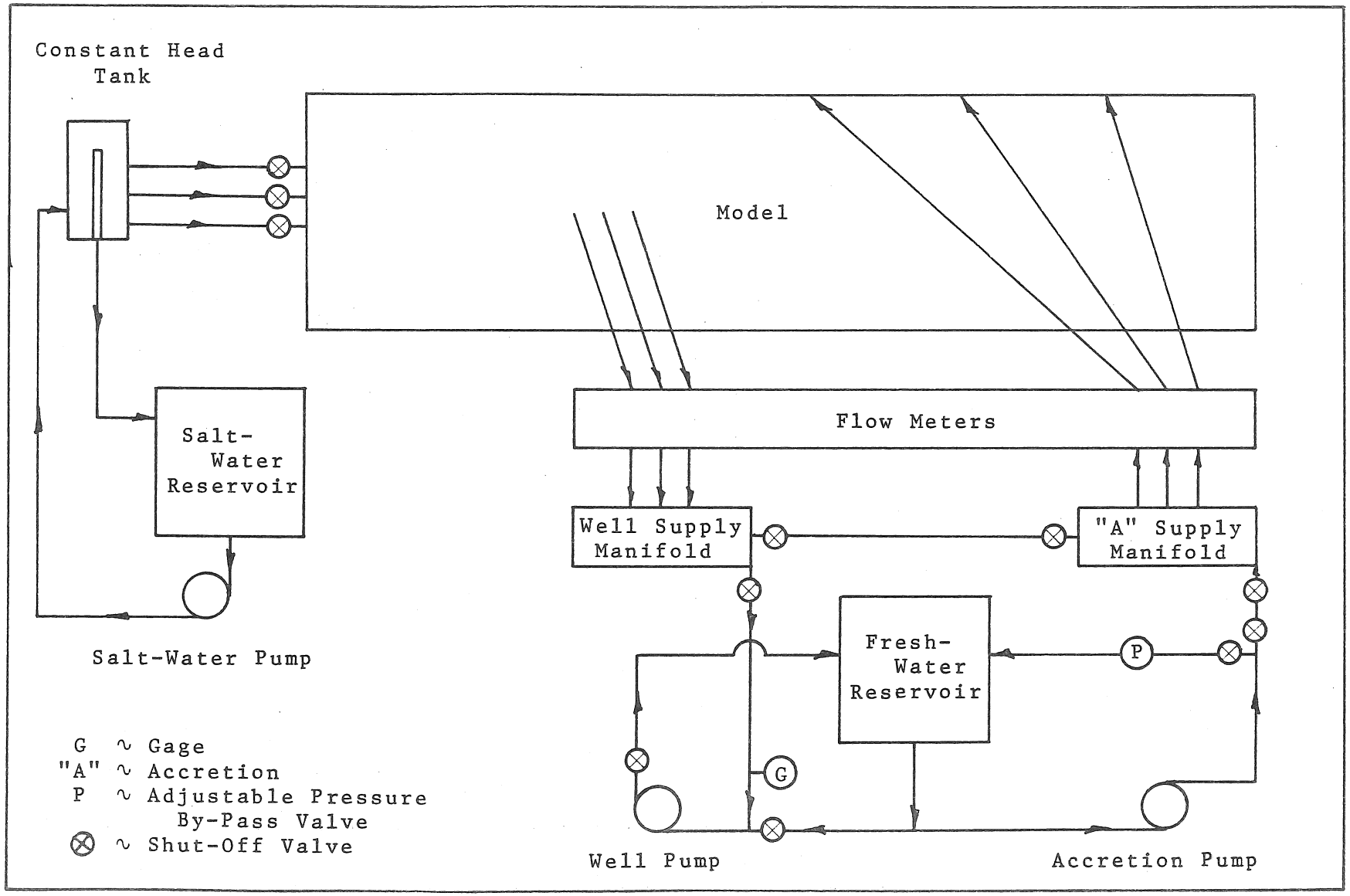

FIGURE 5.17
FLUID SUPPLY NETWORK SCHEMATIC

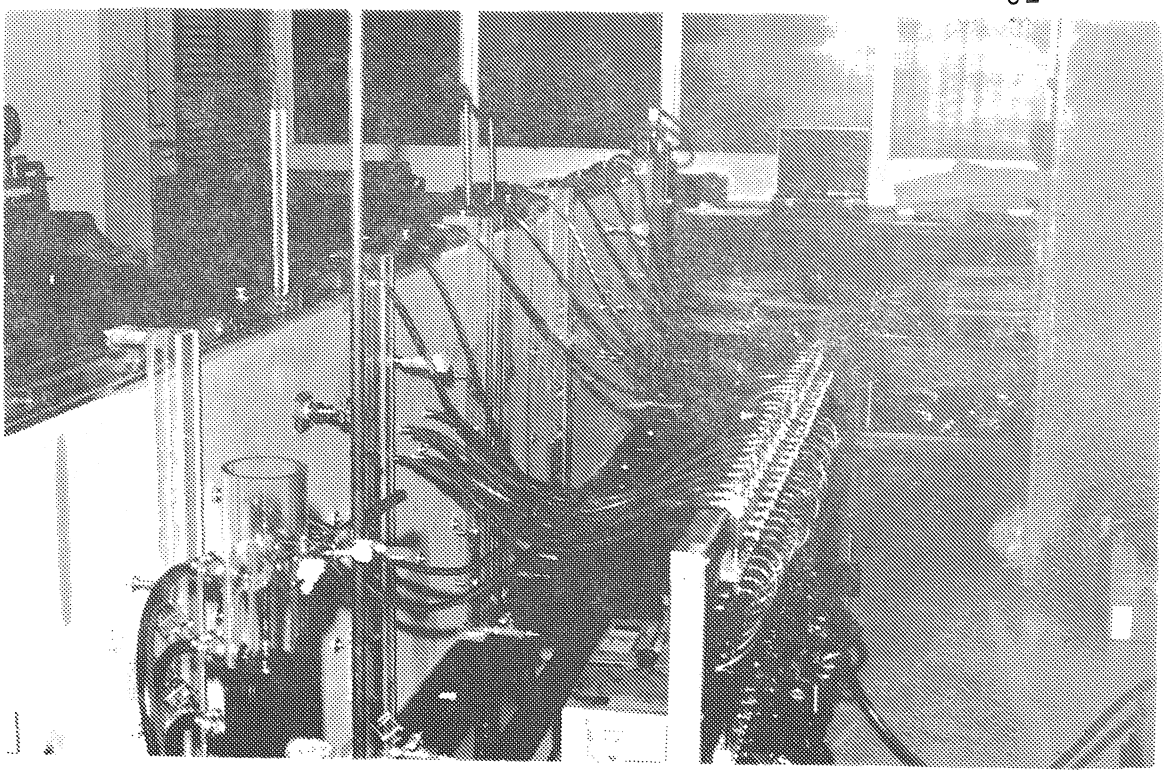

FIGURE 5.18
CONNECTIONS BETWEEN MODEL AND FLUID SUPPLY SYSTEM

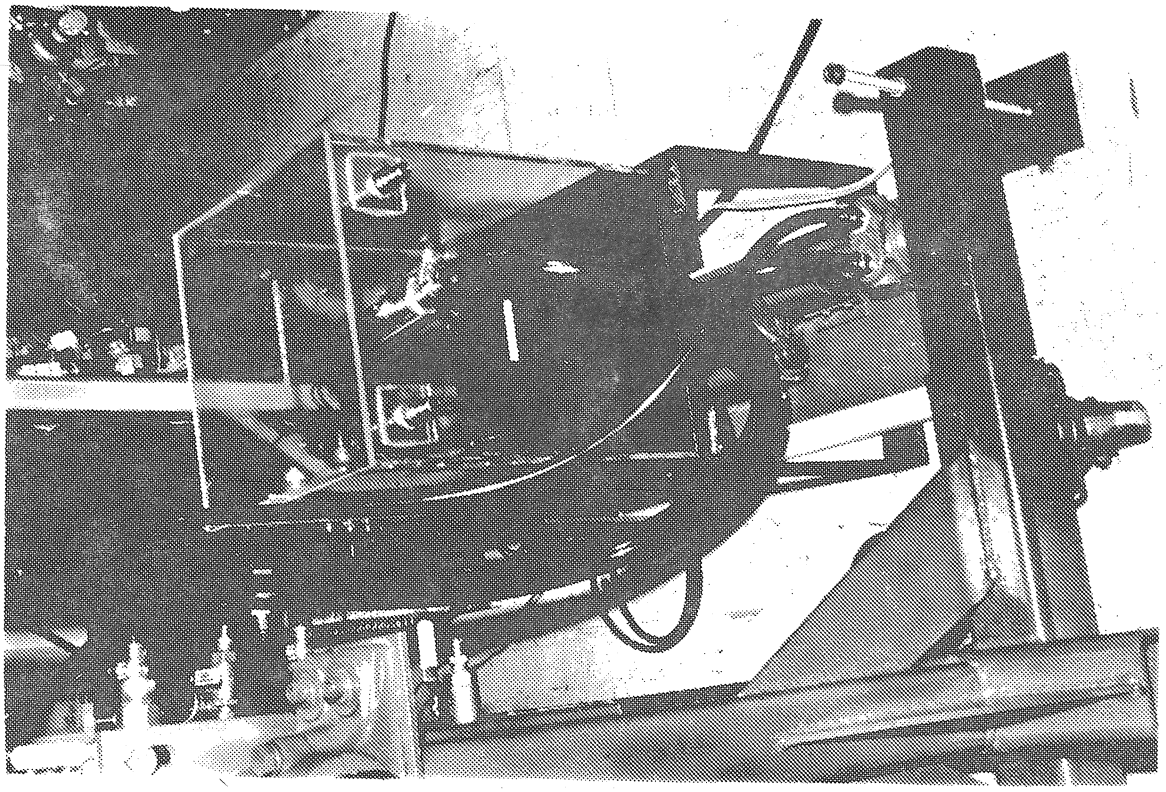

FIGURE 5.19
SALT-WATER RESERVOIR AND PUMP

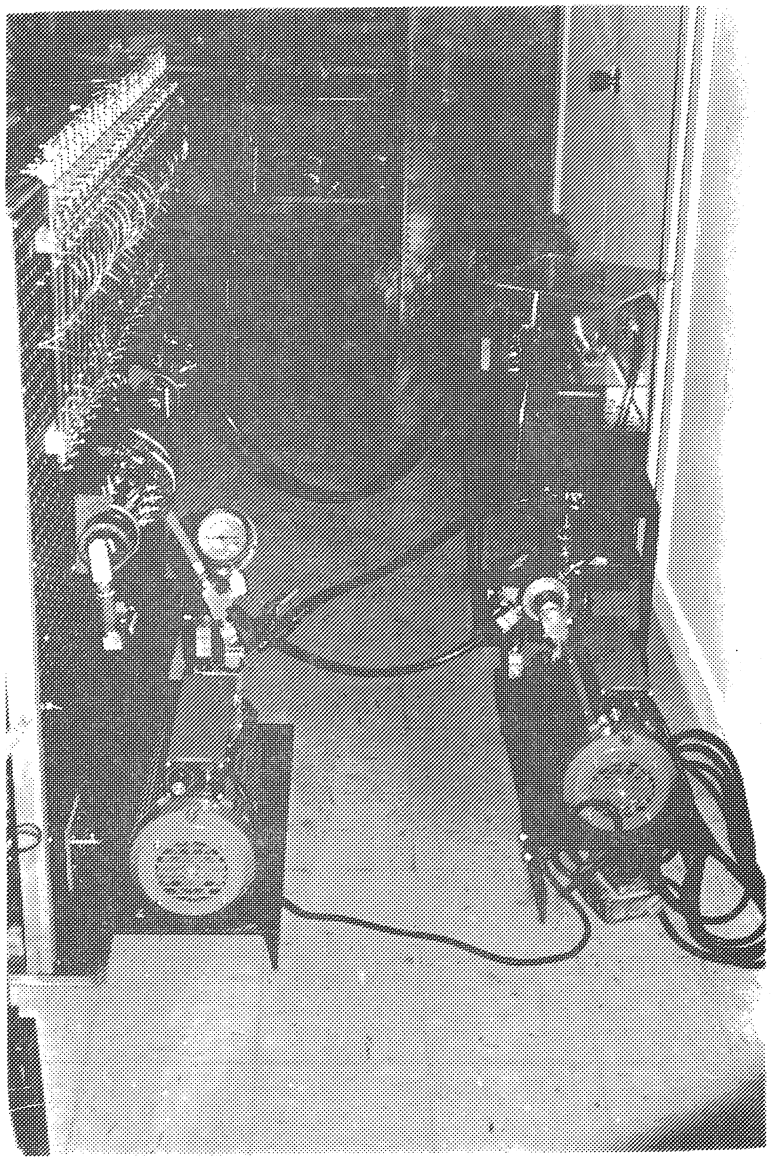

FIGURE 5.21
FRESH-WATER SUPPLY SYSTEM

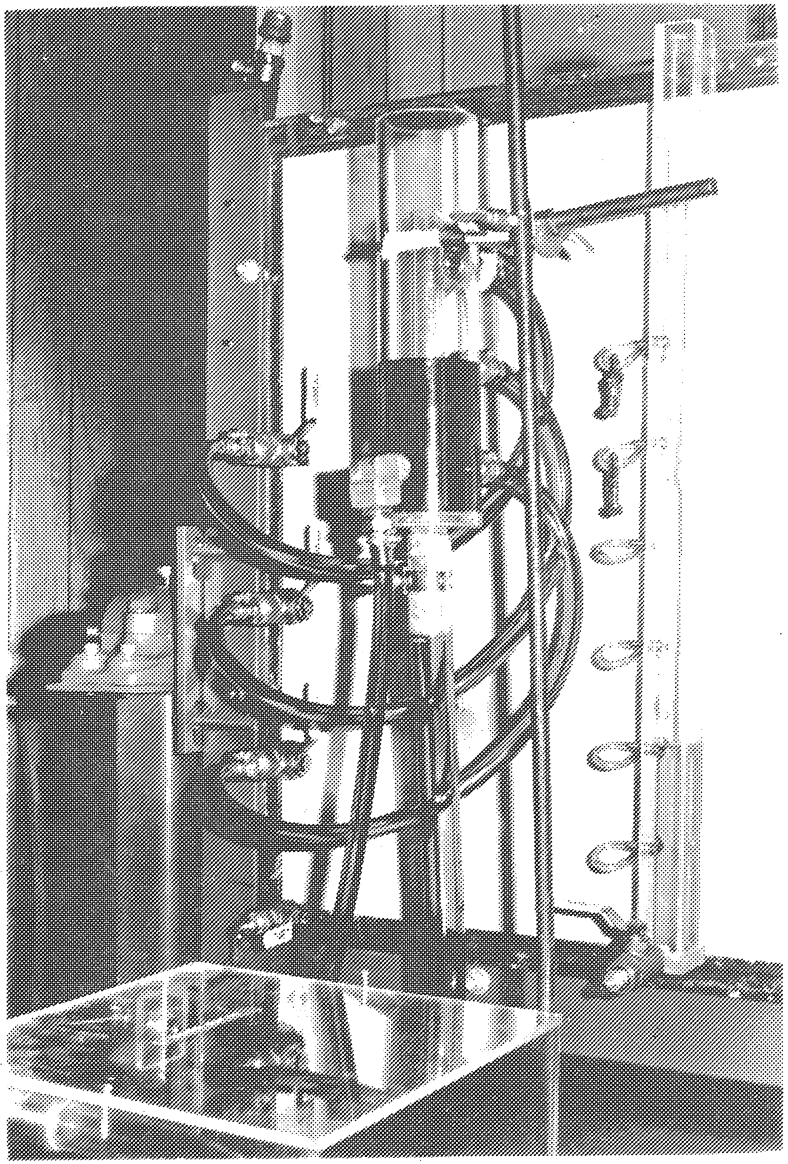

FIGURE 5.20
SALT-WATER CONSTANT HEAD TANK

this tank. Fluid overflowing the center tube of the tank returns to the reservoir. The tank is connected to the Gulf of Mexico end of the model by three tubes and valves as shown in Figure 5.20. The tank's elevation may be raised or lowered in order to set the proper sea level in the model.

Fresh-Water System, General

Figure 5.21 shows the three subsystems of the fresh-water system. At the right top of the figure is the fresh-water reservoir. The accretion pump is at the lower right of the figure. The well pump is at the lower left, and the flow meters are mounted on the peg board at the upper left of the figure.

Fresh-Water System, Accretion

Figure 5.22 shows the fresh-water reservoir and the accretion pump unit. This unit consists of a gear pump, a variable speed, reversible motor and an adjustable pressure by-pass valve. The unit supplies fluid at a pre-selected pressure to a manifold mounted on the flow meter board. This manifold can be seen in Figure 5.23 in the top center of the figure.

Fresh-Water System, Wells

Figure 5.23 shows the well pump unit and its supply manifold. The pump unit consists of a gear pump, a variable speed, reversible motor and a sensitive compound gage. This unit pulls a slight vacuum on the manifold in order to remove fluid from the model at well locations. Fluid removed from the model is returned to the fresh-water reservoir. In addition, a line from the reservoir discharge is kept open to the pump to prevent operating in a "starved" condition.

Fresh-Water System, Flow Meters

Figure 5.24 shows, from left to right, the well supply manifold and the accretion supply manifold with their connections to the bottoms of the flow meters. There are twelve flow meters for each manifold. Figure 5.25 is the opposite view. The two manifolds are connected by a tube which is only used during start-up or shut-down operations; the tube is most clearly seen in Figure 5.24.

Figure 5.26 is an over-all view of the twenty-four flow meter bank. Meters one through twelve supply accretion manifolds and recharge wells; meters thirteen through twenty-four handle well pumping.

Figure 5.27 is a detail view of several flow meters. The operation of the meters is based on Poiseuille's relationship for laminar flow in a tube:

$$Q = \frac{\pi d^4 g}{128 L} \frac{\Delta h}{\nu} \qquad (5.16)$$

where d equals tube diameter and Δh equals head loss.

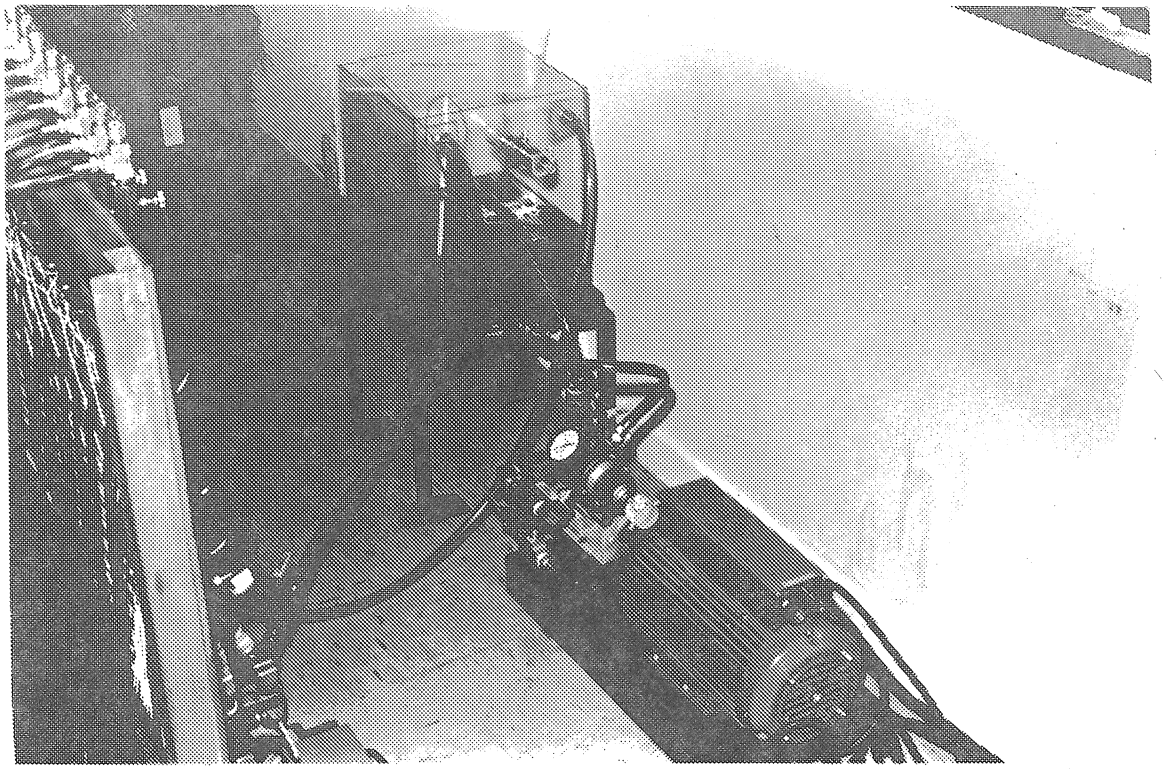

FIGURE 5.22
FRESH-WATER RESERVOIR AND ACCRETION PUMP

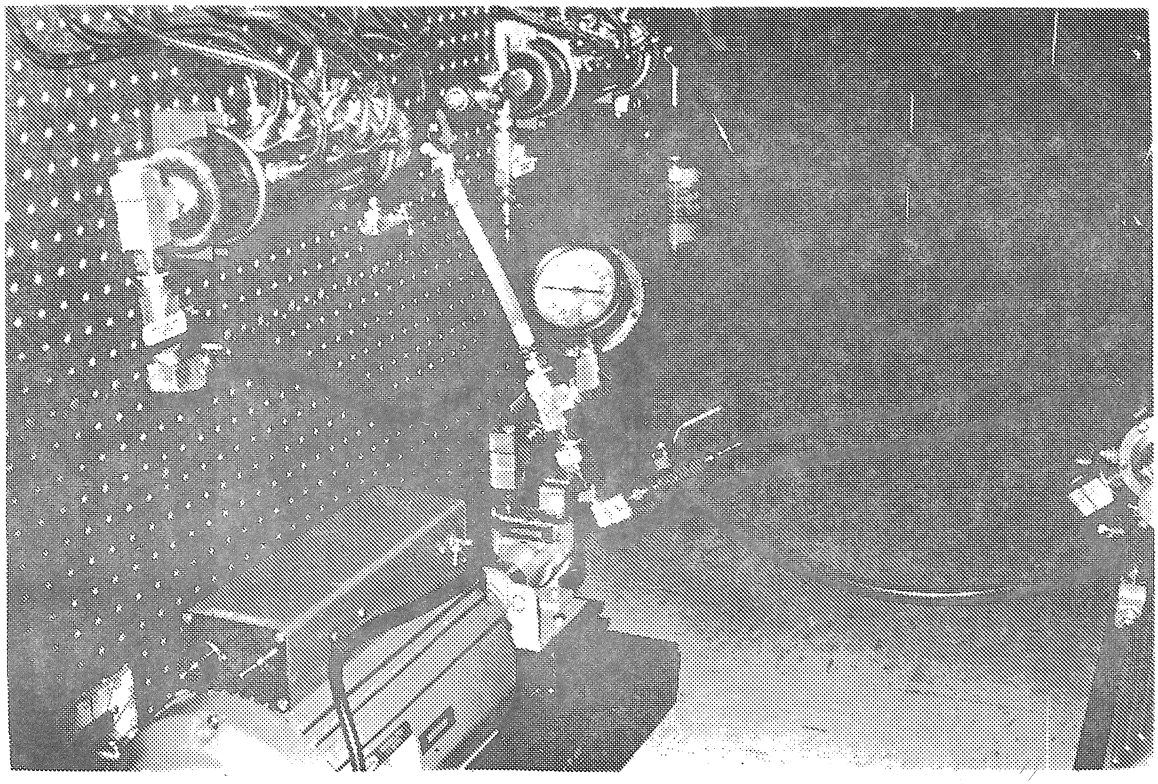

FIGURE 5.23
WELL SUPPLY MANIFOLD AND PUMP

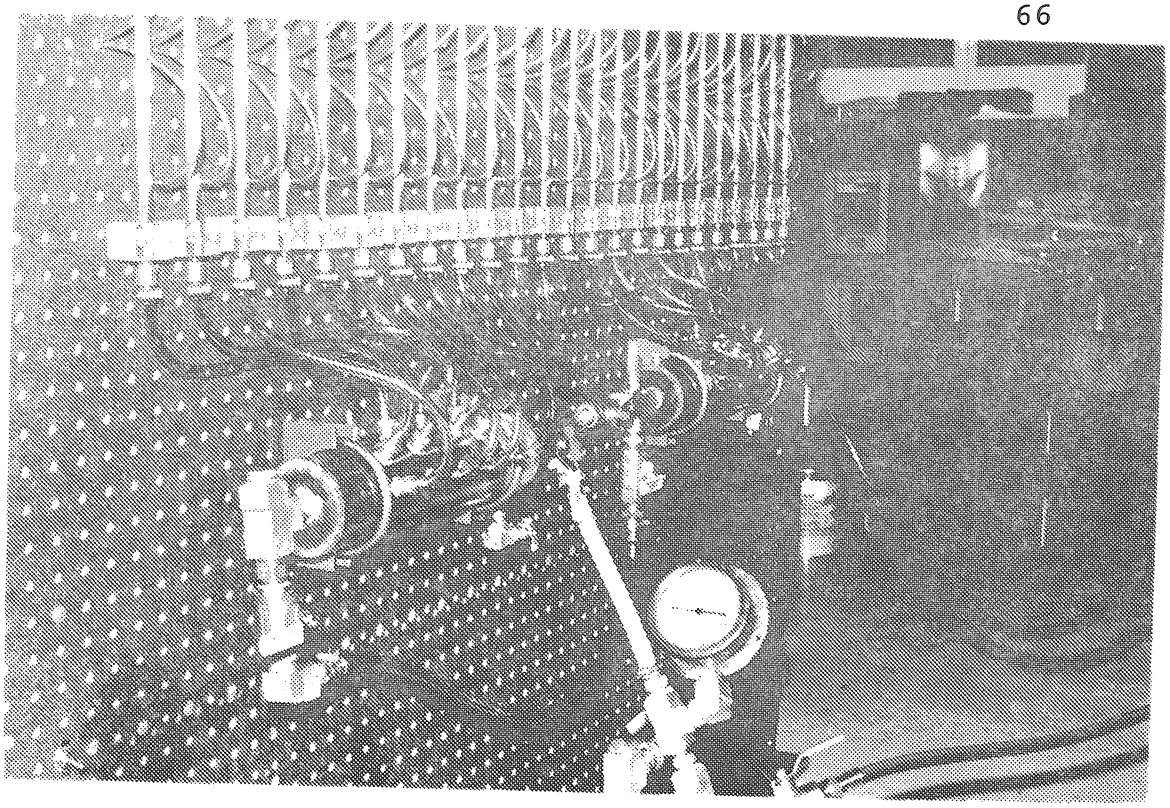

FIGURE 5.24
WELL SUPPLY MANIFOLD AND ACCRETION SUPPLY MANIFOLD

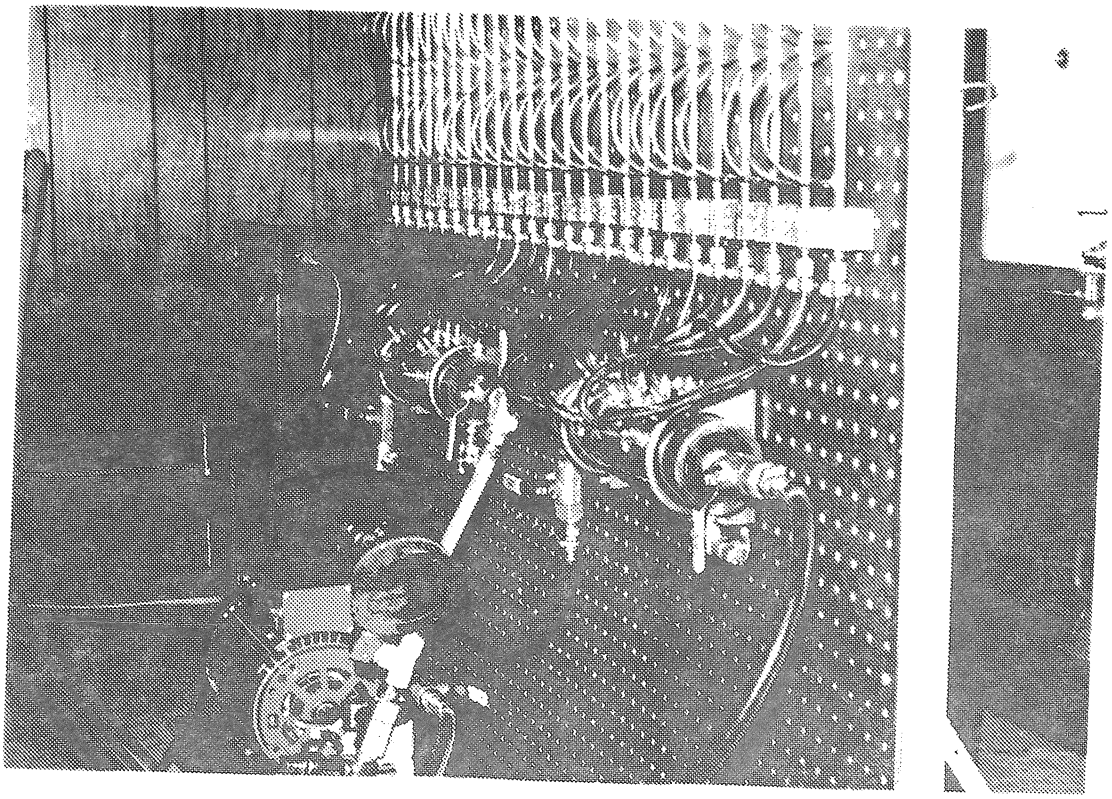

FIGURE 5.25
OPPOSITE VIEW OF FIGURE 5.24

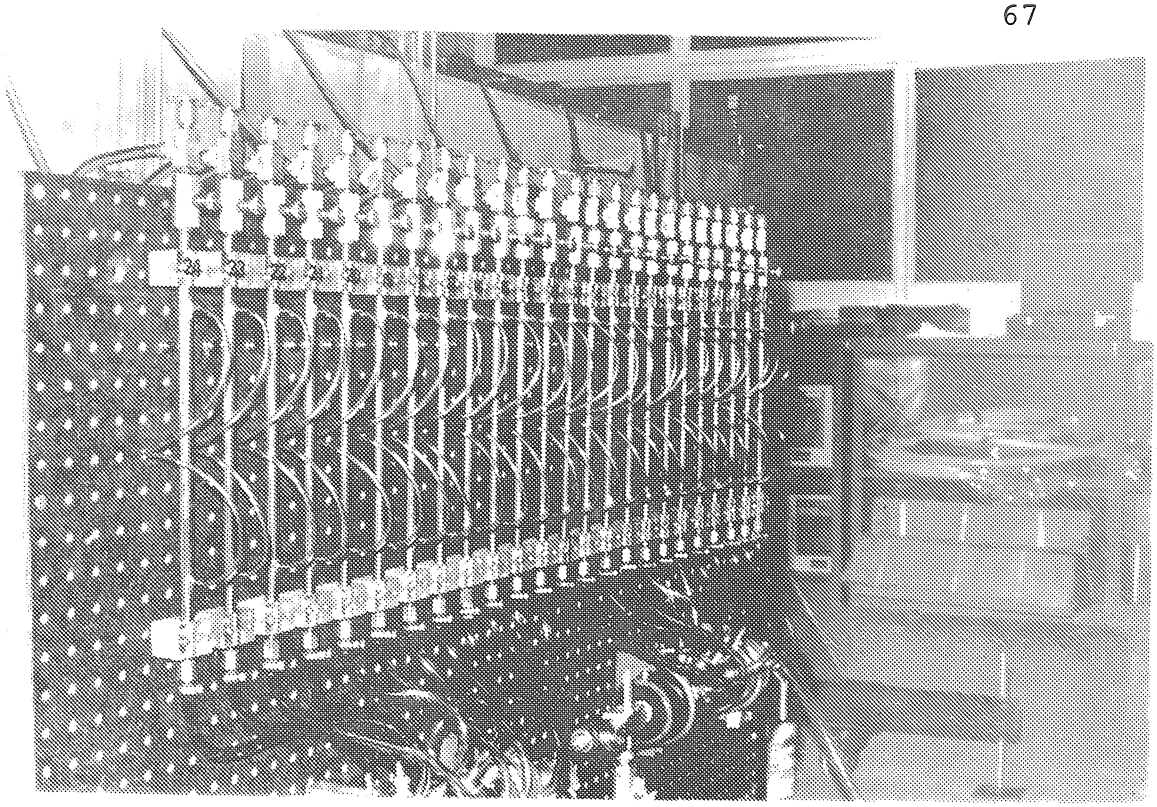

FIGURE 5.26
FLOW METER BANK

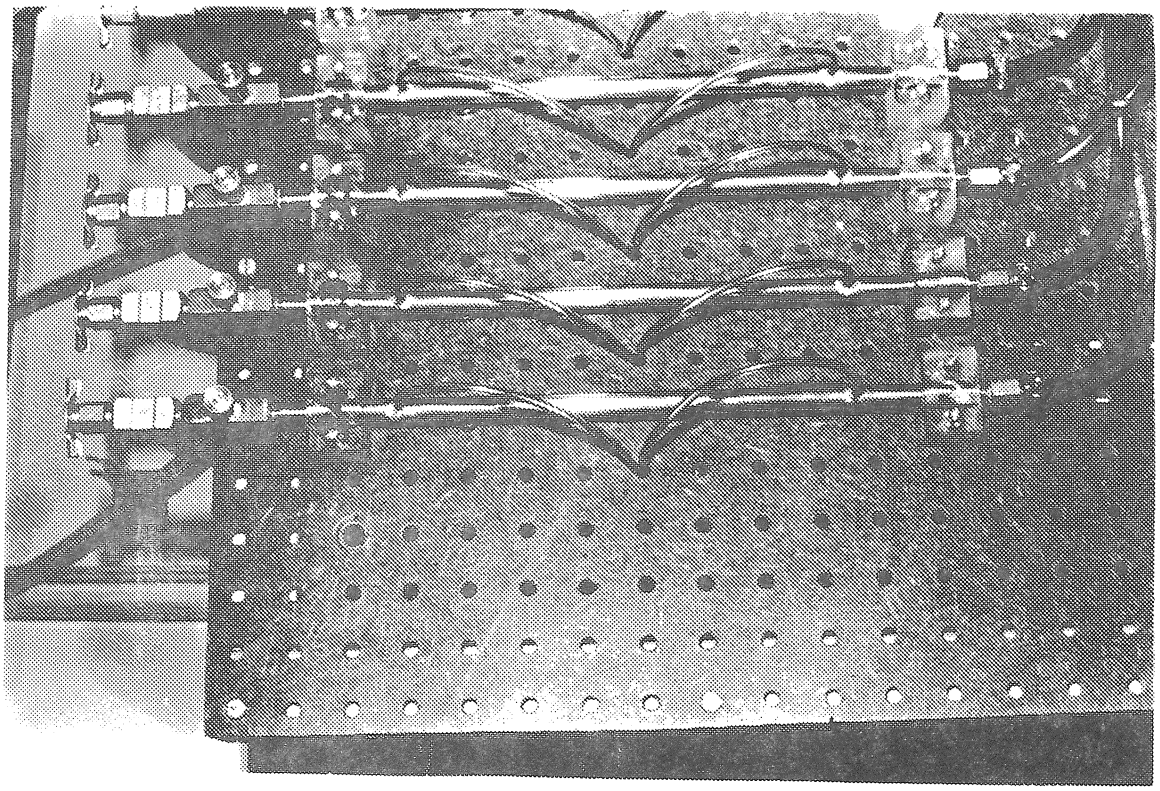

FIGURE 5.27
FLOW METER DETAIL

For a given tube and fluid, the flow rate and pressure drop in the tube are proportional. Therefore, if the pressure drop in a tube is measured, the flow rate may be determined. The flow meter consists of a 12-5/8" length of 1/8" brass pipe with a nominal I.D. of 0.278". The pipe is threaded to accept a hose barb at the bottom end and a regulating needle valve at the top end. Pressure taps are installed in the pipe and are 7.67" apart. This spacing is consistent with the maximum flow rate required of the meter and the pressure sensing capability of the transducers. The pipe is mounted to the peg board with two Plexiglas blocks. A brass tee from the needle valve carries an air bleed at the top and a hose barb for hook-up to the model. Figure 5.28 shows some of the connections to the model. The cluster of tubes in the center of the model is connected to ports simulating Eldridge-Wilde well field. The longer tubes going over the top of the model are connected to accretion manifolds. The two tubes extending out of the figure to the left are for recharge wells near Lake Tarpon. There is an additional well field near the Pasco High which is not shown and which was not hooked up.

The direction of flow for accretion flow meters is from bottom to top. The directions for well pumping flow meters is from top to bottom.

Figure 5.29 shows the back of the flow meter mounting board and the pressure sensing lines from each meter. These lines originate at the pressure taps on the meters as shown in Figure 5.27 and terminate at a rotary valve switching device, seen in the center of Figure 5.29. A more detailed look at this device, and the two pressure transducers that are connected to it,is shown in Figure 5.30. The switching device consists of four fluid switch wafers coaxially mounted in a control unit. Each wafer (Scanivalve, Inc., Model 60 Fluid Switch Wafer, Scan Co. #W1260/1P-12T) has twelve input ports and one output port. Therefore, two wafers can switch twelve pairs of input lines from twelve flow meters into one differential pressure transducer. Four wafers and two transducers are required for twenty-four flow meters. The control unit has twelve click-stop positions, and each position connects two flow meters and two transducers. The pressure transducers used are Celesco #P7D Differential Pressure Transducer, ± 1/2 PSID.

The output of the pressure transducers is sensed and conditioned by a carrier demodulator unit, Celesco Model CD-12, which sends an output signal to a Hewlett-Packard dual channel strip chart recorder. Figure 5.31 shows the carrier demodulator positioned above the recorder.

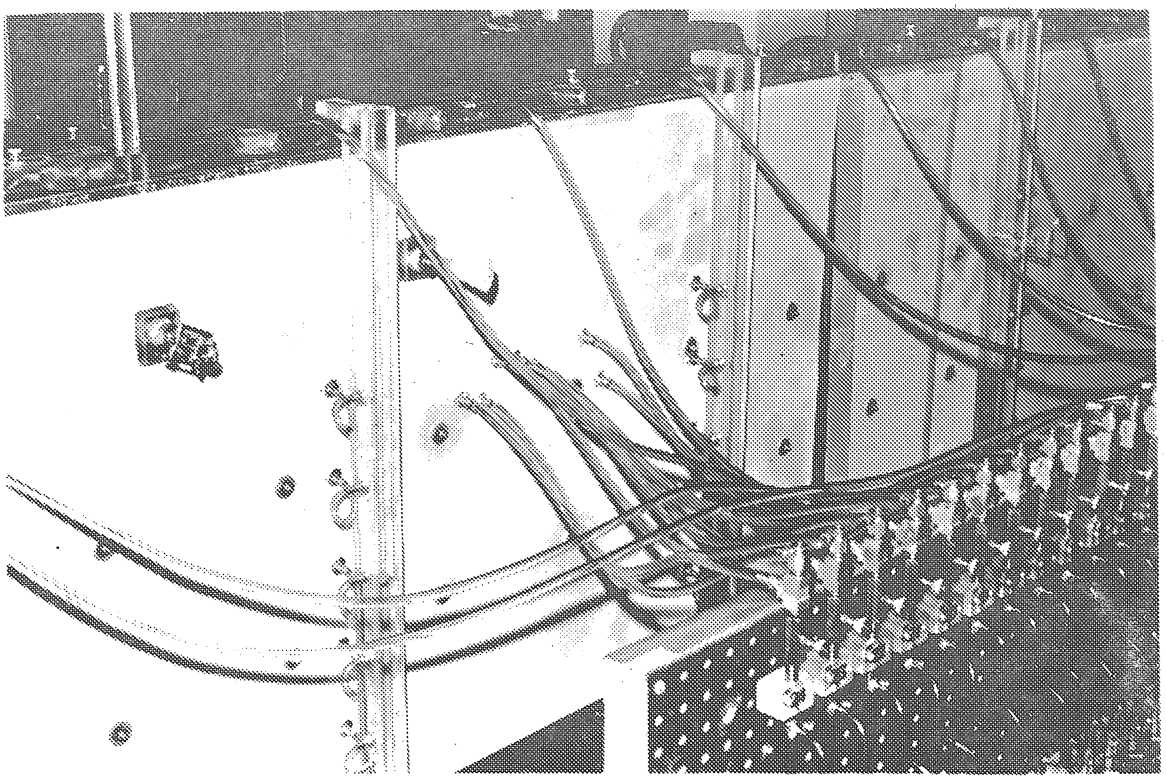

FIGURE 5.28
FLOW METER TO MODEL CONNECTIONS

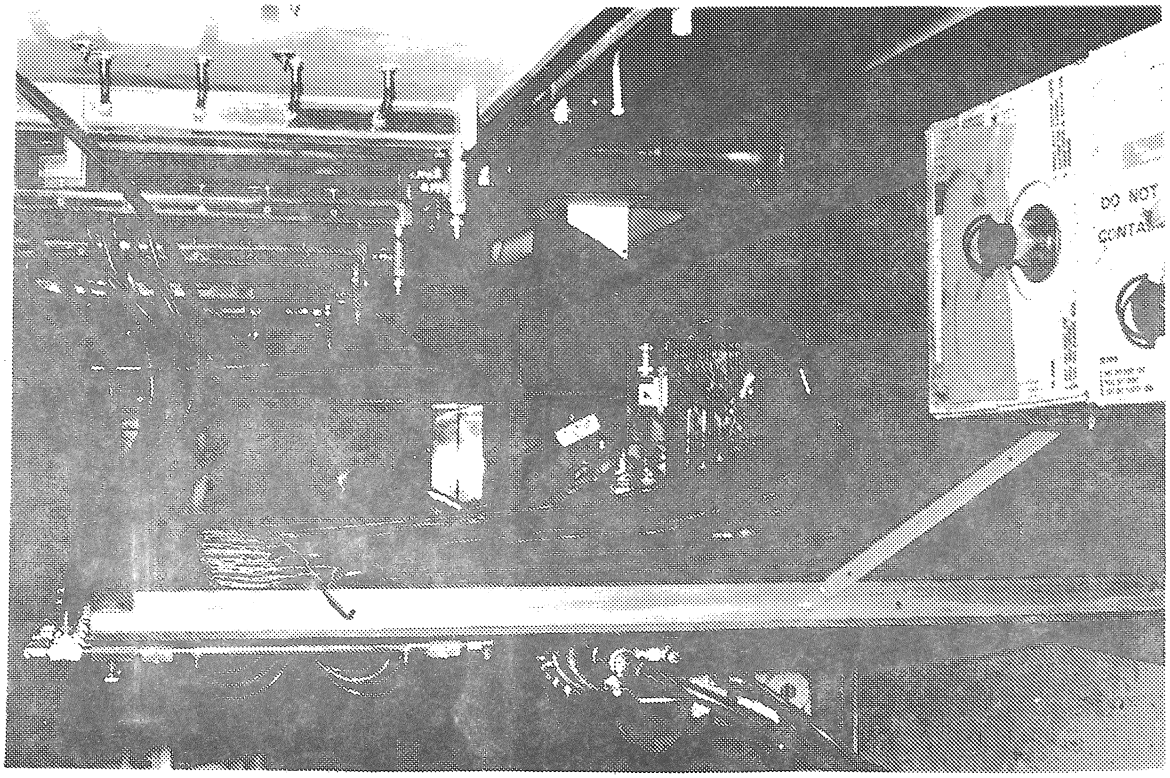

FIGURE 5.29
FLOW METER PRESSURE SENSING LINES

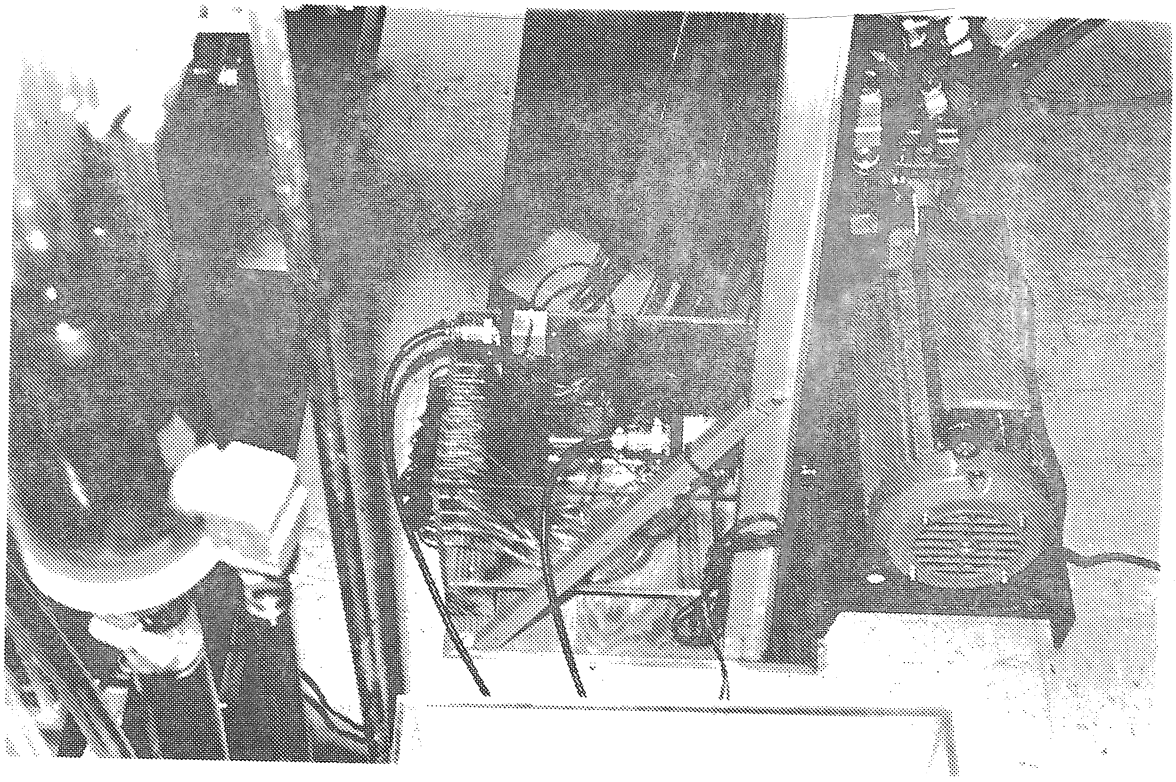

FIGURE 5.30
FLOW METER SWITCHING DEVICE AND PRESSURE TRANSDUCERS

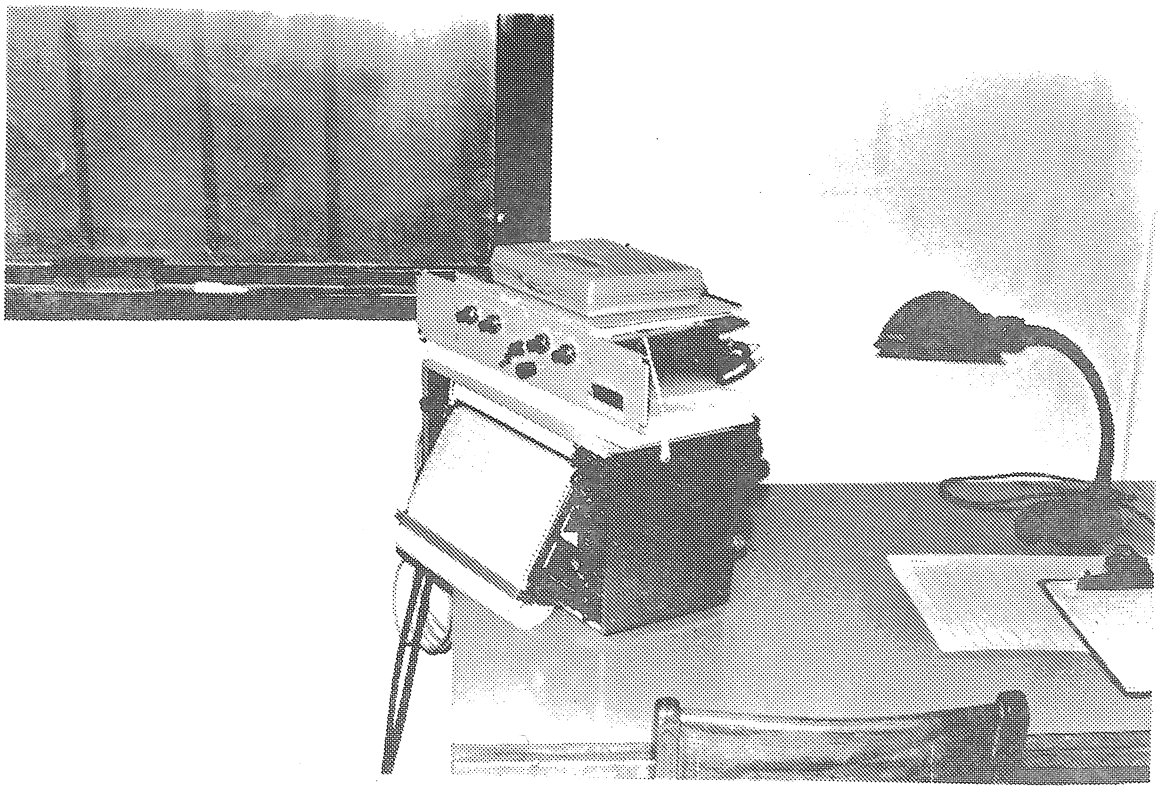

FIGURE 5.31
CARRIER DEMODULATOR AND STRIP CHART RECORDER

Rather than measure pressure drop across the flow meters and then computing the flow rate, the meters were directly calibrated for deflection in inches on the strip chart recorder as a function of measured flow rate. The carrier demodulator and recorder were set to provide zero reading at zero flow rate and near maximum reading at maximum flow rate.

Each flow meter was operated at various flow rates as determined by measurement with a stopwatch and graduated cylinder. The recorder reading and fluid temperature were noted at each point. All data were corrected to 25° C and fitted to a straight-line by the method of least squares. The correlation coefficient for twenty-four meters ranged from 0.997 to 1.000.

Operation

The accretion pump is used to fill the accretion supply manifold, well supply manifold (through cross-over tube), flow meters and pressure sensing lines. Air bleeds are located throughout the system to remove trapped air.

To fill the model, the salt-water pump is started and the constant head tank filled and adjusted. The valves on the accretion flow meters are opened and the valves for the salt-water opened (slightly). The inflow rates are adjusted to bring the salt- and fresh-water levels up together. Once the model is near being full and the interface formed, the pressure by-pass valve on the accretion pump, pump RPM and the accretion flow meters are set to provide the flow rates required for the test under consideration. The salt-water valves are fully opened. The well pump is adjusted by seeing that the well supply manifold is closed to the pump and that the pump RPM is sufficient to maintain a vacuum of ≃ 4" Hg. when recirculating fluid from the fresh-water reservoir. The valve to the well supply manifold is then opened and the well flow meters adjusted. The fluid temperature is monitored throughout the test so that flow rates may be corrected. Excess accretion is removed from the model through various drain ports.

When the model is shut down between tests, it may be drained by gravity or reversing the pumps, or the two fluids may be left in the model where they become horizontally stratified. Starting up again after either procedure is a tedious process and the selection of shut down is left to the subjective evaluation of the operator.

CHAPTER VI

RESULTS, CONCLUSIONS AND RECOMMENDATIONS

Results

The objectives of this project were to (1) develop, (2) construct, and (3) calibrate a Hele-Shaw model for a section of Pinellas County, Florida. Objectives (1) and (2) have been met. Objective (3) has been met from a qualitative point of view, but operational features in the model, in the area of the Pasco High, have presented a problem in obtaining quantitative calibrations. These features are presently being modified to overcome the difficulties; this is discussed later, and the Hydraulic Laboratory will then proceed to a quantitative examination of salt-water intrusion in this area.

Figures 6.1 through 6.13 show the fresh-water/salt-water interface as it proceeds from an equilibrium position through successive stages of penetration and upconing due to pumping in Eldridge-Wilde well field, and then through further stages as fresh-water recharging in the coastal zone is carried out.

Figure 6.1 shows the position of the wedge at a steady-state condition. The wedge is correctly located at the coast and in the approximate present location. Eldridge-Wilde is the cluster of dots in the center of the picture, it is directly above the landward toe of the wedge. The wedge and the Gulf of Mexico are the dark region at the right end of the model. The fresh-water is the light region.

The time ratio is approximately 1 minute of model time = 1 year of prototype time. The sequence beginning with Figure 6.1 and proceeding through Figure 6.7 represents about 100 years of pumping at low rates with low accretion rates set to maintain an equivalent pumping water level of 40 feet. These figures show the progressive penetration of the wedge and upconing under the well field.

Figure 6.7 is the beginning of fresh-water recharge in the coastal zone. The initial location of the upper end of the wedge in this zone is accentuated by the dark line on the interface as shown in Figure 6.8. The recharge points are the two dots located above this line. A recharge period of about 70 years is shown in Figures 6.7 through 6.13.

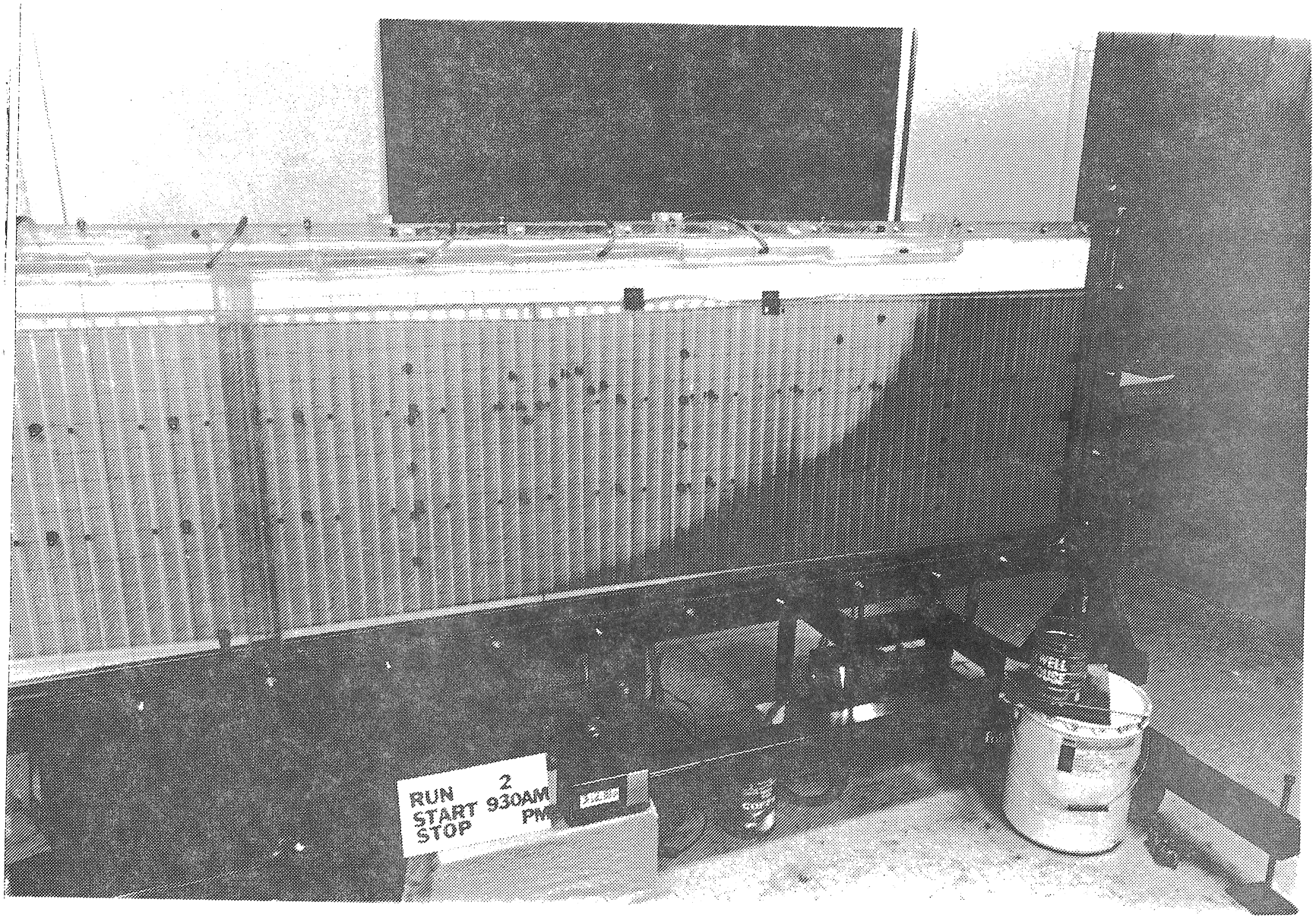

FIGURE 6.1
INTERFACE LOCATION, t_m = 0 Min.

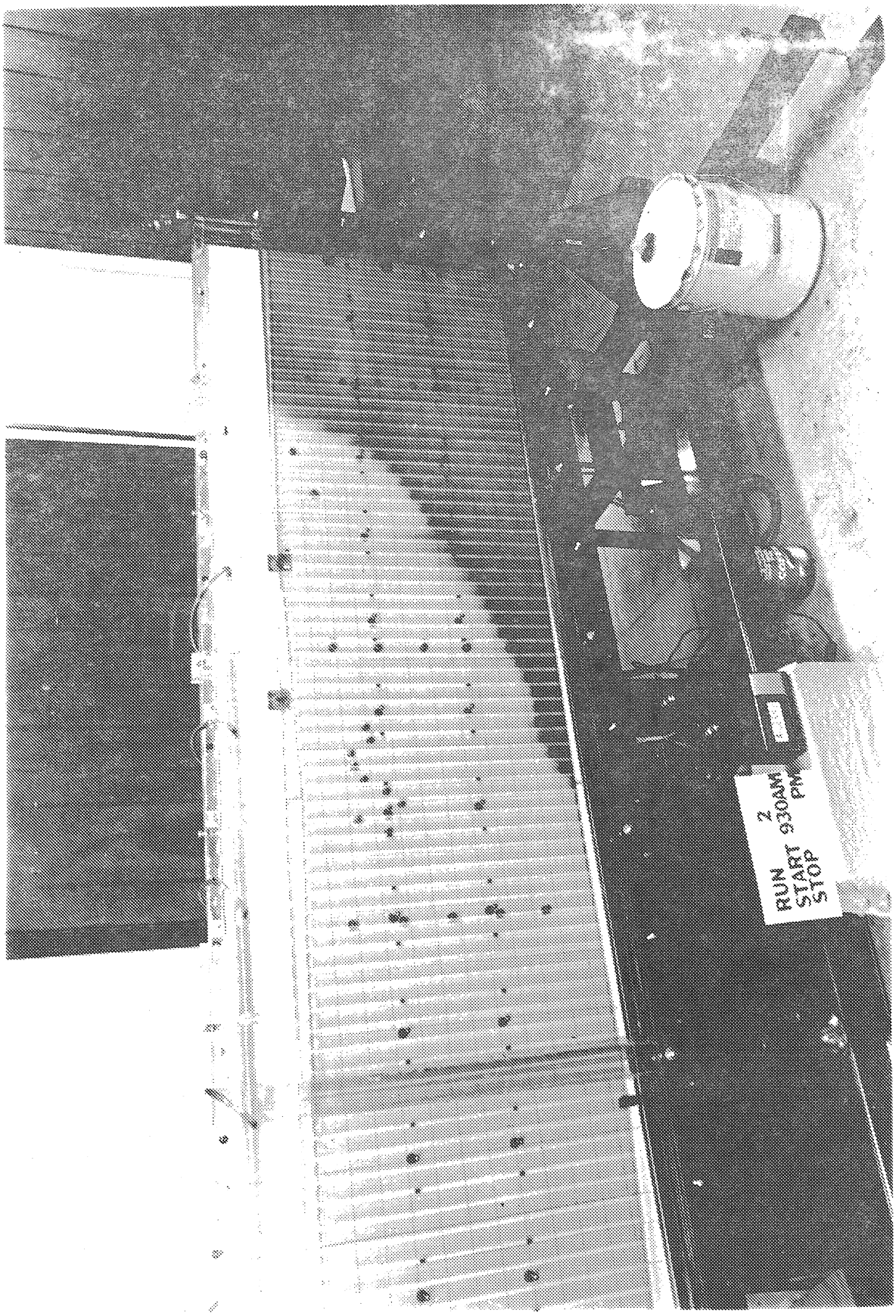

FIGURE 6.2
INTERFACE LOCATION, t_m = 32 Min.

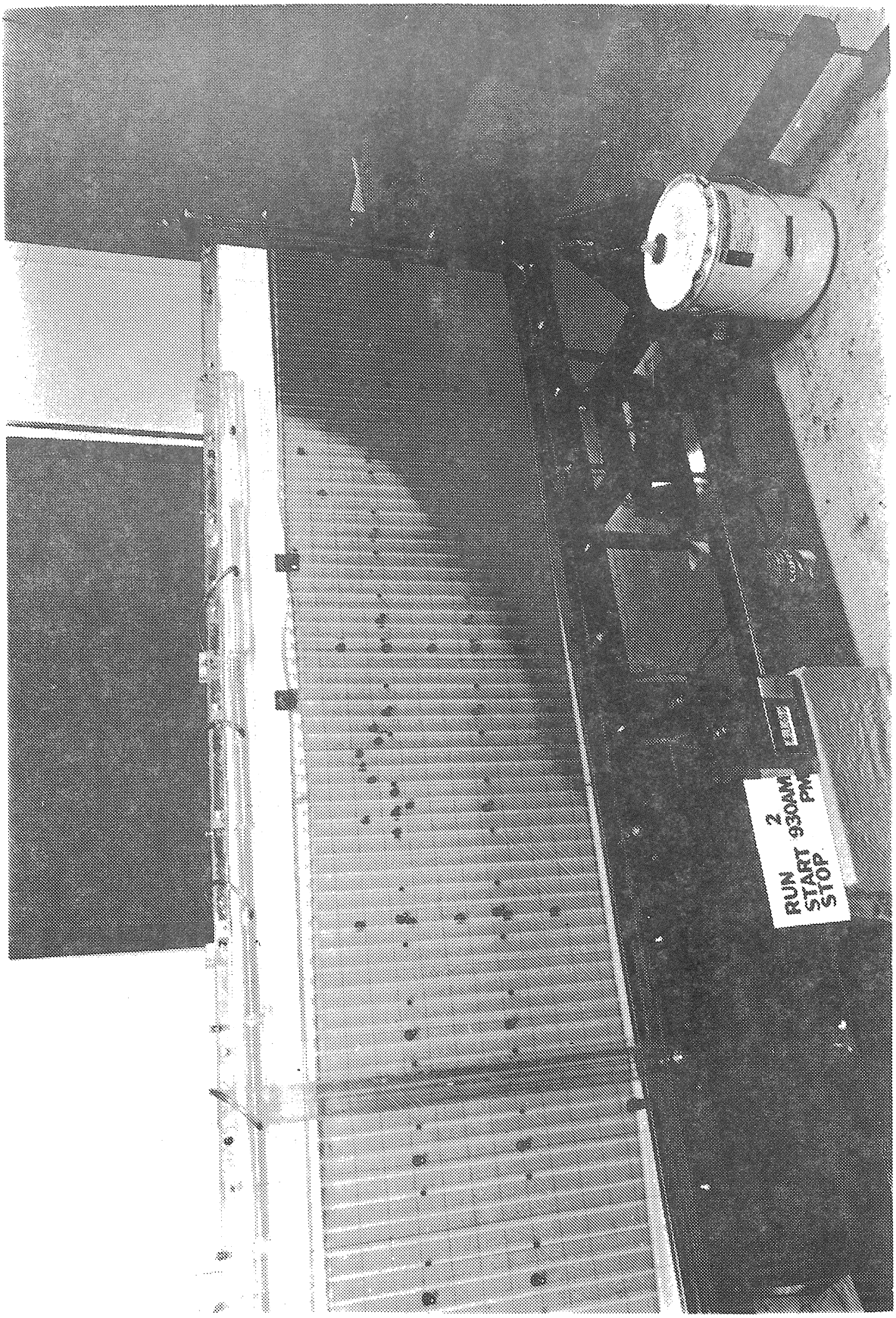

FIGURE 6.3
INTERFACE LOCATION, t_m = 48 Min.

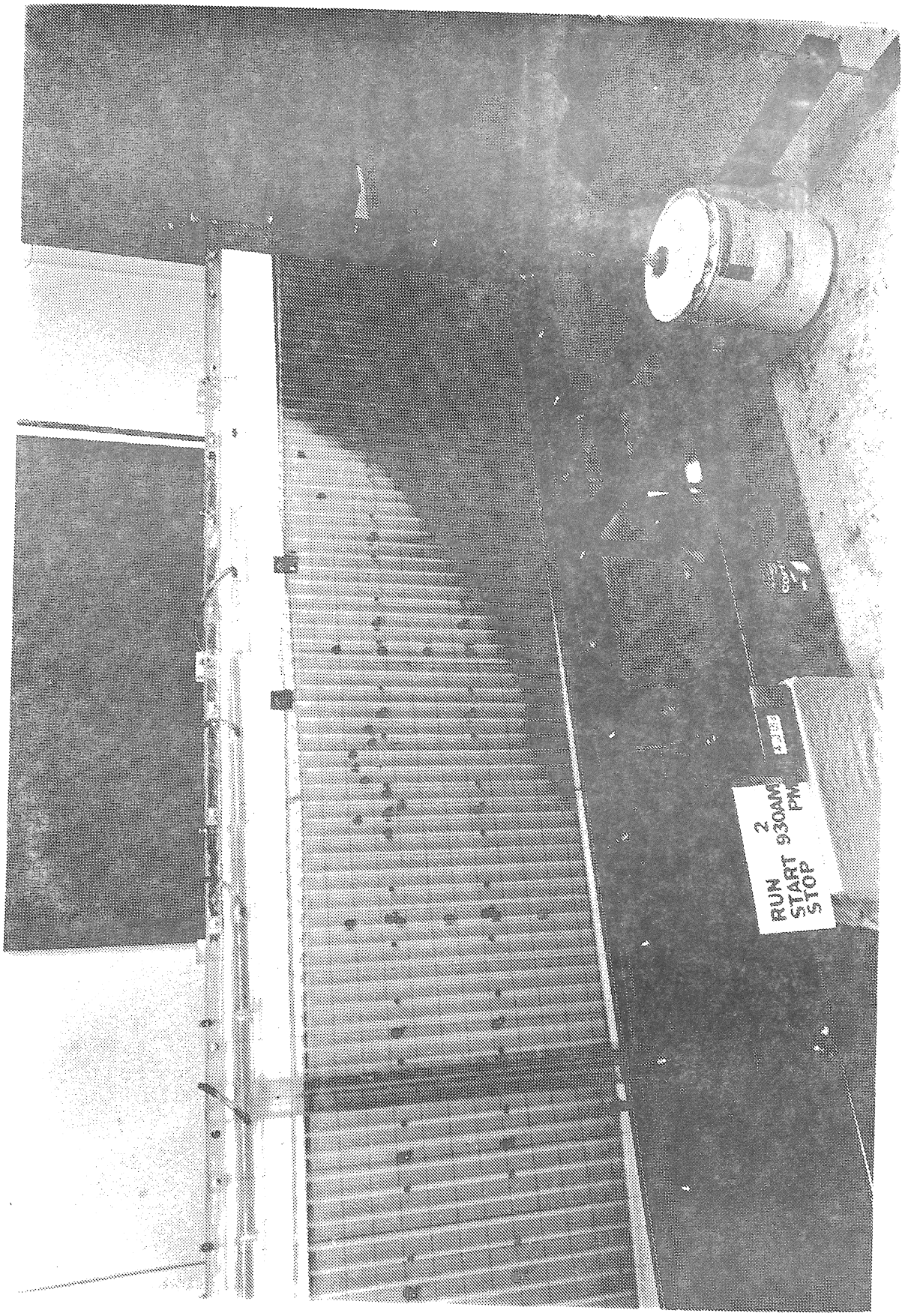

FIGURE 6.4
INTERFACE LOCATION, t_m = 62 Min.

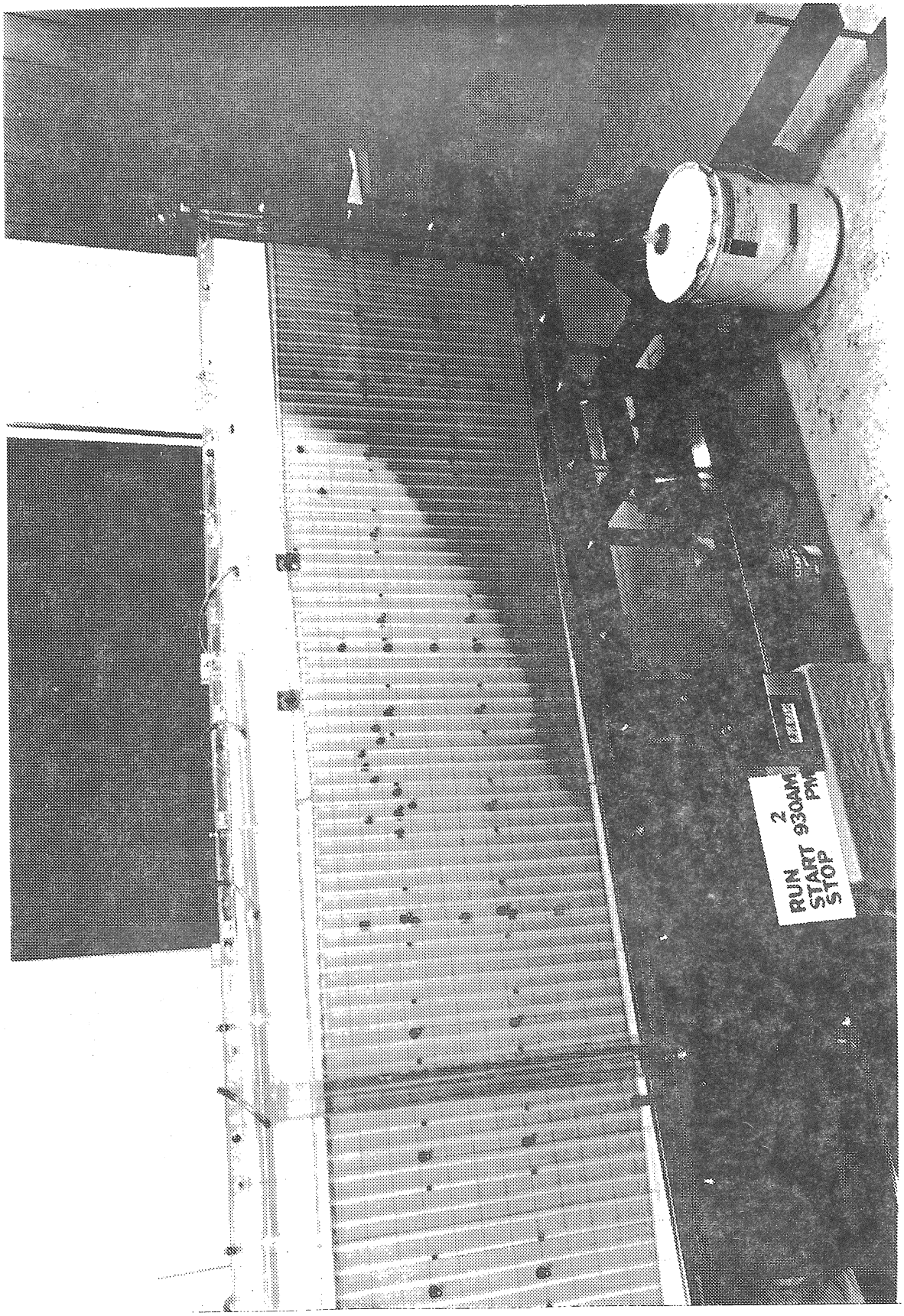

FIGURE 6.5
INTERFACE LOCATION, t_m = 79 Min.

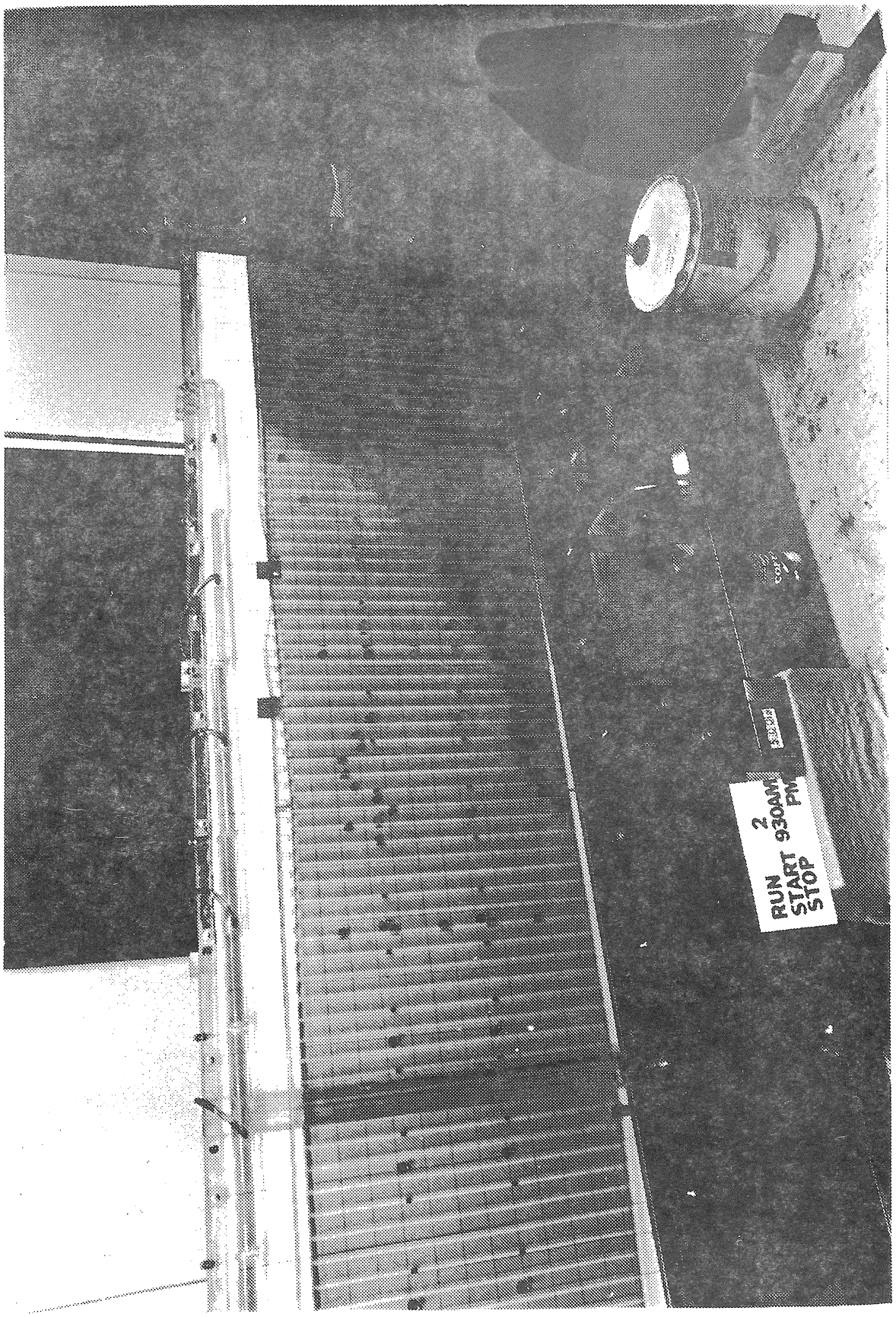

FIGURE 6.6
INTERFACE LOCATION, t_m = 92 Min.

FIGURE 6.7
INTERFACE LOCATION, t_m = 102 Min.

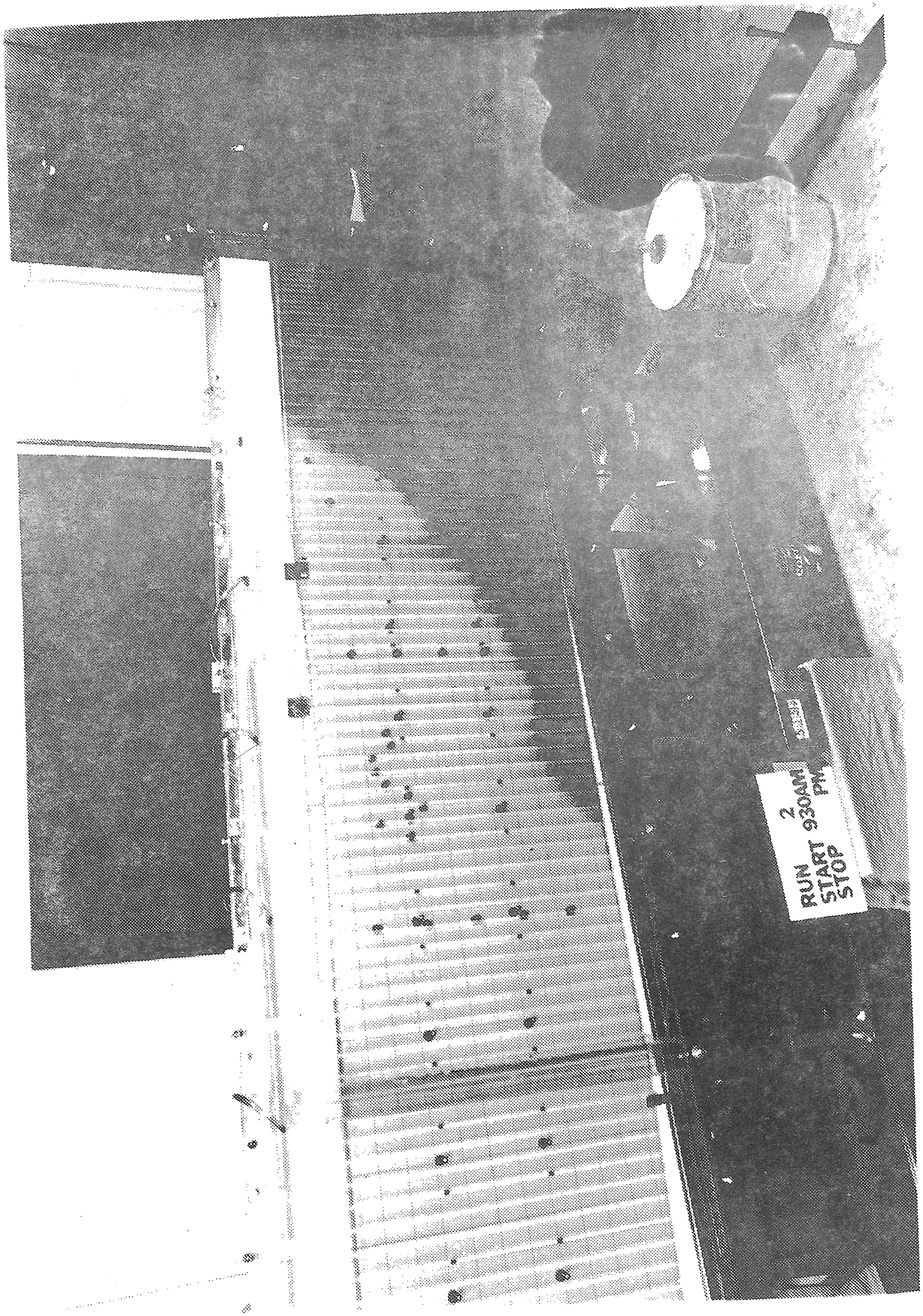

FIGURE 6.8
INTERFACE LOCATION, t_m = 107 Min.

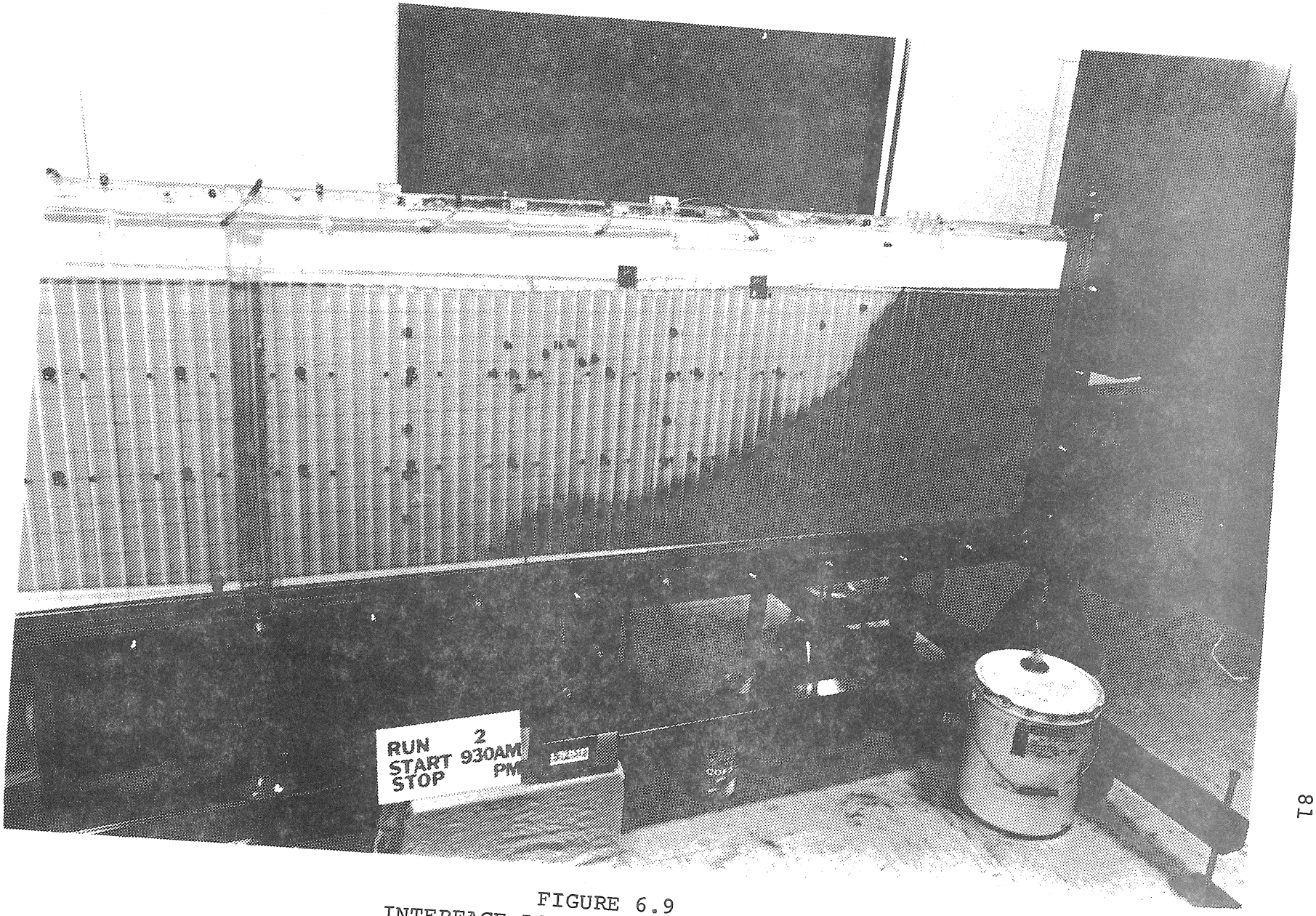

FIGURE 6.9
INTERFACE LOCATION, t_m = 117 Min.

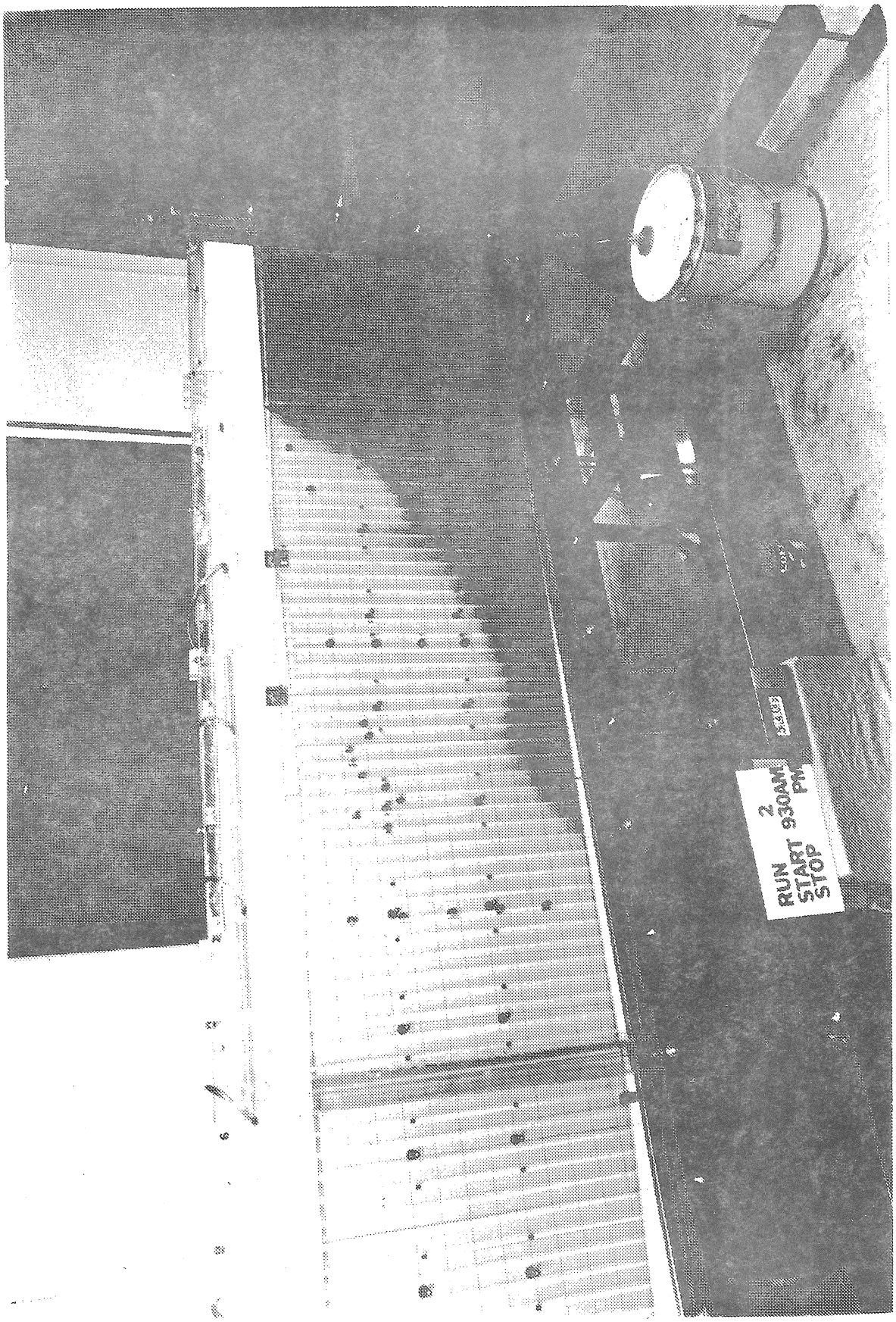

FIGURE 6.10
INTERFACE LOCATION, t_m = 132 Min.

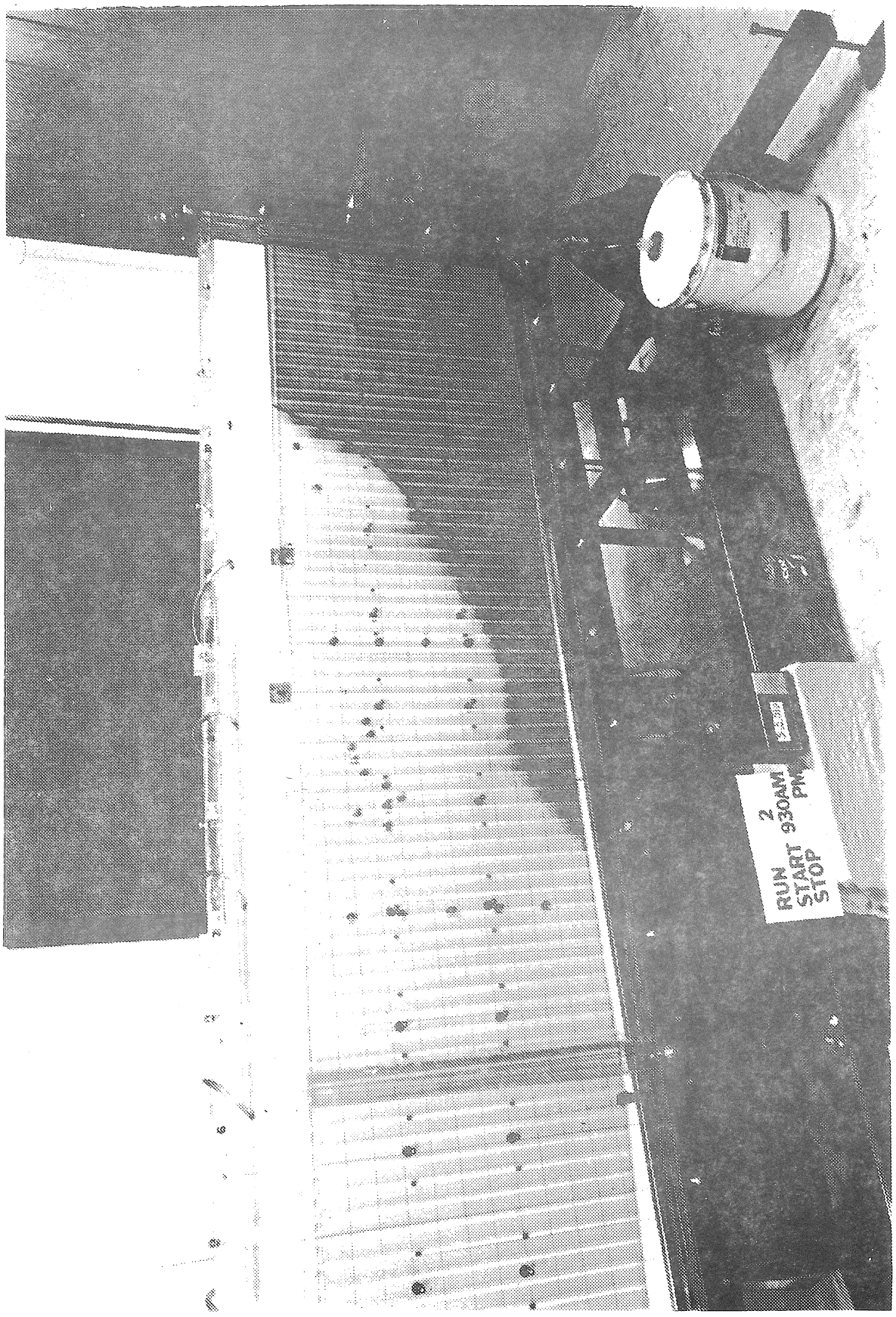

FIGURE 6.11
INTERFACE LOCATION, t_m = 147 Min.

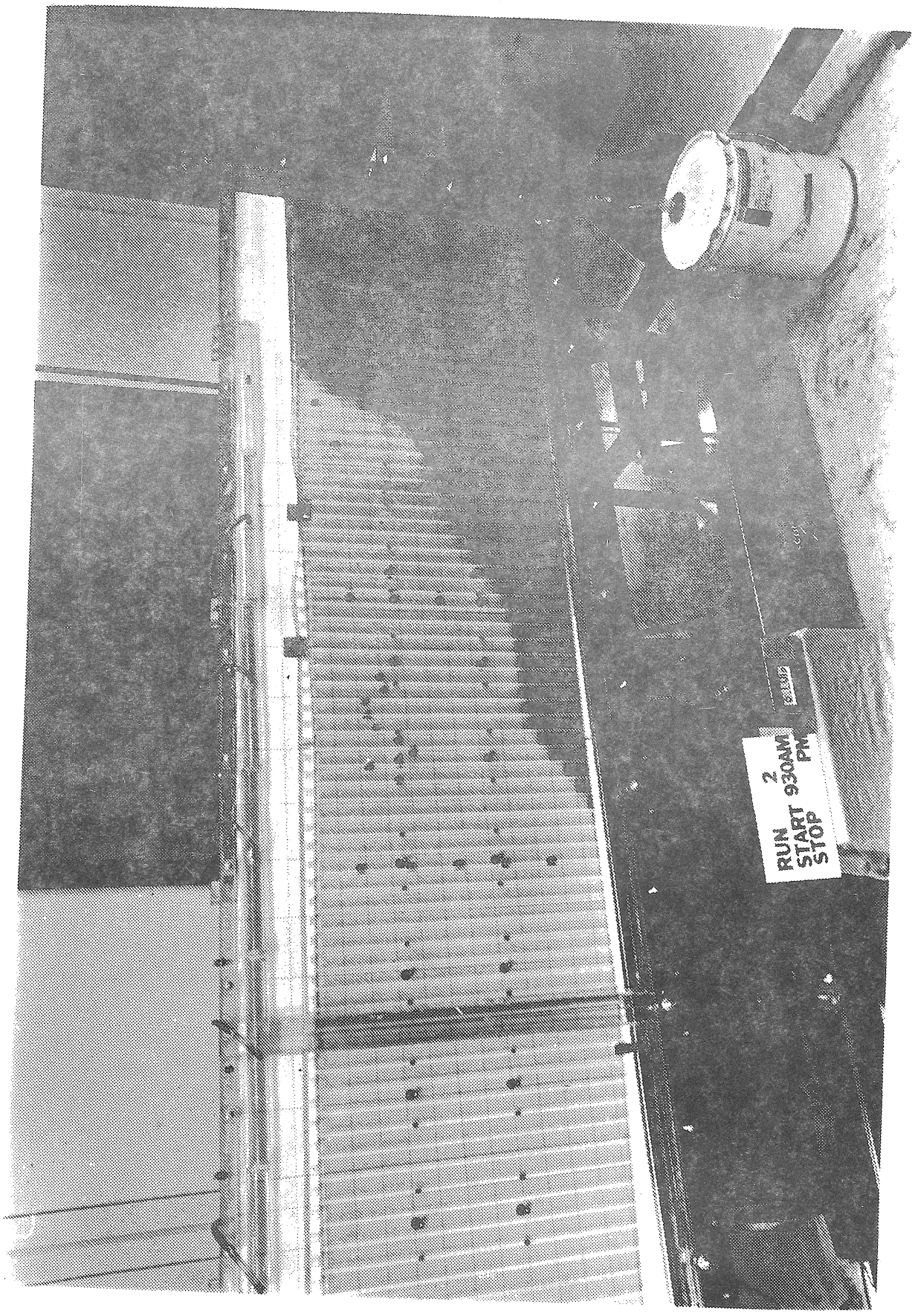

FIGURE 6.12
INTERFACE LOCATION, t_m = 162 Min.

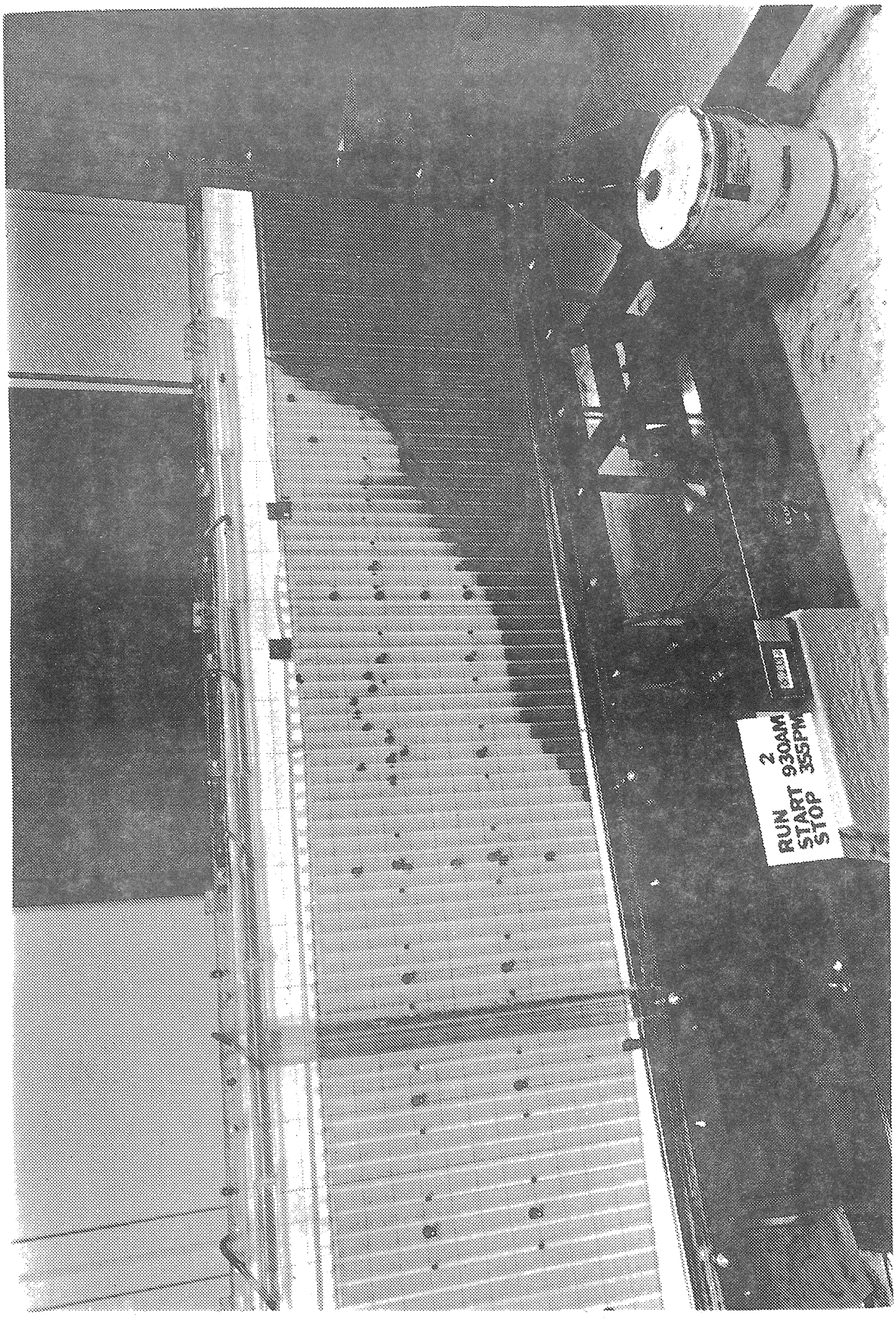

FIGURE 6.13
INTERFACE LOCATION, t_m = 172 Min.

The ultimate effect of the recharging is shown in Figure 6.13 in which the wedge has been depressed and moved seaward in the area under the recharge wells; and, in the area under Lake Tarpon, the wedge has been forced upward. The dark lines on the model were added to bring out the wedge location at the beginning and end of the recharge period.

Conclusions and Recommendations

As can be seen from the preceding figures, the model operation is satisfactory from a qualitative point of view. The problem in obtaining quantitative results at this time involves maintaining the correct water level in the aquifer in the area of the Pasco High. During the run from which the pictures were taken, the water level in this area was much too low and the figures would therefore indicate more penetration and upconing than would be likely.

It is felt that the change in wedge shape due to recharging is a likely result, and that recharge wells would be better located at points farther inland. They might be located in Lake Tarpon or just to the east of the lake. If the recharge water is to be treated waste-water, the proximity of the recharge wells to the Eldridge-Wilde well field would be of great importance.

In order to maintain the correct water level in the aquifer, an overflow manifold system will be installed on the back plate of the model. This system should allow the continuation of the quantitative study in regard to long-term pumping in Eldridge well field, the most advantageous location of recharge wells and the effect of a new well field in the Pasco High area. The use of a tracer dye in the recharge wells would facilitate the evaluation of their effect on the wedge and on Eldridge-Wilde well field.

Objectives (1) and (2) are met in that the model is designed for ease of operation, quick change adjustments, ability to handle silicone oil and other such features as discussed in chapter V.

BIBLIOGRAPHY

Aravin, V. I., and Numerov, S. N. Theory of Motion of Liquids and Gases in Undeformable Porous Media. Trans. A. Moscona. Jerusalem: Israel Program for Scientific Translation, 1965.

Badon-Ghyben, W. "Nota in Verban met de Voorgenomen Putboring nabij Amersterdam", Tijdschrift van net Koninklijk Instituyt van Ingenieurs. The Hague: 1888.

Bear, Jacob. "Scales of Viscous Analogy Models for Ground Water Studies", Journal of the Hydraulics Division, ASCE. Vol. 86, No. HY2, (February, 1960), 11-23.

Dynamics of Fluids in Porous Media. New York: American Elsevier Publishing Company, Inc., 1972.

Bear, Jacob, and Dagan G. "Some Exact Solutions of Interface Problems by Means of the Hodograph Method", Journal of Geophysical Research. Vol. 69, No. 8, (1964b), 1563-1572.

"The Unsteady Interface Below a Coastal Collector", The Transition Zone Between Fresh and Salt Waters in a Coastal Aquifer, Progress Report #3. Technion., Haifa: 1964.

Bear, Jacob, Zaslavsky, D., and Irmay, S. Physical Principles of Water Percolation and Seepage. Paris: UNESCO, 1968.

Black, Crow and Eidsness, Inc. "Water Resources Investigation for the Pinellas County Water System, Pinellas County, Florida", Gainesville, Florida, 1970.

Collins, M. A., and Gelhar, L. W. Ground Water Hydrology of the Long Island Aquifer System, Hydrodynamics Laboratory, Report No. 122. M. I. T., Cambridge Massachusetts: 1970.

Cooke, C. W. "Scenery of Florida Interpreted by a Geologist", State Geological Survey, Bulletin No. 17. Tallahassee: 1939.

"Geology of Florida", Florida Geological Survey, Bulletin No. 29. Tallahassee: 1945.

BIBLIOGRAPHY (Continued)

De Wiest, R. J. M. "Free Surface Flow in Homogeneous Porous Medium", ASCE Transactions. Vol. 127, (1962), 1045-1089.

Glover, R. E. "The Pattern of Fresh-Water Flow in a Coastal Aquifer", Journal of Geophysical Research. Vol. 64, No. 4, (1959), 457-459.

Hele-Shaw, H. S. "Experiments on the Nature of Surface Resistance in Pipes and on Ships", Transactions Institute Naval Architects. Vol. 39, (1897), 145-156.

"Experiments on the Nature of Surface Resistance of Water and Streamline Motion under Certain Experimental Conditions", Transactions Institute Naval Architects. Vol. 40, (1898), 21-46.

"Streamline Motion of a Viscous Film", Rep. of the British Association for the Advancement of Science, 68th Meeting. Vol. 136, (1899), 136-142.

Herzberg, A. "Die Wasserversorgung einiger Nordsee bader", Journal Gasbeleuchtung und Wasserversorgung. Vol. 44, Munich: (1901) 815-819, 824-844.

Hubbert, K. M. "The Theory of Ground Water Motion", Journal of Geology. Vol. 48, No. 8, (1940), 785-944.

Polubarinova-Kochina. Theory of Ground Water Movement. Trans. J. M. R. De Wiest. Princeton: Princeton University Press, 1962.

Rouse, H. Advanced Mechanics of Fluids. New York: John Wiley & Sons, Inc., 1959.

Shames, I. H. Mechanics of Fluids. New York: McGraw-Hill Book Company, Inc., 1962.

Stewart, J. W. "Hydrologic Effects of Pumping From the Floridan Aquifer in Northwest Hillsborough, Northeast Pinellas, and Southwest Pasco Counties, Florida", U. S. Geological Survey, Open File Report, Tallahassee, Florida: 1968.

U. S. Weather Bureau. Climatological Data for the United States by Section, Florida Section. Washington, D. C: U. S. Government Printing Office, 1971.

Vaughan, T. W. "A Contribution to the Geologic History of the Floridan Plateau", Papers from the Trotugas Laboratory, No. 4. Carnegie Institute, Publication 133, (1910) 99-185.